Korrigierte Fassung

A photoactivated adenylyl cyclase as an optogenetic tool to manipulate neuronal signaling and synaptic plasticity

Dissertation

Zur Erlangung des Doktorgrades
an der Fakultät für Mathematik, Informatik und Naturwissenschaften
Fachbereich Biologie
der Universität Hamburg

vorgelegt von

Daniel Udwari

geb. am 7. Juli 1980 in Bad Dürkheim

Hamburg, den 31. Januar 2014

Genehmigt vom Fachbereich Biologie
der Fakultät für Mathematik, Informatik und Naturwissenschaften
an der Universität Hamburg
auf Antrag von Professor Dr. T. OERTNER
Weiterer Gutachter der Dissertation:
Professor Dr. C. LOHR
Tag der Disputation: 28. März 2014

Hamburg, den 07. März 2014

Professor Dr. C. Lohr
Vorsitzender des
Fach-Promotionsausschusses Biologie

Betreuer
Prof. Dr. Thomas G. Oertner
Institut für Synaptische Physiologie
Zentrum für Molekulare Neurobiologie (ZMNH)
am Universitätsklinikum Hamburg-Eppendorf

Co-Betreuer
Prof. Dr. Christian Lohr
Abteilung Neurophysiologie
Zoologisches Institut
an der Universität Hamburg

The research for this thesis was carried out at the Friedrich Miescher Institute for Biomedical Research (FMI) in Basel, Switzerland and at the Center for Molecular Neurobiology (ZMNH) in Hamburg, Germany.

For inquiries about this thesis, please contact daniel@udwari.de

Universität Hamburg
DER FORSCHUNG | DER LEHRE | DER BILDUNG

Universitätsklinikum Hamburg-Eppendorf

ZMNH Center for Molecular Neurobiology Hamburg

FMI Friedrich Miescher Institute for Biomedical Research

Summary

To improve our understanding of brain function, temporally and spatially precise manipulation of neurons and neuronal circuits is needed. This is limited with standard methods based on pharmacological manipulations and electrophysiology. In recent years, novel optogenetic tools have become available which promise to facilitate more precise spatiotemporal control of neuronal activity and signaling. In this thesis, I introduce bPAC (*Beggiatoa* photoactivated adenylyl cyclase), a member of a new class of optogenetic actuators which I characterized in hippocampal neurons. bPAC is a soluble adenylyl cyclase, which produces cAMP upon illumination with blue light. It allows for manipulation of intracellular cyclic AMP signaling, a ubiquitous second messenger system important for neuronal plasticity, learning and memory. bPAC is small compared to similar optogenetic tools (350 amino acids) and very light sensitive, which are desirable attributes in an optogenetic actuator, commending it for *in vivo* and *in vitro* applications. I expressed bPAC in hippocampal organotypic slice cultures using different gene delivery techniques which allow for sparse or regionally limited expression. Neurons express bPAC well and I could reliably use bPAC to elevate intracellular cAMP levels in a controlled manner to concentration ranges similar to what can be achieved with canonical pharmacological tools. Optogenetic cAMP elevation activated conductances underlying slow inward current in these neurons, which was in large part due to cAMP modulation of hyperpolarization activated cyclic nucleotide gated (HCN) channels. Under elevated cAMP concentrations, miniature EPSC frequency, but not amplitude, increased reversibly in CA1 cells. These effects were acute and not lasting. To study the effects of postsynaptic cAMP signaling on neuronal plasticity, I used two approaches: 1) intracellular recordings in postsynaptic neurons with presynaptic channelrhodopsin stimulation, and 2) paired recordings of unitary synaptic connections between two hippocampal pyramidal cells. I show that elevation of postsynaptic cAMP alone is not sufficient to induce synaptic potentiation, nor to modulate plasticity induction in a theta burst protocol.

Taken together, cAMP is a viable tool to elevate neuronal cAMP levels and to study intracellular second messenger signaling with unprecedented temporal and spatial precision.

Zusammenfassung

Methoden zur räumlich und zeitlich präzisen Manipulation von Nervenzellen sind wichtig, um unser Verständnis des Gehirns und seiner Funktionsweise voranzutreiben. Mit den pharmakologischen und elektrophysiologischen Standardmethoden ist dies nur eingeschränkt möglich. In den letzten Jahren stehen zunehmend neuartige optogenetische Werkzeuge zur Verfügung, welche eine größere räumlich-zeitliche Kontrolle über neuronale Aktivität und Signalwege versprechen. In dieser Arbeit stelle ich bPAC (*Beggiatoa* photoaktivierte Adenylatzyklase) vor, Teil einer neuen Klasse von optogenetischen Effektoren, und charakterisiere bPAC in hippocampalen Neuronen. bPAC ist eine lösliche Adenylatzyklase, die bei Beleuchtung mit blauem Licht zyklisches Adenosinmonophosphat (cAMP) herstellt. Die Lichtabhängigkeit erlaubt eine nicht-invasive Manipulation von intrazellulären cAMP-abhängigen Signalkaskaden, einem ubiquitären Second-Messenger-System, welches unter anderem für neuronale Plastizität, Lernen und Gedächtnis wichtig ist. bPAC ist klein im Vergleich zu ähnlichen optogentischen Effektoren (350 Aminosäuren) und sehr lichtempfindlich, zwei wertvolle Attribute in einem optogenetischen Werkzeug, wodurch bPAC für *in vivo* und *in vitro* Anwendungen geeignet ist. Ich benutzte verschiedenen Transfektionstechniken, um bPAC in organotypischen Kulturen in einzelnen Neuronen oder in spezifischen Regionen des Hippocampus zu exprimieren. Ich konnte zeigen, dass mittels bPAC die intrazelluläre cAMP-Konzentration in einer kontrollierten und reproduzierbaren Art und Weise erhöht werden kann. Dabei können ähnliche cAMP-Konzentrationen wie mit klassischen pharmakologischen Methoden erreicht werden. Optogenetische Erhöhung der cAMP-Konzentration führt zu einer Öffnung von Membrankanälen und zu einem langsamen Einwärtsstrom, welcher zu einem großen Teil durch cAMP-abhängige Modulation von hyperpolarisationsaktivierten zyklonukleotid-gesteuerten Kanälen (HCN) verursacht wird. Während der lichtinduzierten erhöhten cAMP-Konzentration in CA1 Neuronen steigt die Frequenz, jedoch nicht die Amplitude von Miniatur-EPSCs reversibel an. Diese Effekte sind akut und reversibel. Um die Auswirkungen der postsynaptischen cAMP-Signalkaskaden auf neuronale Plastizität zu untersuchen, verfolgen wir zwei Ansätze: 1) Intrazelluläre Messungen, kombiniert mit Channelrhodopsin-Stimulation,

und 2) Messung der synaptischen Verbindung zwischen zwei hippocampalen Pyramidenzellen(paired-patch Experimente). Ich konnte zeigen, dass die Erhöhung von postsynaptischem cAMP nicht ausreicht, um eine synaptische Potenzierung zu induzieren. Die Induktion synaptischer Plastizität durch Theta-Burst Stimulation war durch postsynaptische cAMP Erhöhung ebenfalls nicht verändert. Zusammenfassend lässt sich sagen, das bPAC ein neues und äußerst potentes Werkzeug ist, um die cAMP-Konzentration in individuellen Nervenzellen kontrolliert zu erhöhen und dadurch intrazelluläre Signalwege mit hoher zeitlicher und räumlicher Präzision zu untersuchen.

Table of Contents

1. Introduction

1.1. Optogenetics

In recent years, the field of optogenetics has become more and more part of the standard toolbox for neuroscientists, and optogenetic tools are now widely used *in vitro* and *in vivo*. The term optogenetics was defined by Gero Miesenböck as "the branch of biotechnology which combines genetic engineering with optics to observe and control the function of genetically targeted groups of cells with light, often in the intact animal"[1]. The available optogenetic tools include actuators that are used to manipulate neuronal activity or signaling, most prominently channelrhodopsin-2, and sensors to probe various states of neurons, such as calcium (GCaMP, GECO) or voltage (VSFPs) (Fig. 1.1). A later and more restrictive definition by Karl Deisseroth focuses on the actuators: "Optogenetics is the combination of genetic and optical methods to achieve gain or loss of function of well-defined events in specific cells of living tissue"[2].

Predominantly channelrhodopsin-2 has been used to induce action potentials with light flashes in select populations of neurons, both for *in vitro* and *in vivo*

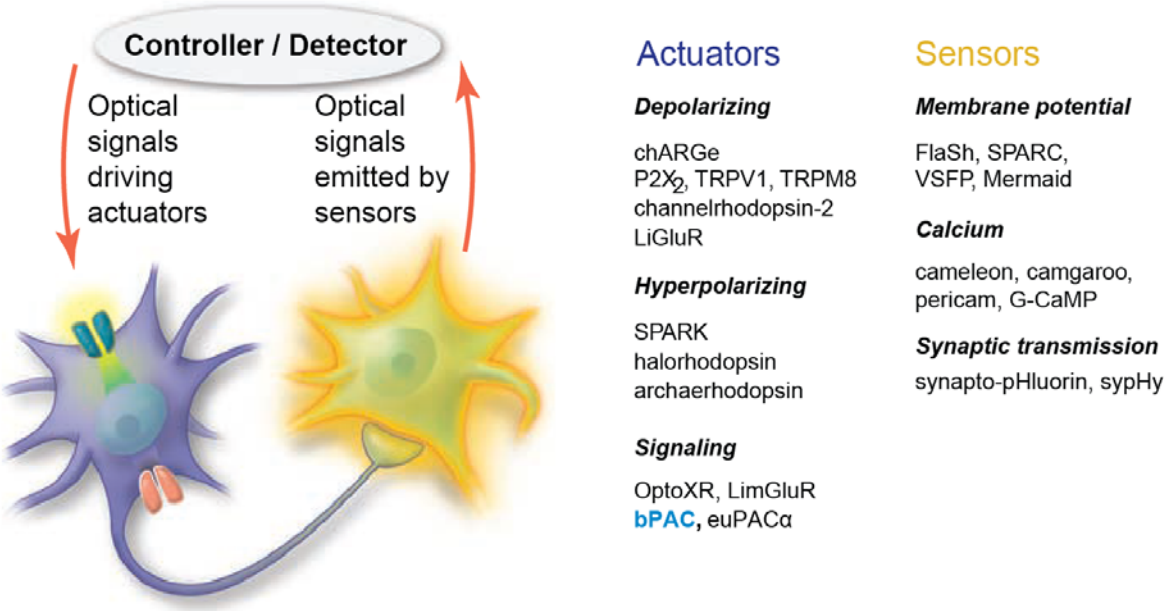

Figure 1.1: Optogenetic actuators and sensors. Actuators translate light stimuli emitted from an illumination system ('controller') into a biologically relevant response. Sensors translate responses into differential photon output, which can be read out by a detection system ('detector'). Figure modified from Miesenböck[1].

studies. Due to the widespread use and the avalanche of important new findings arising from the use of channelrhodopsin-2, optogenetics has been named 'Method of the Year' by the journal *Nature Methods* in 2010[3].

Optogenetics as a method for interfering with intracellular signaling has been less widely used. One important class of tools for studying signaling are the opto-XRs, which are chimeric 7 trans-membrane G-Protein coupled receptors[4,5]. The X is a placeholder for the type of receptor (R) engineered into the opto-XR. They allow for fast activation of signaling pathways with very low dark activity. The OptoXRs are engineered from bovine rhodopsin, where the intracellular loops were replaced with the intracellular domains from a GPCR that signals via the pathway of interest. For example, OptoXRs with the intracellular domains of the α_1 and $ß_2$-adrenergic receptors(opto-α_1R, opto-$ß_2$R) have been constructed, which activate $G\alpha_q$- or $G\alpha_s$-dependent signaling pathways, respectively. Blue light rapidly increases cAMP signaling downstream of $G\alpha_s$ in HEK cells expressing opto-$ß_2$AR[5]. Opto-XRs depend on intracellular mechanisms to increase cAMP signaling. In the discussion (chapter 6) I will compare opto-XRs to bPAC, the optogenetic tool which I have used for my thesis.

Targeting and expression levels

The key advantage of optogenetics over other methods of stimulation and sensors such as calcium-sensitive dyes is that the expression of optogenetic tools can be targeted specifically to cells of a defined type. Targeting is, however also challenging and controlling expression levels of optogenetic tools is more difficult than controlling concentration of a chemical indicator. One challenge in optogenetics is the control of expression levels and cell type specificity. For expression *in vivo,* only few approaches are viable, including transgenic animals, *in utero* electroporation, and the use of viral vectors. For *in vitro* experiments with cell or tissue cultures, additional techniques available are biolistic transfection (gene-gun), single cell electroporation, and techniques for transfecting dissociated cultures such as lipofection and calcium phosphate transfection.

Targeting expression to the desired cell type is mainly achieved by the choice of promoter, which is active in specific cell types or at specific times. Certain viral vectors also have some cell or tissue specificity, and precisely timed *in vivo*

electroporation is also used to target specific classes of cells. Single-cell electroporation is the only technique that allows transfecting individual, morphologically identified cells in tissue. Expression levels of the desired optogenetic construct in the target cells can be controlled in several ways. The amount of vector DNA introduced can be controlled (i.e. by changing the duration of the electroporation pulse, virus concentration etc.) and promoters of different strengths can be chosen. As expression changes over time, the choice of time point for an experiment is also not to be neglected and should be standardized. In the case of AAVs, different serotypes affect which cell- and tissue types are transduced, and how expression is regulated over time[6,7]. These factors should be taken into account when choosing a transfection system for optogenetic tools.

1.2. Photoactivated adenylyl cyclases

Photoactivated adenylyl cyclases were first described in the early 2000s in the laboratory of Masakatsu Watanabe, where they could show that the well-known phototaxic and photoavoidance behaviors of the flagellate protist *Euglena gracilis* are regulated by a novel type of blue-light activated flavoprotein which they named PAC (Photoactivated Adenylyl Cyclase), consisting of two subunits, PACα and PACβ.[8,9] PACα was introduced as an optogenetic tool some years later, and it was shown that intracellular cAMP signaling in eukaryotic cells and fly behavior could be modulated with PACα from *Euglena* (in this thesis abbreviated as euPACα)[10]. Part of the work presented in this thesis is the discovery and characterization of a photoactivatable adenylyl cyclase (bPAC) from *Beggiatoa,* a hydrogen sulfide oxidizing bacterium and its comparison with euPACα (see chapter 3). Both euPACα and bPAC are class III adenylyl cyclases, the most abundant AC class, whose members have similar catalytic domains and mechanisms[11]. Both euPACα and bPAC are also soluble adenylyl cyclases; they are not anchored to the cell membrane but rather diffuse throughout the cytosol[12]. Recently, several other photoactivatable adenylyl cyclases have been found in bacteria[13,14], but their applicability as optogenetic tools has not been demonstrated yet. Discovery of additional PACs from different species, or molecular engineering of existing PACs might extend the PAC toolkit in the future.

1.3. The hippocampus and the trisynaptic pathway

The hippocampus is one of the most intensively studied parts of the brain, which is in part due to its major role in certain types of memory and memory formation, but also because of its very ordered structure. It is part of the limbic system in the forebrain, and one of the evolutionarily oldest brain structures. It consists of archicortical tissue, which comprises fewer layers than neocortical tissue (three instead of six), and is an elaboration of the inner border of the cortex[15]. The major fraction of excitatory input to the hippocampus arrives via the entorhinal cortex (EC), which innervates the dentate gyrus (DG) via the perforant pathway. The DG granule cells in turn project to the CA3 region of the hippocampus proper, more specifically to CA3 pyramidal neurons, which in turn project to CA1 pyramidal cells. This nonreciprocal connection from EC to CA1 is called *the trisynaptic circuit*[15,16] (see also Fig. 1.3).

The pyramidal cells in the CA1 region mainly project back to the EC, either via the subiculum, or directly. Throughout the arc that is formed by CA3 to the CA1 region of the hippocampus, the basic layering is similar. The pyramidal cell layer or *stratum pyramidale* contains the densely packed somata of the pyramidal cells.

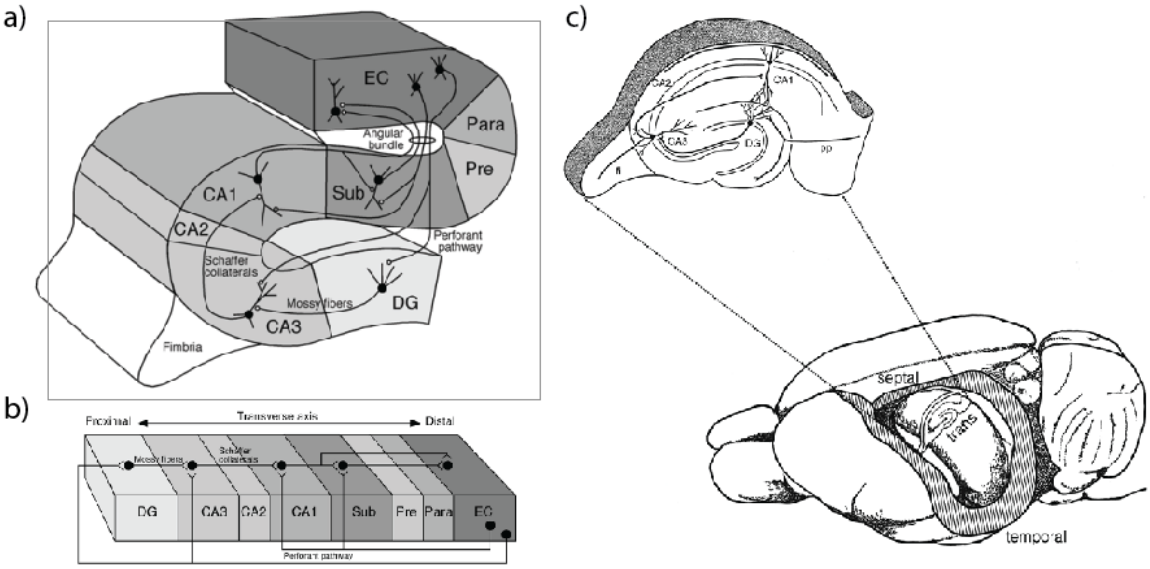

Figure 1.3: Anatomy of the hippocampus and basic connectivity: (a) Schematic of hippocampal regions and their basic connectivity (b) linearized schematic of *(a)*. (c) Anatomical position of the hippocampus in the rat brain. A transversal cross-section is shown above, same orientation as in *(a),* with the EC and parts of the Sub cut off. All illustrations from reference No.[15], p. 38 & 46.

The dendritic arborizations of the pyramidal cells extend throughout the other layers of the hippocampus. In CA1, from the pyramidal cell layer towards the hippocampal fissure which separates the CA regions from the DG, the proximal layer is the *stratum radiatum* (SR). The layer closest to the fissure is the *stratum lacunosum moleculare*. The *stratum oriens* lies in the other direction, is relatively cell free, and contains the basal dendrites of the pyramidal cells and the *alveus* forms the innermost layer. The Schaffer collateral axons of the CA3 pyramidal neurons project predominantly to the *stratum radiatum* and to the *stratum oriens* where they synapse onto CA1 pyramidal neuron and interneuron dendrites. In the CA3 region, an additional layer exists between the *stratum pyramidale* and the stratum radiatum, namely the *stratum lucidum*, which receives the majority of excitatory inputs from DG onto CA3 cells.

1.4. Organotypic hippocampal cultures from rats

The model system used for all experiments in this thesis was organotypic hippocampal slice cultures from rats, growing on porous PTFE membranes[17]. This model system has advantages compared to other ways of studying live hippocampal tissue. Compared to dissociated hippocampal cell cultures, the tissue integrity is high, and basic connectivity of DG, CA1 and CA3 is intact[17]. Compared to acute tissue slices classically used for electrophysiological experiments of the hippocampus, a big advantage is the long term survival of organotypic cultures in the incubator, which allows for several rounds of region-targeted gene delivery. Connectivity between CA3 and CA1 regions is much lower in acute slices, since many axonal connections run diagonally through the hippocampus and are cut during slice preparation[18]. In organotypic hippocampal slices this is not the case, as CA3 to CA1 projections extend while the slices develop in culture. However, the connectivity is not exactly the same as *in vivo*, and a caveat must be considered: recurrent circular wiring in an organotypic slice can lead to elevated recurrent activity which makes e.g. extracellular stimulation experiments difficult due to frequent epileptiform discharges within the slice.

1.5. Properties of pyramidal neurons and their synaptic inputs

Pyramidal neurons are the principal excitatory cells on each end of the Schaffer collaterals, and the CA3-CA1 connection is probably the most widely studied synapse in the brain. CA1 pyramidal neurons have a soma, an axon, and two distinct dendritic arborizations: the apical dendrites are longer, reach out through the *stratum radiatum* to the *stratum lacunosum moleculare*, where they form the apical tuft. The basal dendrites extend across the *stratum oriens*[15,19] (Fig 1.5a). CA3 and CA1 pyramidal neurons have differential morphologies and inputs. The somata of CA3 cells are generally larger than those of CA1 cells, and their dendritic tufts branch earlier. Unique to CA3 pyramidal cells is the presence of large spiny structures on the apical dendrites close to the soma. These thorny excrescences are located in the *stratum lucidum*, most synapses from mossy

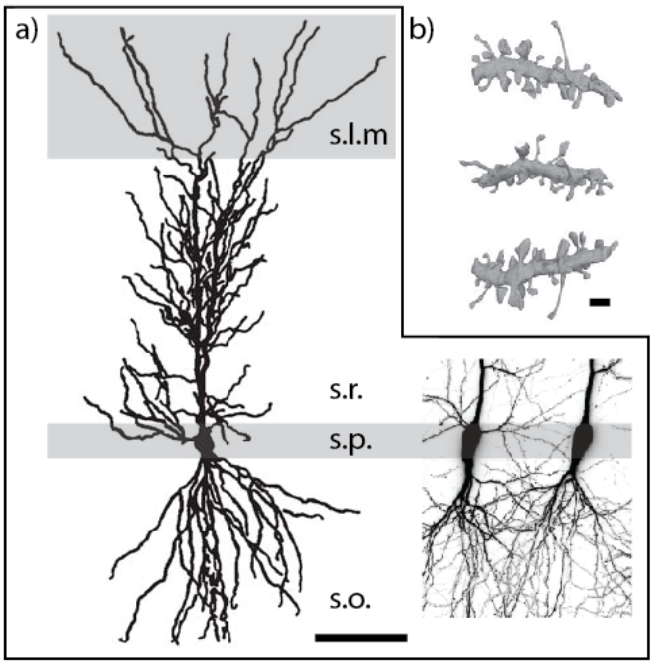

Figure 1.5: CA1 pyramidal neurons are strongly arborized and spiny. (a) left: 2D reconstruction of a typical CA1 pyramidal neuron. Major layers are marked. s.l.m., *stratum lacunosum moleculare*, s.r., *stratum radiatum*, s.p., *stratum pyramidale*, s.o., *stratum oriens.* Scale bar = 100 µm. Adapted from [132].. Lower right: Two-photon image of two CA1 pyramidal neurons in a rat hippocampal organotypic culture, layers aligned to the left neuron. Spines visible. Neurons expressing tDimer2-RFP. Image by D.U. (b) Different views of one 3D-reconstruction showing a piece of dendrite with differently shaped spines. Scalebar = 1µm (Image by Kristen Harris, taken from [20])

fibers are made here[15,20]. Both types of pyramidal neuron receive their excitatory inputs mainly onto dendritic spines, small protrusions of the dendritic membrane that are highly variable in shape and size (Fig.1.5b).

Excitatory synapses

Excitatory synapses onto pyramidal cells consist of a presynaptic bouton and a postsynaptic spine. Boutons contain one or more active zones, where neurotransmitter vesicles containing glutamate undergo exocytosis when the release machinery is activated by Ca^{2+}-influx from voltage-gated calcium channels[21]. Glutamate diffuses across the synaptic cleft, where it binds to glutamate receptors, the main ionotropic glutamate receptors are AMPARs, kainate receptors and NMDARs. These receptors have different functions: AMPARs, permeable to Na^+ and K^+, open fast and desensitize quickly. NMDARs on the other hand are normally blocked by a Mg^{2+} ion even when they bind glutamate. Only a concurring depolarization of the postsynaptic membrane repels the Mg^{2+} ions and unblocks the NMDARs, allowing for influx of cations including Ca^{2+}.

Inhibitory synapses and modulatory input

In addition to excitatory synapses (either coming from the hippocampus itself or from other brain areas), there are many inhibitory and modulatory inputs to hippocampal pyramidal cells. These either come from local GABAergic interneurons (many different subtypes, see[22]) or from afar. The hippocampal CA1 region receives cholinergic, adrenergic, noradrenergic, serotonergic and dopaminergic inputs, binding their respective neurotransmitter receptors[20]. I would like to point out two types of modulatory inputs, noradrenergic and dopaminergic. Both can elevate cAMP via GPCR signaling ($G\alpha_s$) downstream of a subgroup of their receptors (specifically ß-adrenoreceptors and D_1 dopamine receptors). Noradrenergic inputs to the hippocampus come predominantly from the *locus coeruleus*. Dopaminergic inputs innervating the hippocampus mainly derive from the ventral tegmental area (VTA). Both dopaminergic and adrenergic signaling has been shown to play a role in the modulation of hippocampal long-term plasticity[23–25].

1.6. Cyclic AMP is a ubiquitous second messenger system

Intracellular signaling via cAMP is a prototypic second messenger system. The vast majority of organisms have adenylyl cyclases which produce cAMP as a signaling molecule, including all animals, most protists and prokaryotes, and it has also been found in higher plants[26–28]. In eukaryotes, cAMP signaling is mediated mainly by G-protein coupled receptors (GPCRs), which stimulate (via $G\alpha_s$ signaling), or inhibit (via $G\alpha_i$ signaling) certain types of adenylyl cyclases. GPCRs are a receptor class activated by a wide range of different molecules (such as hormones, neurotransmitters and pheromones[29]) or other extracellular signals (the most prominent being opsins, which can detect photons with very high sensitivity[30]). GPCRs are not the only activators of adenylyl cyclases; some isoforms can be activated by calcium-calmodulin, another important second messenger system, constituting a convergence point for the two systems[31].

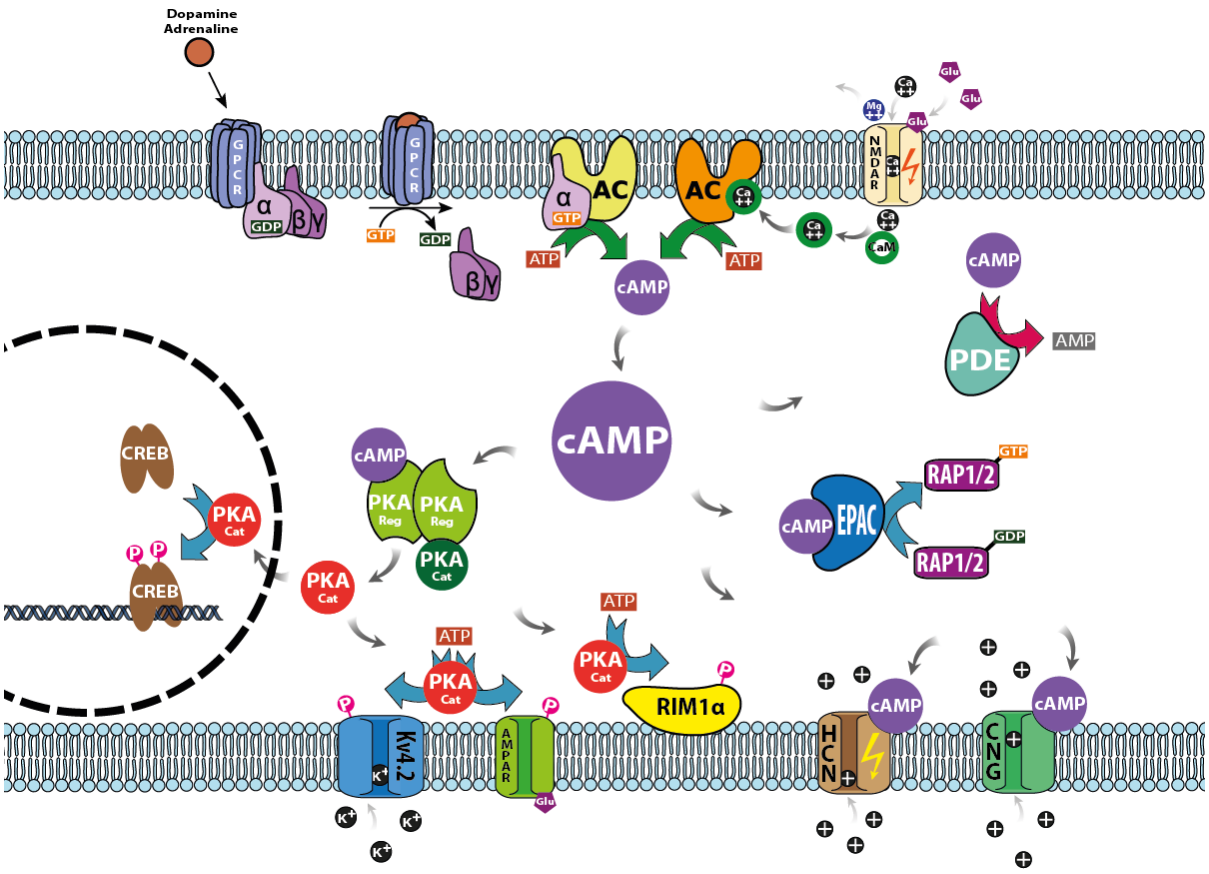

Fig 1.6: Scheme of endogenous cAMP signaling in neurons. (figure by D.U.)

cAMP signaling in the nervous system

I will give a concise overview of cAMP signaling with a focus on the nervous system, referring in this subsection to figure 1.6. Cyclic AMP is produced by adenylyl cyclases, which are generally membrane-bound, although soluble ACs exist in neurons[32]. Activation of $G\alpha_s$ signaling cascades by neurotransmitters such as dopamine and adrenaline leads to activation of adenylyl cyclases and increase in cAMP levels. Likewise, Ca^{2+} influx, via NMDARs and subsequent binding to Calmodulin (CaM) activates certain ACs. Downstream of cAMP, several effectors exist, the most widely known is certainly protein kinase A (PKA). cAMP binding to the regulatory subunits of PKA releases the catalytic subunits (PKA_{cat}, shown in red). Phosphorylation targets for PKA_{cat} include the transcription factor CREB (cAMP response element binding protein), regulating for example genes important for neuronal plasticity[33]. PKA also phosphorylates some ion channels, for example AMPARs, where PKA phosphorylation regulates receptor trafficking [34] and conductivity[35]. Another ion-channel that is modulated by PKA phosphorylation is Kv4.2, an A-type potassium channel, important for regulating membrane excitability in neurons[36]. RIM1α is an example for a presynaptic protein where phosphorylation by PKA has been shown to play a role in some forms of presynaptic plasticity[37], but there are others, for example synaptotagmin-12[38].

Independent of PKA, cAMP can directly bind two families ion channels: cyclic nucleotide gated channels (CNG) and hyperpolarization activated cyclic nucleotide modulated channels (HCN)[39]. CNG channels are directly gated by cAMP, and are nonselective cation channels[40]. They play an important role in olfaction and phototransduction[41], but are also expressed in hippocampal neurons[42]. HCN channels have been studied extensively in the heart, where they are responsible for pacemaker currents, also known as ‘funny’ currents[43]. In the CNS generally, also specifically in the hippocampus, HCN currents (here known as I_h for hyperpolarization activated currents) play a role in the regulation of neuronal excitability[44]. HCN channels are mixed cation conducting channels. Unlike other voltage gated channels, they are activated by hyperpolarization of the membrane, typically below -60 mV, which means close to the resting

membrane potential of a hippocampal neuron[45]. cAMP directly binds to HCN channels, shifting the voltage activation threshold to more depolarized potentials.
A third major target of cAMP signaling is exchange protein directly activated by cAMP (EPAC), which has only in recent years moved into the focus of study[46]. EPAC signaling in the CNS is not as well understood as PKA signaling, but nevertheless there are several studies linking EPAC signaling to neuronal function and synaptic plasticity[47–50]. Degradation of cAMP is regulated by phosphodiesterases (PDE)[51].

Localized cAMP signaling

Looking at the plethora of downstream effectors of cAMP, one question arises immediately: How can specific targeting of extracellular signals to intracellular pathways be maintained? Figure 1.6, a simplified scheme to illustrate general principles of cAMP signaling, omits an important component of cAMP signaling, namely compartmentalization of cAMP signaling into signaling units[52]. A-kinase anchoring proteins (AKAPs) play an essential role in this. AKAPs bind to PKA, PDEs and ACs which is prerequisite for local and differential cAMP signaling[53,54]. Especially phosphodiesterases are implicated in shaping cAMP gradients in subcellular compartments[55]. This has been shown in neurons[56], and compartmentalized cAMP signaling has been found to play a role in neuronal plasticity[57–60].

Approaches to study cAMP signaling

cAMP signaling has been studied with different approaches, and I will discuss the different approaches in chapter 6. The two main concepts are pharmacology and genetic manipulation. Pharmacological tools include blockers for PDEs (IBMX, Rolipram), activators of ACs (Forskolin), blockers of PKA (H89, KT5720), and cell permeable, PDE resistant cAMP analogs (Sp-cAMPS). Genetic interference can target either components of the cAMP signaling cascades directly or associated proteins such as AKAPs, and there are mouse models with altered cAMP signaling available[61]. Finally, the advent of optogenetics now also brings new tools to investigate cAMP signaling.

cAMP signaling in synaptic plasticity, learning and memory

Evidence for involvement of cAMP signaling in synaptic plasticity was first shown more than four decades ago for the gill withdrawal reflex of *Aplysia* studied by Eric Kandel[62]. Later, groundbreaking genetic studies in *Drosophila* have shown pivotal roles for components of the cAMP signaling cascade for learning, specifically the *dunce* and *rutabaga* genes, coding for a PDE and AC, respectively[63]. The transcription factor CREB (cAMP response element binding protein) regulates a variety of plasticity genes implicated in long-term memory [64]. It is linked to cAMP signaling via PKA, which transfers to the nucleus, phosphorylating CREB and thereby activating it, promoting transcription[64]. There are many more studies linking cAMP signaling to learning and memory, including effects of I_h on learning curves[65] and plasticity regulation by AMPAR phosphorylation[34]. I will put these in context of this thesis in the discussion.

2. Aim of the Thesis

Optogenetics is relatively new branch of biotechnology, but its applications have extended tremendously in recent years. However, tools to directly modulate intracellular signaling with light are still not regularly used. Photoactivatable adenylyl cyclases (PACs) are novel members of the optogenetic toolbox, and in collaboration with the lab of Peter Hegemann in Berlin, I characterized the newest developments in this direction in neurons, focusing on a PAC from the bacterium *Beggiatoa*.

First, I wanted to establish a stable expression system for bPAC, and characterize bPAC in neurons in organotypic hippocampal cultures from rats. For this characterization, two things were essential: an optic system to stimulate the photoactivatable adenylyl cyclase, and a readout system, for which we chose an electrophysiological method: overexpression of cyclic nucleotide gated channels and current measurements with patch-clamp. The second goal was to study neuronal cAMP signaling with a focus on synaptic plasticity, making use of bPAC with the advantages of an optogenetic tool for manipulating cAMP. Using bPAC I could stimulate cAMP with a cell-type specificity and temporal precision far above what can be achieved with bath application of chemical activators.

As bPAC is a novel optogenetic tool, we first wanted to characterize effects of *acute* bPAC stimulation on the electrophysiological properties of neurons. In a next step, we wanted to make use of the temporal and spatial precision of bPAC to study the modulatory effects of cAMP signaling on long-term plasticity of the CA3-CA1 synapse, the central object of study in the Institute for Synaptic Physiology. To separate pre- and postsynaptic sites of plasticity induction, optogenetic tools are superior to pharmacological tools, because they can be targeted to specific regions or cells. To this end, I had to implement methods for targeted gene delivery. Taken together, our goal was to establish bPAC as an optogenetic tool to investigate synaptic signaling *in vitro* and set the course for a potential use *in vivo* in the future.

3. Characterization of bPAC and comparison with euPACα

3.1. Characterization of bPAC in neurons with a co-expressed CNG-channel

To characterize bPAC in hippocampal neurons, we chose an approach allowing for electrophysiological readout of cAMP levels. For this, I co-expressed a modified cyclic nucleotide gated channel, CNG-A2 (C460W/E583M)[66] together with bPAC, or alternatively with euPACα.I recorded from CA1 cells in whole-cell mode during bPAC illumination, while pharmacologically blocking NMDARs, GABARs, and VGSCs. Cells were voltage clamped at -65 mV (Fig. 3.1.1). We published the results of these experiments in the Journal of Biological Chemistry in December 2010[67]. The simultaneous discovery of bPAC by Mark Gomelsky and coworkers was published back-to-back in the same issue[68]. In their paper, they describe the same gene and gene product, here named BlaC, and characterize its function in *E. coli*, but not in eukaryotic cells.

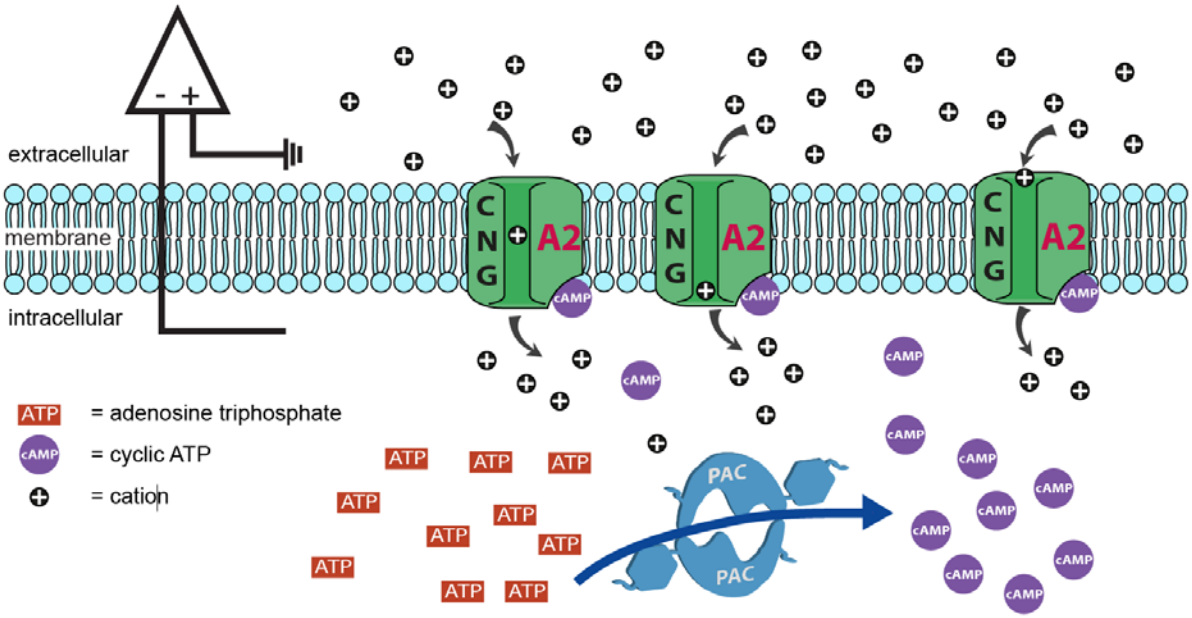

Figure 3.1.1: PAC / CNG Scheme. Experimental setup for PAC characterization. PAC catalyzes the reaction ATP → cAMP upon blue light illumination. cAMP binds directly to co-expressed CNG-A2 channels (in addition to endogenous targets). CNG-A2 conductances open, CNG-A2s are non-selective cation channels.

3.2. Publication in JBC 2011

Disclaimer

The following section has been published. For this thesis, the original manuscript has been included in full. Numbering of figures and references has been reformatted. The author of this thesis contributed all experiments on hippocampal neurons to the publication (figures 3.2.4 and 3.2.5).

THE JOURNAL OF BIOLOGICAL CHEMISTRY VOL. 286, NO. 2, pp. 1181–1188, January 14, 2011

Light-modulation of cellular cAMP by a small bacterial photoactivated adenylyl cyclase, bPAC, of the soil bacterium *Beggiatoa*

Manuela Stierl[1], Patrick Stumpf[2], Daniel Udwari[3], Ronnie Gueta[2], Rolf Hagedorn[1], Aba Losi[4], Wolfgang Gärtner[5], Linda Petereit[6], Marina Efetova[6], Martin Schwarzel[6], Thomas G. Oertner[3], Georg Nagel[2], and Peter Hegemann[1*]

From the [1]Humboldt-Universität zu Berlin, Experimental Biophysics, Invalidenstr. 42, D-10115 Berlin, Germany, the [2]University of Würzburg, Botany I, Julius-von-Sachs-Platz 2, D-97082 Würzburg, Germany, the [3]Friedrich Miescher Institute for Biomedical Research, Maulbeerstr. 66, CH-4058 Basel, Switzerland, the [4] University of Parma, Dept. of Physics, Parma, Italy, the [5] Max-Planck-Institute for Bioinorganic Chemistry, Postfach 1013 56, D-45410 Mülheim, Germany, and the [6] Free University Berlin, Dept. of Biology, Takustr. 6, D-14195 Berlin, Germany.

Abstract

The recent success of Channelrhodopsin (ChR) in optogenetics has caused increasing interest also in enzymes that are directly activated by light. We have identified in the genome of the bacterium *Beggiatoa* a DNA sequence encoding an adenylyl cyclase directly linked to a BLUF-type light sensor domain. In *E. coli* and *Xenopus* oocytes, this photoactivated adenylyl cyclase (bPAC) showed cyclase activity that is low in darkness but increased 300 fold in the light. This enzymatic activity decays thermally within 20 s in parallel with the red-shifted BLUF-photointermediate. bPAC is well expressed in pyramidal neurons and, in combination with cyclic nucleotide gated (CNG) channels, causes efficient light-induced depolarization. In the *Drosophila* central nervous system, bPAC mediates light-dependent cAMP increase and behavioral changes in freely moving animals. bPAC seems a perfect optogenetic tool for light-modulation of cAMP in neuronal cells and tissues, and for studying cAMP-dependent processes in live animals.

Introduction

Non-invasive manipulation of intercellular processes by light-activated proteins has recently developed as an emerging scientific field[69]. The wide application of channelrhodopsin (ChR) in the neurosciences as an inheritable protein with retinal as a ubiquitous chromophore has strongly promoted the young field of optogenetics[70,71]. ChR is so well appreciated in this context because it modulates the *membrane voltage* as a universal parameter relevant for basically all neuronal cells. The protein is small, non-toxic, the cofactor retinal is available in all animal cells, and a once transformed organism inherits the light-sensitivity to the next generation. This success stimulated the demand for novel genetically encoded light-activated proteins that modulate other general cellular parameters such as the second messengers Ca^{2+}, cAMP, cGMP, or IP_3. To become useful tools for cell biology and neuroscience, such light-gated enzymes would have to work well in all classical experimental systems and use ubiquitous cofactors as light sensors.

A promising example in this direction were the light-gated adenylate cyclases PACα and PACβ of the unicellular flagellate *Euglena gracilis* (euPACs), where they serve as an $\alpha_2ß_2$ photoreceptor complex that senses light for photophobic responses and phototaxis[8,9]. However, both euPACs are large proteins with two BLUF-photoreceptor domains (F)[72] and two cyclase domains (C) in a FCFC arrangement (Fig. 3.2.1a) functioning in the flagellate as a tetrameric complex. The purified protein complex shows some cyclase activity in the dark that is stimulated 80-fold in the light. In *Xenopus* oocytes and in HEK cells, the activity of euPACα was much higher than that of euPACβ[10] suggesting that euPACα would be an appropriate tool for manipulating cAMP-levels in host cells and animals. In fact, ubiquitous expression of euPACα in *Drosophila* leads to a lethal cAMP increase, whereas pan-neuronal euPACα expression yielded strong effects on the grooming behavior of adult fruit flies in response to blue light[10]. Despite these promising experiments, PAC proteins were not widely accepted for the study of neuronal or developmental cAMP-dependent processes. The main obstacles are the large molecular weight of above 100 kD, low solubility, significant dark activity, and the only moderate activation by light[10].

Here we introduce a novel PAC from *Beggiatoa*, a sulfide oxidizing bacterium that colonizes large areas of sea ground in form of widely extended microbial mats[73]. *Beggiatoa* possesses a chemolithoautotrophic metabolism, which allows utilization of oxygen or nitrate as electron acceptors during sulfide oxidation[74]. A recently deposited genome sequence revealed the presence of a gene, putatively encoding a 350 amino acid protein, consisting of a blue light sensing BLUF-domain linked C-terminally to an Type III adenylyl cyclase (Fig. 3.2.1a)[27]. All amino acids considered as critical for the catalytic mechanism are conserved as highlighted in Fig. 3.2.1b. The amino acids are arranged in such a way that we expect the protein to function as a homo-dimer in accordance to crystal structures of other Type III cyclases (Fig. 3.2.1c).

We proved the bPAC activity first in *E. coli*, analyzed the spectral properties on the purified protein, and tested the applicability and kinetics in *Xenopus* oocytes, rat hippocampal pyramidal cells, and in the *Drosophila* CNS in light and darkness. In spite of its small size, bPAC performed in most respects superior to euPAC. bPAC shows lower dark activity and a better stimulation of the activity in the light. We demonstrate that light-induced cAMP elevations in neurons are highly reproducible and proportional to the light dose, making non-invasive light-control of cAMP possible in cell biology and the neurosciences.

Experimental Procedures

Cyclase activity in E. coli: E. coli-optimized synthetic DNA encoding the photoactivated cyclase bPAC of Beggiatoa sp. (Acc.No. GU461307) was purchased from Mr. Gene (Regensburg, Germany) and was cloned in frame behind the N-terminal His_6-tag and SUMO epitope into a pET SUMO vector (Invitrogen). The protein was expressed in *E. coli* strain BTH101 at 30°C in 200 µM IPTG for 2h. Both transformed and non-transformed cells were plated on MacConkey agar (Difco) pH 7.5 containing 1% maltose, and incubated at 30°C over night in darkness or in white light (average intensity: 8 W m^{-2} white light).

Protein purification: For purification the bPAC SUMO fusion construct was expressed in *E. coli* strain BL21 DE3 at 18°C in LB induced with 60µM IPTG for 48h. bPAC was purified on Co-NTA resin (Clontech, USA) in 50 mM NaH_2PO_4 (pH 7.5), 300 mM NaCl, 0.1 mM phenylmethylsulfonyl fluoride (PMSF) buffer

according to suppliers instruction. The eluate was dialyzed 2x against 200 volumes buffer and concentrated by ultrafiltration (Amicon Ultracel, M.W.C.O. 10000, Millipore).

Oocyte electrophysiology: Oocytes from *Xenopus laevis* and human CFTR cRNA were prepared as described before[75]. We used bPAC-DNA codon-optimized for expression in human cells (0810735_Beggiatoa_Mammal_pMK, Genbank accession number GU461307 or GU461306). The DNA (Mr. Gene, Regensburg, Germany) was inserted between the *BamHI* and *BsiWI* of the pGEMHE vector[76], a derivative of pGEM3z (Promega, Madison, WI, USA) including a C-terminal myc-tag. The Nhe-linearized plasmids were used for the in vitro generation of cRNA with the mMESSAGE mMACHINE T7 Ultra kit (Ambion, Austin, TX, USA). For the CNG-channel assay, 100 pg bPAC mRNA and 20 ng RNA encoding the olfactory CNG-channel variant C460W/E583M[77] (kindly provided by J. W. Karpen, Oregon) were injected into oocytes and incubated for 3 - 5 days at 16-18 °C in Ringer solution (96 mM NaCl, 5 mM KCl, 2 mM $CaCl_2$, 1 mM $MgCl_2$, 5 mM MOPS or 5 mM HEPES (pH 7.5) with streptomycin (1 mg/ml), penicillin (1 mg/ml). For the CFTR assay, we injected 20 pg bPAC RNA and 1 ng CFTR RNA. Current recordings were performed with a GeneClamp 500 (Axon) at sampling rates between 500 Hz and 5 kHz. For recordings under pulsed light conditions, oocytes were excited with 450 nm light of a 75 W Xenon lamp (Osram). The oocyte in the TEVC experiment was protected from intense ambient light so that exposure did not exceed 84 nW/cm^2. Oocytes were monitored with a binocular under orange (> 515 nm) light.

Immunological quantification of $cAMP_i$: cAMP was detected by a competitive immunoassay (Correlate-EIA, Assay Designs, Ann Arbor, MI, USA) as described previously[10]. Cyclase activity of purified recombinant protein was also assessed with this assay by incubation of 10 µg bPAC in 24 µl of a solution of 300 mM KCl, 50 mM Hepes-Tris, pH 7.4, 1 mM $MgCl_2$, 100 µM MgATP at room temperature (21°C). The reaction was stopped with 220 µl 0.1 M HCl.

Spectroscopy: Single wavelength kinetics were recorded in a Cary300bio (Varian, Palo Alto) UV/Vis-spectrometer at 489nm. The protein was excited with a 455 nm LED (1W Royal Blue, Luxeon Star, effective power 0.9 mW mm^{-2}). For recordings of transient absorption spectra a faster setup was used comprising a Shamrock 303i Imaging Spectrograph with an Andor iStar ICCD (Andor

Technology, Belfast). The spectrum of the late photoproduct was recorded 2 s after application of a 500 ms flash of a 455 nm LED (0.9 mW mm^{-2}). The probe light from a short arc xenon-lamp (XBO 75W) was applied by an optical fiber, transferred to a spectrograph and then mapped on the ICCD-chip of the camera. To minimize actinic effects the probe light was choppered with a VS-25 shutter (Uniblitz, San Francisco) to 90ms dark/ 10ms light. Furthermore the intensity was reduced until 10 subsequent dark spectra appeared constantly. The spectra shown in Fig. 3.2.3a are averages of 10 discrete spectra, further smoothed by low-pass filtering the amplitude representation of the Fourier series expansion.

Electrophysiology of hippocampal neurons: Hippocampal slice cultures from Wistar rats were prepared at postnatal day 4–5 as previously described[17], according to Swiss veterinary regulations. Neurons were co-transfected with DNA encoding bPAC, CNG-A2 (C460W/ E583M) and a RFP (tdimer2, a gift from R. Y. Tsien, San Diego) under control of the neuron-specific Synapsin1 promoter using a Helios Gene-Gun (Bio-Rad). Whole-cell patch-clamp recordings were conducted at 30°C in artificial cerebrospinal fluid (ACSF)[78] containing 1 µM tetrodotoxin (TTX), using potassium gluconate intracellular solution. For photo-stimulation of bPAC, a 100W mercury arc lamp was controlled by a mechanical shutter (Uniblitz), attenuated by a series of neutral density filters and an eGFP excitation filter (BP470/40). Light intensity was measured at the back aperture of the objective (LUMPlan 60x 0.9NA) and divided by the field of view (0.1 mm^2).

Generation and analysis of transgenic Drosophila*:* The bPAC cDNA was subcloned into the pUASt fly transformation vector via EcoRI and KpnI restriction sited and transgenic flies were generated by standard procedures (BestGenes Inc., Chino Hills, CA, USA). Flies containing elav-Gal4 and appropriate PAC transgenes were F1 progeny of homozygous parental lines. cAMP was quantified from groups of ten brains dissected in *Drosophila* ringer under red light and 10 min with blue light (455nm, 20 mW mm^{-2}) when appropriate. Immediately afterwards, brains were processed following manufacturer's instructions (Cat.-No 900-066, Assay designs, Ann Harbor, MI, USA).

Grooming assay: For behavioral experiments we used female *Drosophila* aged 3 to 5 days post eclosion in an assay modified after[10]. Illumination regimes contained either dim-red light (> 650 nm, 10 mW mm^{-2}) or intense blue light (455 nm, 40 mW mm^{-2}) to provoke 'freezing behavior' in a light-dependent manner.

Delay times for behavioral changes were determined from videotapes of individual animals.

Statistical analysis: Numerical data are presented as mean ± SEM. Statistical differences were analyzed using Student's t test.

Results

To test the function of the protein encoded by the published bPAC sequence, we cloned bPAC into a cAMP-deficient *E. coli* strain in which lactose and maltose cannot be fermented[79]. On MacConkey agar plates, cAMP-deficient bacteria produce ammonia and form slow growing white colonies (Fig. 3.2.1d). Expression of bPAC rescued their maltose metabolism, as seen from the improved growth and red color of transformed colonies in Fig. 3.2.1d. Differences between light- and dark-grown plates were not detected. We concluded that bPAC is a functional adenylyl cyclase.

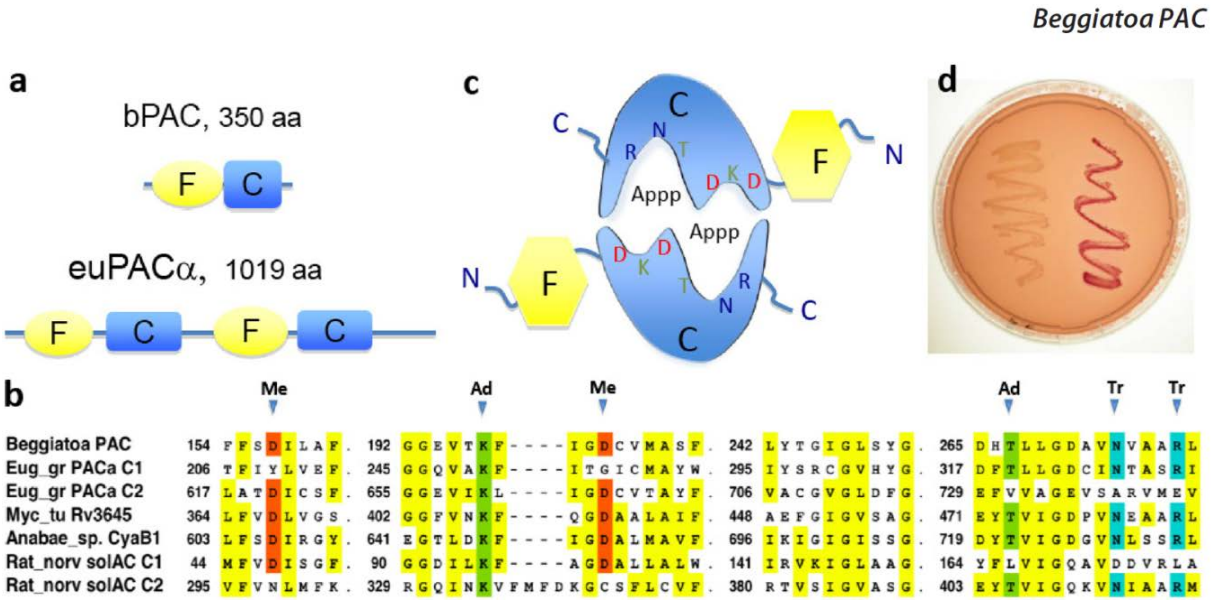

Figure 3.2.1: Concept of light–activated cyclase. (a) Schematic arrangements of the photoreceptive BLUF domain (F) and the catalytic domain (C). (b) Part of the bPAC cyclase amino acid sequence aligned to the corresponding regions of other TypIII cyclases: metal-binding Asps (Me) are underlaid in red, essential adenine binding Lys or Thr in green and transition state-stabilizing Asn and Arg in blue. (c) Model of the dimeric bPAC with flavin binding BLUF domain (F) in yellow and the catalytic domain (C) in blue. (c) Cyclase activity in an adenylate cyclase-deficient *E. coli* strain before (left) and after (right) transformation with bPAC on a MacConkey agar plate. Red color indicates rescue of maltose metabolism due to cAMP production.

To test the light-dependence of the new cyclase in a eukaryotic cell, we have expressed bPAC in *Xenopus* oocytes in conjunction with two cAMP-dependent ion channel systems (Fig. 3.2.2a). First, 100 pg of bPAC-RNA were injected into oocytes in combination with RNA encoding an olfactory cyclic nucleotide-gated cation channel (CNG-channel)[66]. After 3 - 4 days of expression, we measured large light-induced inward currents that peaked ~50 s after the light pulse (Fig. 3.2.2b). Current decay was slow and the resting conductance was reached after ~5 min in the dark. In a second approach, we employed the cystic fibrosis transmembrane conductance regulator (CFTR), an anion channel with indirect cAMP-dependence and higher sensitivity. The cAMP-dependent protein kinase (PKA) phosphorylates CFTR, thus triggering transition to the open state (Fig. 3.2.2a). CTFR currents had slower rise times, peaking ~100 s after the light pulse, but decayed faster compared to the CNG currents (Fig. 3.2.2b). To estimate absolute cAMP levels under light and dark conditions, oocytes expressing bPAC only (2 ng bPAC-RNA) were tested for cAMP using an ELISA assay. After 4 days of expression in the dark, cAMP levels were 3.5 µM, slightly

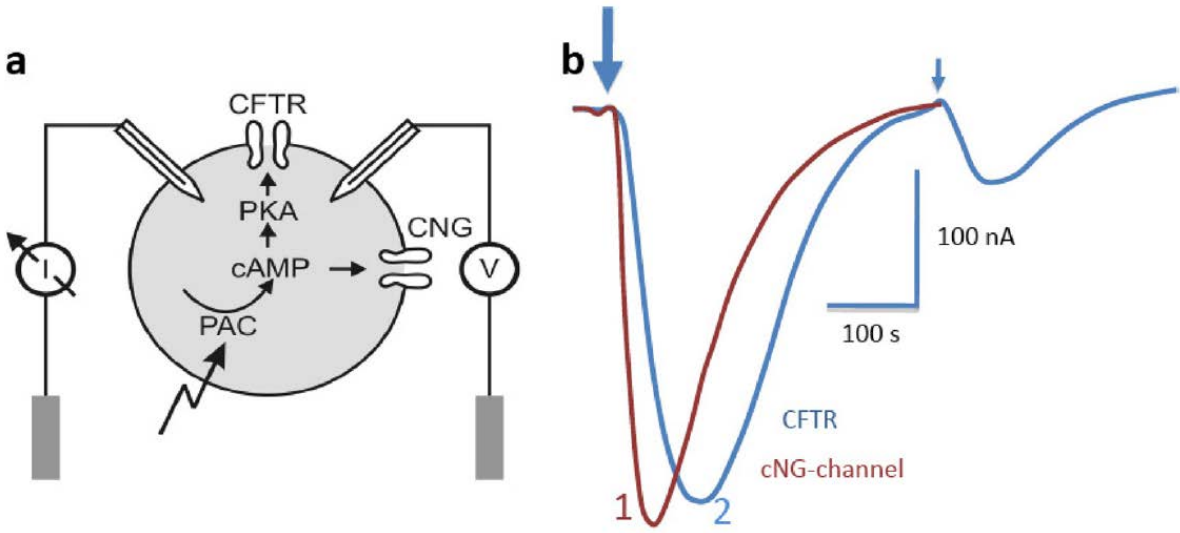

Figure 3.2.2: bPAC activity in Xenopus oocytes. (a) Principle of the electrical assay. CFTR is activated by phosphorylation via an oocyte-endogenous cAMP-dependent protein kinase (PKA) whereas the CNG-channel is directly activated by cAMP binding. (b) Photocurrents evoked by a 500 ms light pulse (450 nm) after coexpression of bPAC and CNG-channel (dark red trace), and currents evoked by an 8 s (large arrow) or 100 ms (small arrow) light pulse after co-injection of bPAC and CFTR (blue trace). Currents were measured at -40 mV for CFTR and CNG channels. In both test systems the current reached values up to about -0.3 µA.

but significantly above the level of control oocytes (2.0 µM). Following a 1 min light pulse, cAMP levels reached values up to 140 µM. Assuming bPAC dark activity was responsible for the 1.5 µM increase above baseline, these values correspond to a ~100 fold increase in cyclase activity after illumination.

To investigate the relation between the bPAC photoreceptor states and enzymatic activity, we expressed bPAC in *E. coli* and purified it via affinity chromatography. The absorption spectrum of the purified bPAC showed the

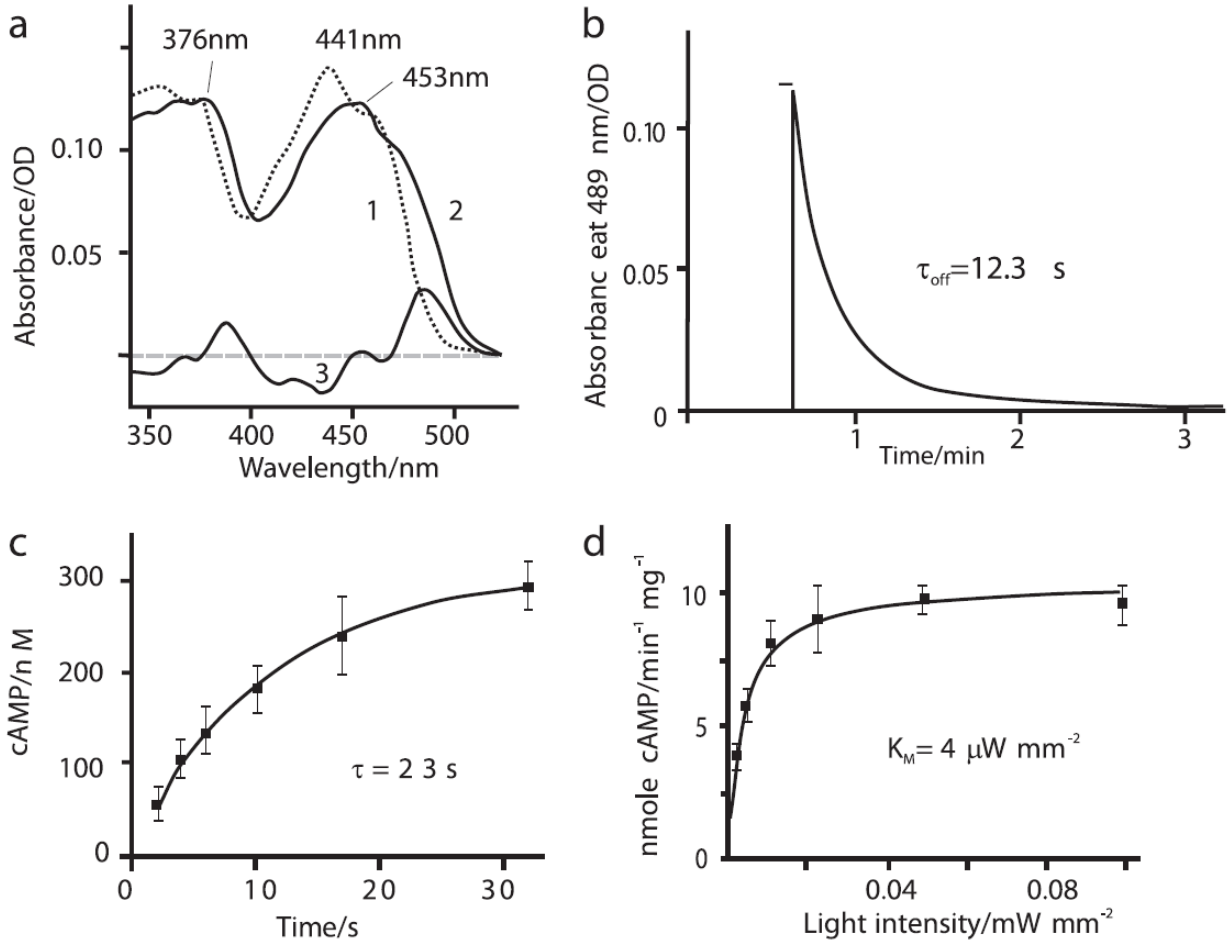

Figure 3.2.3: Spectral properties. (a) Absorption spectra of purified bPAC in its dark-adapted (trace 1) and light adapted (trace 2) state. The difference between the two is shown as line (trace 3). (b) Decay of the red-shifted intermediate that is considered as the signaling state. The fit is seen as a white line. The protein was excited for 3 s with a 455 nm LED and the absorbance change was recorded at 489 nm. (c) cAMP concentration at different time delays in the dark after a 4 s 475 nm light pulse; 300 mM KCl, 50 mM Tris-Hepes, pH 7.5, 21°C, n = 3 with double determinations for each cAMP value. (d) Light (475 nm) intensity dependence of cAMP production by purified bPAC, conditions as in C, illumination for 60 seconds and immediate quenching with 9 fold volume of 0.1 M HCl. n = 2 with double determinations for each cAMP value. Plotted are mean values with S.D. and a Michaelis-Menten fit curve, yielding a K_M of 3.7 ± 0.4 µW mm^{-2}.

typical BLUF-fine structure with a maximum at 441 nm[80] (Fig. 3.2.3a). Upon irradiation, the absorption band became less structured and was shifted by 12 nm to longer wavelengths, in accordance to the photochemical properties of other BLUF photoreceptors. The recovery of the dark state (Fig. 3.2.3b) was relatively fast with a τ_{off} = 12 s at pH 7.5 in phosphate buffer at room temperature. Next, we measured the timing of cyclase activity *in vitro*. After a light flash of 4 s, cAMP continued to rise in the dark with a time constant τ = 23 ± 2 s at pH 7.4 (Fig. 3.2.3c), which is in fair agreement with the decay of the BLUF-signaling state.

A parameter of great practical importance is the light-intensity dependence of bPAC's enzymatic activity. We measured cAMP concentrations in test tubes with purified bPAC protein after illumination for one minute with blue light of variable intensity and obtained a Michaelis-Menten-type saturation curve (475 nm, Fig. 3.2.3d) with a half saturation constant of 3.7 ± 0.4 µW mm^{-2}. This low value is consistent with a photocycle in the range of 10 seconds and demonstrates the very high sensitivity of bPAC to light. Dark activity of bPAC was 33 ± 5 pmole cAMP per min and mg protein. For the maximal activity in the light, we obtained a value of 10 ± 2 nmole cAMP per min and mg protein (Fig. 3.2.3d), corresponding to a 300-fold increase in enzymatic activity. This large dynamic range combined with its high sensitivity to light made bPAC a promising tool to modulate brain function.

To test its applicability to neurons, we have expressed bPAC in CA1 pyramidal cells in conjunction with CNG channels and dimeric red fluorescent protein (tdimer2). Red fluorescent labeling of PAC-transfected cells is advantageous since the wavelength for RFP excitation (~540 nm) is well beyond the BLUF absorption, which makes it easy to select cells for electrophysiological recordings without activating bPAC. Ten days after transfection, neurons were viable and had a normal appearance (Fig. 3.2.4a). Dim light pulses of 100 ms duration (470 nm, 0.12 mW mm^{-2}) evoked large inward currents (Fig. 3.2.4b), indicating rapid cAMP production in the transfected neurons. As expected, extension of pulse duration induced stronger and longer lasting CNG currents (Fig. 3.2.4c). At high light intensities (100 mW mm^{-2}), CNG currents rapidly saturated, but were still fully reversible (gray curves in Fig. 3.2.4c). In control experiments with non-transfected neurons, identical illumination did not evoke any currents. At all

tested light doses, CNG currents peaked rapidly (< 3 s) and were highly reproducible, indicating precise control of intracellular cAMP concentration ($cAMP_i$) by light. Pharmacological stimulation of endogenous AC with 100 µM forskolin and simultaneous inhibition of phosphodiesterases with 100 µM IBMX also activated CNG currents, but with a much slower time course (3-4 min rise time, Fig. 3.2.4d). Interestingly, even though combined forskolin/IBMX application is considered a very strong stimulation leading to 'chemical LTP'[81], forskolin/IBMX application did not fully occlude light-induced CNG currents, suggesting that bPAC outperformed the pharmacological cocktail.

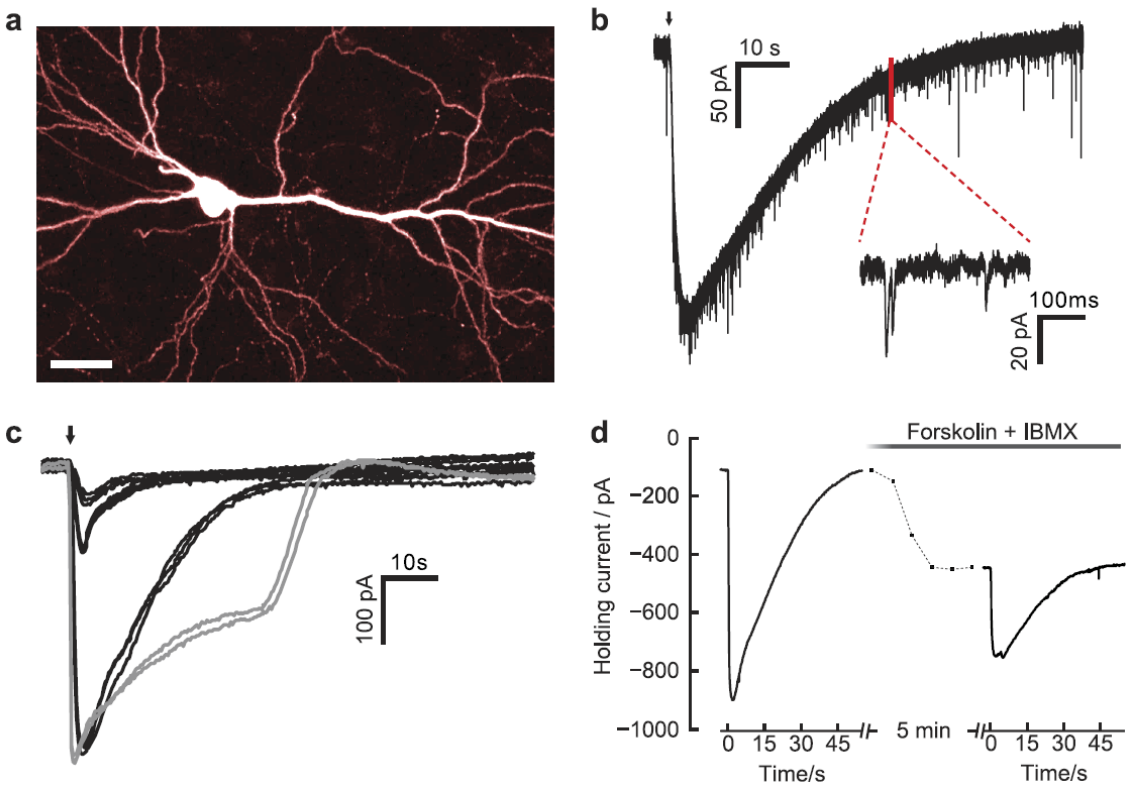

Figure 3.2.4: Assessing bPAC function in hippocampal neurons. (a) CA1 pyramidal cell expressing bPAC, CNG-A2, and RFP (Two-photon imaging at 980 nm, scale bar: 30 µm). (b) Light-evoked cAMP-gated current at 0.14 mW/mm (2). Arrow: 100 ms light pulse. Enlarged insert shows miniature EPSCs. (c) Light-evoked cAMP-gated currents in one pyramidal cell at 4 different light doses (black traces: 0.14 mW/mm^2 for 50, 100, 1000 ms; gray traces: 109 mW/mm^2 for 1 s). Traces were low pass filtered at 10 Hz to remove miniature EPSCs. At all stimulation intensities, currents were fully reversible and highly reproducible. CNG currents saturated at 0.14 $mW*s/mm^2$. (d) Light-evoked cAMP-gated currents before and after forskolin (100 µM) + IBMX (100 µM) wash-in. During forskolin/IBMX wash-in (dashed line, 5 min), holding current increased from -108 pA to -446 pA. Forskolin/IBMX application only partially occluded light-induced currents.

To directly compare the activities of bPAC and euPACα, we performed a second set of experiments on hippocampal neurons by co-transfection with euPACα, CNG and RFP, using the same amounts of DNA than in bPAC experiments. In response to light pulses of saturating intensity, both PACs were able to induce large photocurrents (up to 1 nA), sufficient to induce action potential firing in many neurons under current clamp conditions. bPAC-induced currents peaked later than those of euPAC (bPAC: ½ peak after 723 ms ± 101 ms; euPACα: ½ peak after 227 ms ± 40 ms) and were much longer lasting (bPAC: τ_{decay} 19.0 s ± 2.8 s; Fig. 3.2.5a and b, euPACα: τ_{decay} = 2.7 s ± 0.1 s), confirming the slow

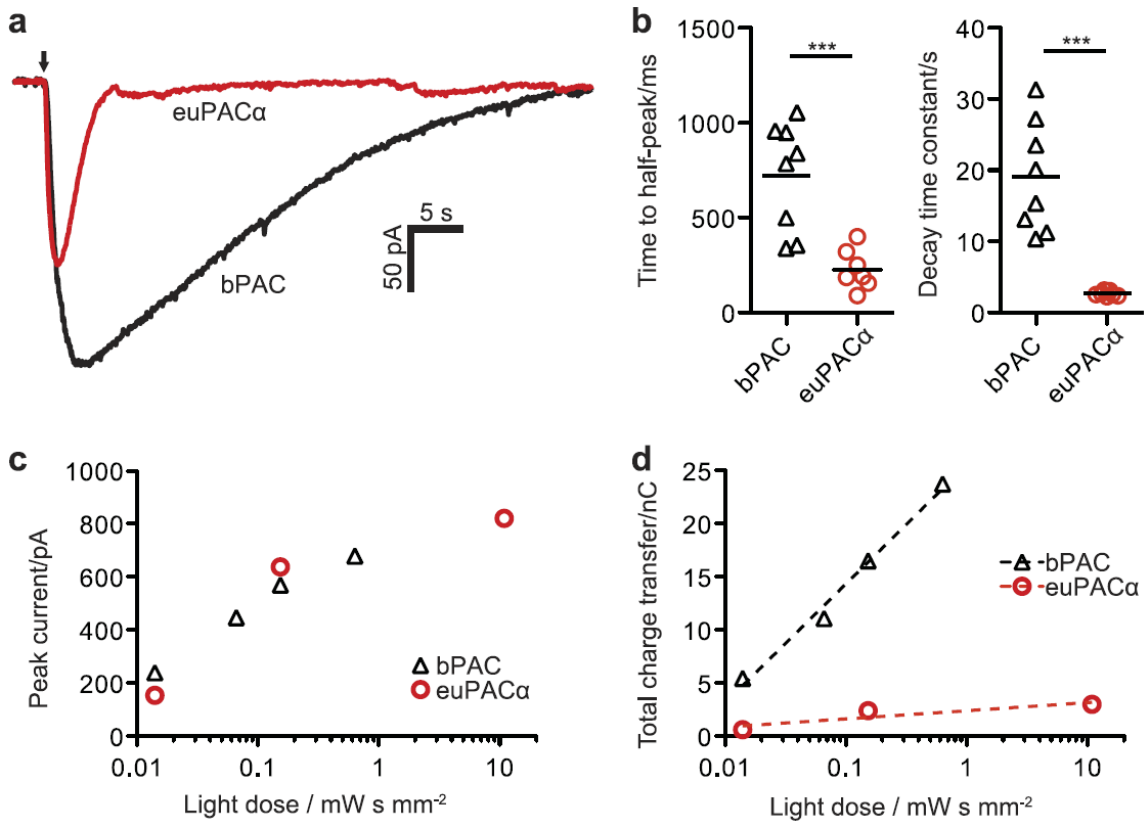

Figure 3.2.5: Comparing bPAC and euPACα-induced currents in neurons. (*a*) Following a 100 ms light pulse (140 µW mm^{-2}, blue arrow), cAMP elevation was much longer lasting in CA1 pyramidal cells expressing bPAC, CNG-A2, and RFP (black trace) compared to cells expressing euPACα, CNG-A2, and RFP (red trace). Traces were low-pass filtered to remove miniature EPSCs. (*b*) Time to half-peak current and current decay time constant were significantly longer in bPAC- compared to euPACα-expressing neurons (bPAC: n = 8 conditions (3 light doses, 5 cells); euPAC: n = 7 conditions (4 light doses, 3 cells); ***, $p < 0.001$). (*c*) Under sub-saturating conditions, light-dose dependence of peak currents was similar for bPAC- and euPACα-expressing neurons. (*d*) Total charge transfer (integrated current) was ~8 times higher in bPAC- compared to euPACα-expressing neurons.

inactivation of bPAC. As a consequence, at light intensities that kept cAMP below CNG current saturation, peak currents were similar for both PACs (Fig. 3.2.5c), but in bPAC transfected cells the integrated current (total charge transfer) was significantly larger (Fig. 3.2.5d). *Vice versa*, to produce comparable amounts of cAMP in euPACα-expressing neurons, light dose had to be increased by at least three orders of magnitude. Since bPAC is able to produce large cAMP elevations in response to dim blue light pulses it will be eligible for studies cAMP-mediated processes in cells deep below the surface of the brain. The previously described euPACα, on the other hand, might be advantageous for experiments in which sub-second temporal control is necessary and light dose is not a limiting factor.

Applicability of bPAC was also tested in *Drosophila*. We targeted expression of bPAC to the *Drosophila* central nervous system (CNS) using euPAC as control.

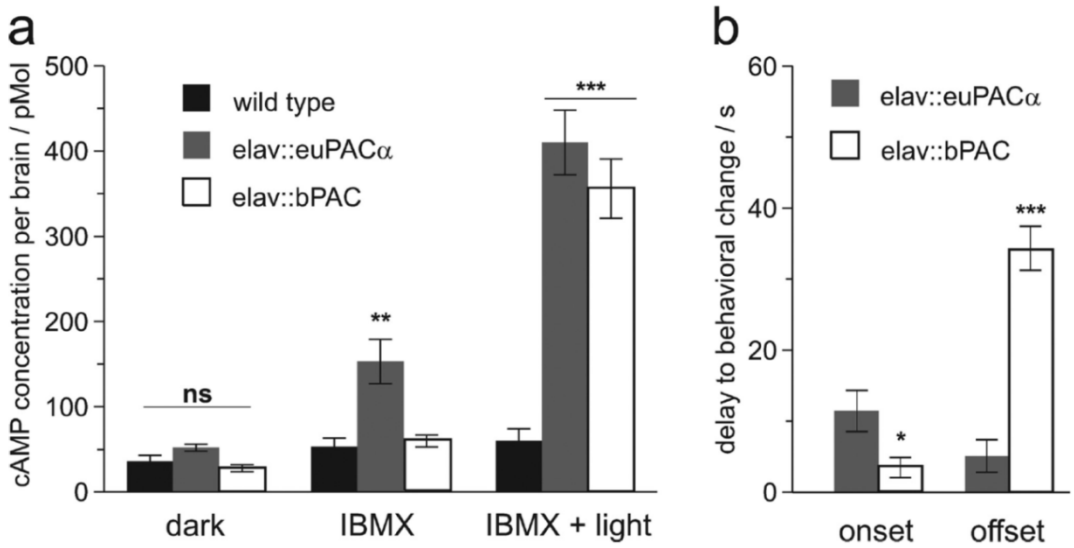

Figure 3.2.6: Transgenic bPAC and euPACα exhibit different levels of dark-activity and affect grooming behavior in freely moving *Drosophila*. (*a*) Expression of euPACα transgenes (elav::euPACα) resulted in distinctive dark activity, which was revealed by the phosphodiesterase blocker IBMX. Dark activity was not observed upon bPAC expression (elav::bPAC) or in wild type Canton-S control animals. Photoactivation of either PAC transgene resulted in a 10-fold increase in cAMP with no statistical difference between final concentrations of cAMP derived from either euPACα or bPAC (n = 11 per group). 100 µM IBMX was used to block phosphodiesterase activity; light activation of cyclase transgenes was performed in 100 µM IBMX and irradiation (5 min, 455 nm, 40 mW mm^{-2}). (b) Photoactivation of pan-neuronally expressed PAC transgenes affects grooming activity resulting in stereotypic 'freezing behavior' (7). bPAC expressing flies freeze significantly faster in blue light than euPACα flies (n = 11 per group). They also take significantly longer to resume grooming behavior in the dark. Data represent means ± SEM; *, $p < 0.05$; **, $p < 0.01$; ***, $p < 0.001$; ns, not significant.

We used the neuron-specific elav-Gal4 driver and quantified cAMP levels in dissected brains (Fig. 3.2.6a). Basal cAMP dark levels did not significantly differ between genotypes ($p > 0.05$). Addition 100 mM IBMX increased dark levels of cAMP in euPAC-expressing *Drosophila* but had no effect on bPAC transgenes, indicating significant dark activity of euPAC, but not bPAC ($p < 0.01$, further details in MM and figure legends). After photo-activation, both transgenes showed strongly increased levels of brain cAMP ($p < 0.001$).

In a small animal like *Drosophila*, photoactivation of PAC transgenes can be achieved through the cuticle of live animals. As previously described, grooming activity stops when cAMP is elevated throughout the CNS[10]. Here we used this effect to compare *in vivo* applicability of bPAC and euPACα, focusing on the delay of behavioral changes after short illumination. Compared to euPAC transgenes, bPAC-expressing flies exhibited a significantly faster response onset ($p < 0.05$). After light-off, it took on average 34 s until bPAC flies resumed grooming, confirming bPAC's more powerful and prolonged cyclase activity ($p < 0.01$, Fig. 3.2.6b).

Discussion

With the experiments described above we introduce an adenylyl cyclase with properties that are for application superior in most respects over the previously described PACα of *Euglena gracilis*. We demonstrate that bPAC is functional in bacteria, fruit flies, frog oocytes and rodent neurons, and can be purified from *E. coli* for biophysical studies. The advantages of bPAC over euPACα are the following: (i) bPAC DNA is only about one third the size of euPACα and it is more conveniently handled in host vector systems, especially if viral vectors with limited maximal packing volume are used. (ii) Owing to the fact that only one photoreceptor domain is present modification of the photoreceptor kinetics[82] and the enzymatic active state lifetime will be more straightforward. (iii) It is likely that bPAC is active as a homodimer, like most prokaryotic type III cyclases, resulting in a three or six times smaller complex than the tetrameric euPAC. (iv) Light stimulation of the purified euPAC complex resulted in an 80 fold cyclase activity[9] whereas we determined a 300 fold increase in activity for bPAC. (v) Due to the long life time of the active state, the half saturating light intensity is low and bPAC

needs ~1000 times less light than euPACα to generate comparable steady state levels of cAMP in neurons.

The temporal precision of cAMP control by light is limited by the inactivation time of PAC, but also by the activity of endogenous cyclic nucleotide phosphodiesterases (PDE). The correlation between the life time of the BLUF signaling state and activity of the cyclase tells us that the cyclase is not only activated by the BLUF domain but also inactivated by its transition back to the dark state. Moreover the high PDA activity in hippocampal neurons, achieves a tight correlation between the BLUF signaling state and the cAMP level (19 s, Fig. 3.2.5b). In oocytes, this correlation is lost due to low PDE activity and long diffusion pathways (Fig. 3.2.2b). Thus, neurons are ideal candidates for light-control of cAMP signaling with high temporal accuracy. These kinetic comparisons have never been done for any euPAC because no recombinant full length euPAC could be purified in an active and soluble state.

An important issue for application of light-activated enzymes is the difference in activity in light and darkness (dynamic range). Dark activity may pose an experimental problem since it changes the properties of transfected cells or tissues even during PAC expression before the actual experiment is started. The absence of any measurable dark conductance has been a great advantage of the channelrhodopsins. In contrast, most light-activated enzymes with a flavin-based BLUF- or LOV-type photoreceptor domain show significant dark activity and their light activation is less than 10-fold[83,84]. This is also true for proteins with engineered photoreceptor function as the light activated Rac (10-fold)[85] or the light modulated DNA-binding protein the Moffat group has recently designed (5.6 ± 2.5 fold)[86]. An exceptional case is the designed light activated kinase YF1, the activity of which is high in the dark and suppressed 1000-fold in the light[87]. However, due to the microbial target this kinase can hardly be employed in animals and, second, in most experiments activation of the enzyme and not inactivation is preferred. This large dynamic range of bPAC with 300 fold light-activation suggests that any potential problem associated with dark activity could be remedied simply by using a weaker promoter to drive bPAC expression. Thus, careful analysis of intracellular cAMP levels is mandatory in any experimental application of PAC transgenes and various analytical techniques are available,

e.g. immunodetection by ELISA, electrophysiological quantification or use of FRET-based imaging techniques[10,88,89].

Across many species, the cAMP system in neurons has been shown to be crucial for learning and memory[90]. Classical examples are the *Drosophila* learning mutants dunce and rutabaga that affect cAMP metabolism in opposite directions. From presynaptic short-term plasticity to cAMP-inducible gene expression and long-term plasticity, synapses transiently or persistently change their transmission characteristics in response to elevated $cAMP_i$[91,92]. To manipulate $cAMP_i$ in neurons, most studies have used mutant animals or pharmacological agents (e.g. forskolin), methods that lack the precise temporal resolution, single-cell specificity and quantitative control that can be readily achieved with light-activated PAC [10,93]. As an application example, optical control of $cAMP_i$ will allow to dissect which forms of synaptic plasticity are triggered by pre- or postsynaptic signals, a distinction that has been notoriously difficult to make in the past. Furthermore, the sharp drop of bPAC's absorption spectrum at 500 nm might allow to combine it with red-shifted variants of ChR2 [94] for independent optical control of $cAMP_i$ and the membrane voltage E_m. This combination could be useful to probe second messenger systems within individual cells, or to activate two populations of neurons by blue and green light, respectively. In summary, we show that the PAC from *Beggiatoa* is well tolerated by neurons and allows for rapid and reproducible control of $cAMP_i$ using very moderate levels of blue light.

- End of published manuscript -

4. Acute effects of bPAC stimulation in hippocampal neurons

Characterization of bPAC in the previous chapter was performed in neurons co-expressing PAC together with a CNG-A2 channel. bPAC-mediated activation of co-expressed CNG-A2 channels (resulting in significant cation conductances) likely overshadowed endogenous effects of cAMP elevation. Therefore, to investigate effects of bPAC activation on endogenous targets, I expressed bPAC together with the fluorescent protein tdimer2 alone. Transfection was achieved either by biolistics, single cell electroporation, or by local AAV-transduction with a viral construct containing bPAC and tdimer2-FP conjoined with a 2A ribosome skip sequence[95] (see chapter 7.5).

A typical recording of a CA1 pyramidal cell expressing bPAC only is shown in Fig. 4.1. In this case, a biolistic transfection was done with bPAC together with tdimer2, and a blue light stimulus was applied. Two immediate effects of bPAC activation are apparent: a slow-onset inward current during blue light illumination, which was reversible after light-off, and an increase in the frequency of endogenous activity (EPSCs) during illumination. Both observations were further investigated (chapter 4.1 and 4.2) and discussed hereafter (chapter 4.3).

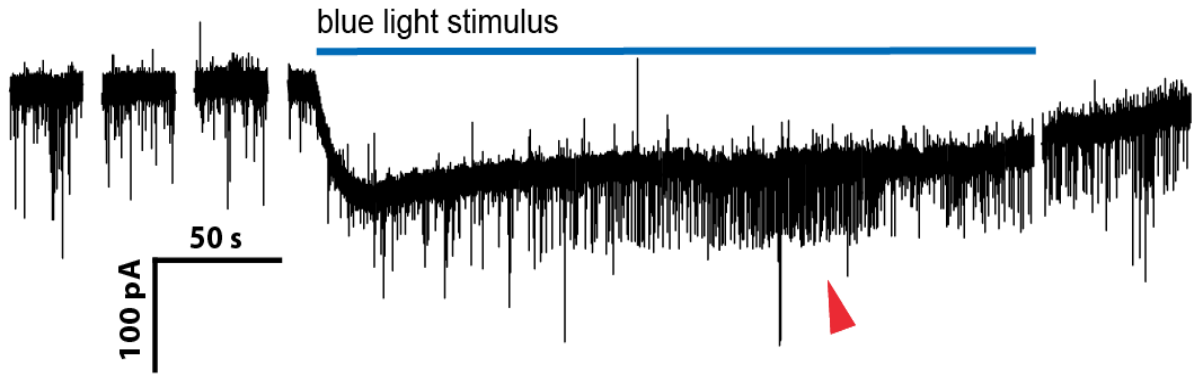

Figure 4.1: bPAC activation in CA1 pyramidal cells results in inward currents and increase in EPSC frequency. In this early example, a significant decrease in holding current occurred during the blue light (blue bar). There was also a delayed increase in EPSC frequency (red arrow). Whole-cell mode, voltage-clamp at -65 mV.

4.1. bPAC activation led to slow inward currents, mainly mediated by I_h

To further investigate the bPAC-induced inward currents, I recorded CA1 pyramidal neurons while illuminating bPAC continuously through the objective. (Fig. 4.1.1). Based on our previous experiments (Fig. 2.3.5), we assume that bPAC was fully activated during light stimulation. The amplitude of the steady-state inward current was measured from filtered traces (low-pass filtered, Bessel) 90 s after onset of light illumination. In these experiments, spiking activity was blocked in the whole organotypic culture (bath applied 1 µM TTX). The onset of the inward current was in the ms range (Fig.4.1.1c), but the time to peak/2 ranged from 5 s to more than 30 s (Fig.4.1.1b). After light off, inward currents went back to baseline within tens of seconds (Fig. 4.1.1a), reflecting degradation of cAMP. Accompanying the inward current was a reduction in membrane resistance (R_{mem}), indicating that the inward current was due to opening of channels in the membrane. (Fig. 4.1.1d). Next, I investigated the nature of bPAC-mediated inward currents. To determine the reversal potential of the inward current, I performed voltage-step protocols in the dark and during steady-state

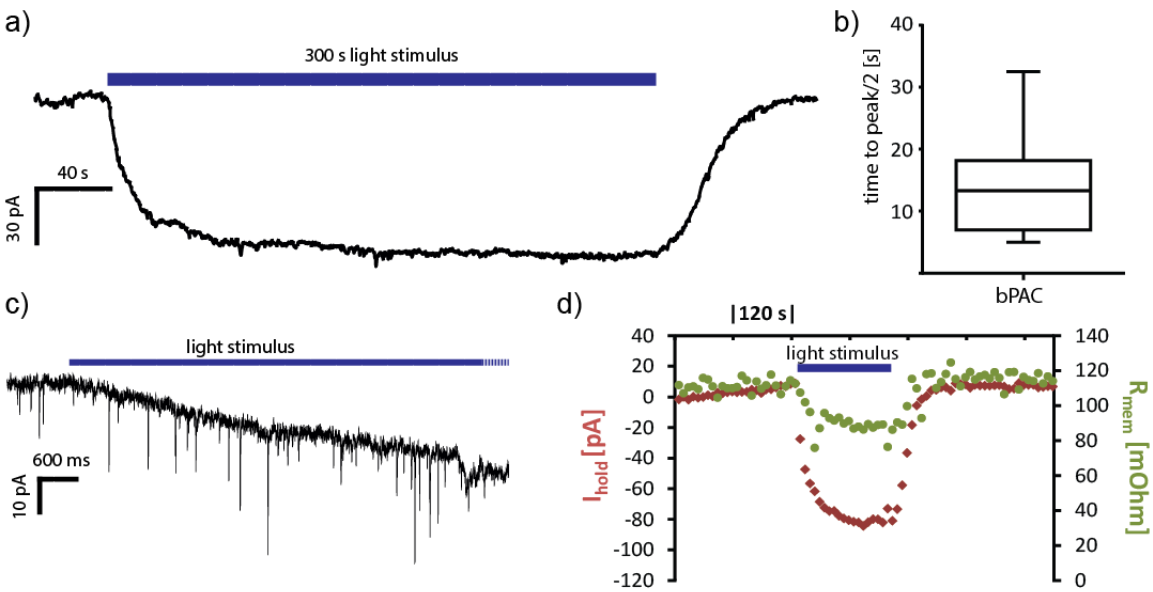

Figure 4.1.1: bPAC-induced inward currents are slow, reversible, and accompanied by a decrease in R_{mem}. (a) Example trace of a low-pass filtered bPAC-induced I_{inward}. 300 s300s light stimulus (~ 1 mW / /mm^2) (b) Time to half-peak for bPAC-induced I_{inward} was 13.8 ± 8.0 s (mean ± SD, n=14). (c) Example showing onset of a bPAC-induced inward current without additional filtering. (d) Example showing the bPAC-induced I_{inward} coincident with reduction in $R_{mem.}$ bPAC stimulation led to about 20% reduction in R_{mem}.

bPAC activation (Fig. 4.1.2.a). Subtracting the current response of one condition from the other led to a series of values for the I-V relationship, which was fit with a polynomial equation to find the zero crossing. The determined reversal potential was approximately -47 mV. There are several potential mechanisms for the bPAC-mediated inward current, as cAMP has a variety of downstream targets. Several pharmacological compounds are available to probe cAMP signaling. The major canonical target for cAMP is protein kinase A (PKA), which in turn phosphorylates (among other targets) different ion channels[96], a putative mechanism for the cAMP-mediated inward current. I inhibited PKA with H89, a competitive inhibitor of the PKA catalytic subunit. H89 reduced the current somewhat, but not significantly. CNG channels are endogenously present in pyramidal neurons[42], and they could be partially responsible for the cAMP-mediated inward currents. Yet, blocking CNG channels with L-*cis*-diltiazem (1 mM in the intracellular solution) had no discernible effects. Another candidate mechanism was cAMP modulation of I_h-currents, which are mediated by hyperpolarization activated cyclic nucleotide gated channels (HCN-Channels). These channels are expressed in CA1 pyramidal neurons and have been shown to play a physiological role in the hippocampus[97–99]. When I blocked HCN-Channels with ZD7288 (20 µM), a selective inhibitor[100], bPAC-mediated inward currents were significantly reduced (Fig. 4.1.2 b). To further specify which fraction of the steady state inward current was attributable to modulation of HCN channels, I did several wash-in experiments, which showed that blocking HCN channels reduces the inward current by ca. 40% (Fig. 4.1.2c and d). The other 60% of the cAMP-induced inward current could not be accounted for in this set of experiments. The reversal potential of an isolated I_h-current is given in the literature at typically -30 mV[44]. The reversal potential I measured was at a more hyperpolarized value (-47 mV). The current-voltage curve was determined by measuring holding currents in voltage clamp mode at different membrane potentials (-100 to +40 mV in 20 mV steps), both in the dark and during bPAC activation with blue light, and subtracting dark currents from light currents (Fig. 4.1.2 a). Thus, the cAMP-induced inward current is most probably composed of several components downstream of cAMP. I will discuss the mechanisms of HCN modulation resulting in inward currents in chapter 4.3. Also, I will elaborate on other downstream targets of cAMP that could contribute to the slow inward

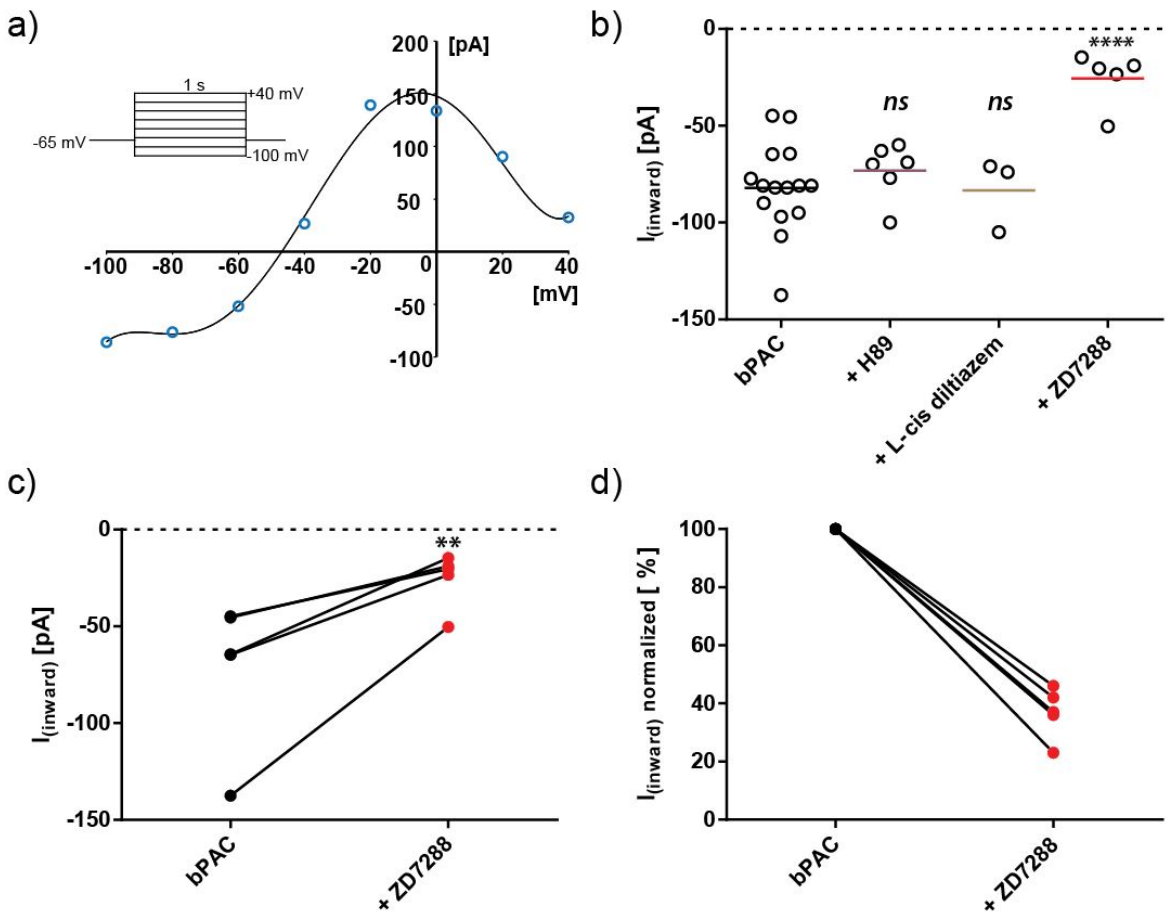

Figure 4.1.2: bPAC-induced inward currents are predominantly caused by cAMP modulation of I_h. (a) Current-voltage (I-V) relationship of bPAC mediated inward current. Reversal potential was determined to be -47 mV.(b) bPAC-induced inward currents, measured at steady state (90 s after light on). Inward currents had an amplitude of -82.0 ± 23.1 pA, n = 15, mean ± SD. H89 and L-cis diltiazem in the bath did not significantly influence the amplitude, but ZD7288 did (H89: -73.2 ± 14.4 pA, n = =6 , ns; LcD: -83.3 ± 18.8 pA, n = =3, ns; ZD: -25.6 ± 14.17 pA, n = 5, p < 0.0001. All: mean ± SD, 1way ANOVA with Dunnett's multiple comparisons test). (c) Wash-in experiments with ZD7288 showed a consistent reduction of I_{inward} in all cases (p < 0.01, ratio paired t-test). (d) I_{inward} was reduced to 63 ± 8.7 % of baseline value in ZD wash-in experiments (mean ± SD).)

currents, potentially accounting for the residual 60% of light-induced current after block of HCN channels.

4.2. Miniature EPSC frequency increased during bPAC activation

Miniature excitatory postsynaptic currents (mEPSCs) are small synaptic currents occurring independently of action potentials. They are primarily mediated by single synaptic vesicle fusion events, therefore representing the postsynaptic

response to a single quantum of neurotransmitter. I looked at excitatory mEPSCs, currents which are mainly mediated by AMPA receptors. To isolate AMPA receptor-mediated mEPSCs , tetrodotoxin (1 µM) to prevent action potentials, bicuculline (10µM) to block fast inhibitory currents, and CPPene (10 µM) to block NMDA receptors were always included in the bath solution. Also, I chose an intracellular solution based on cesium gluconate to block potassium channels. To measure mEPSCs, the cell was held in voltage clamp at -65 mV, and series resistance was rigorously controlled for, as mEPSCs measurements are sensitive to changes in R_s. Usually, mEPSC measurements are done in a certain time window after breaking the membrane seal. In this case, I had to do it a different way, as I wanted to measure mEPSCs in two conditions (with bPAC active and inactive). I first recorded a baseline of ~ 5 min before activating bPAC for a period of time (usually 5 minutes). After light off, I recorded for another 10 min or more. These recordings were than analyzed using ClampFit software (Molecular Devices) and the inbuilt Template Fit function, which allowed for automatic detection of mEPSCs and thereby unbiased relative quantification of frequency and amplitude. The amplitude and timestamp of each detected event was logged by ClampFit, and subsequent analysis in Excel was done to find the frequency and average amplitude of the respective experimental segment (Baseline: 5 min after break-in until light on, bPAC: whole 5 min of light on, Post bPAC: 5 min after light off. I found that the baseline mEPSC frequency and amplitude varied strongly between different measurements in individual CA1 pyramidal cells. During bPAC illumination, mEPSC frequency but not amplitude increased consistently (Fig. 4.2.1). After light off, mEPSC frequency regressed towards baseline in all cases but one. In this dataset, data from different experiments were pooled, with different transfection techniques (2 different viruses, pAAV-Syn-bPAC-2A-tdimer2 and pAAV-CamKII-bPAC$_{S27A}$-2A-tdimer2; gene-gun transfection with bPAC and tdimer2) and different ages. The frequency distribution in figure 4.2.1c shows a bimodal distribution with a group of 4 cells with a high relative mEPSC frequency increase during light (> 200 %). Interestingly, 3 out of 4 of these strongly responding cells were recorded in relatively young cultures (DIV 8). A change in mEPSC frequency, but not in amplitude, is traditionally interpreted as a presynaptic effect. As cAMP levels were only raised postsynaptically in this experiment, it is not obvious how this

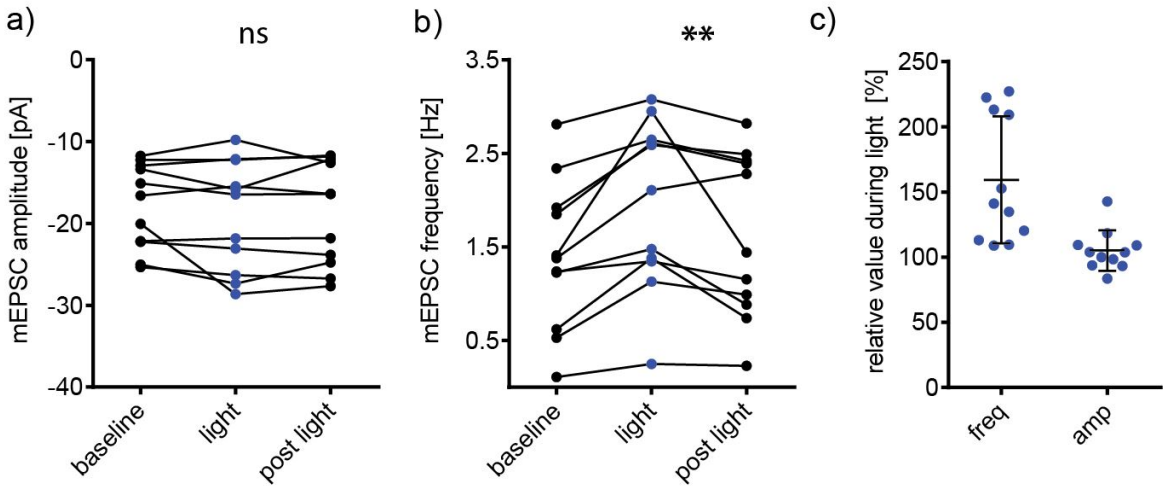

Figure 4.2.1: bPAC activation induces an increase in mEPSC frequency but not amplitude. (a) mEPSC amplitude did not change during stimulation of bPAC by blue light (blue dots), or after. n = 11 neurons, ns (b) mEPSC frequency was consistently increased during stimulation of bPAC. n = 11 cells, **. (c) Relative frequency and amplitude compared to baseline (= 100 %) for each data point. Frequency, 159 ± 49 % SD during light, amplitude, 109 ± 21 % SD.. Statistics for (a) and (b): 1way ANOVA followed by Dunnett's multiple comparisons test.

effect on mEPSC frequency can be explained. I will discuss this in the following chapter 4.3.

4.3. Discussion – acute effects of bPAC activation

bPAC-induced inward currents

The strong endogenous inward currents induced by bPAC stimulation was not expected when starting the experiments. There is little to be found in the literature about cAMP-induced inward currents in neurons, but there are some reports from more than two decades ago about a similar phenomenon in heart cells[101,102]. The pharmacological experiments lead to the conclusion that the bPAC-mediated slow inward current I observed in pyramidal cells consists of multiple components. HCN channels play a large role, which is consistent with the two mentioned reports from heart cells, where HCN conductances play an important role. Furthermore, the inward current is accompanied by a decrease in membrane resistance, which indicates the opening of conductances (such as

HCN channels, which are non-specific cation channels) as opposed to closing of channels or modulation of ion pumps.

HCN channels are known to be expressed in the hippocampus, and they can regulate neuronal excitability[103]. They are modulated by cAMP by direct binding of the molecule, causing a shift in the activation properties towards more depolarized potentials. At a certain potential below their activation threshold (in our case at -65 mV, where our cells are voltage-clamped at), HCN channels are more conductive when they bind cAMP.

Which other mechanisms contribute to the bPAC-mediated inward currents? Inhibition of PKA with H-89 did not significantly decrease the currents. There was also no obvious contribution of endogenous CNG channels revealed by LcD application. However, given the limited cell permeability (intracellular binding site) and high price of LcD, I could perform only a small number of experiments, and the results should be interpreted with caution. Besides these obvious candidates, there is the possibility of PKA-mediated phosphorylation and thus activation of a large number of endogenous channels. As we were most interested in potential effects of cAMP on synaptic plasticity, I decided not to investigate the molecular components of the inward current in further detail. During induction of synaptic plasticity (see chapter 5), the slow inward current proved to be very useful as a positive control for bPAC activation.

bPAC-induced increase in mEPSC frequency

I have shown that during bPAC activation in postsynaptic CA1 cells, the frequency of mEPSCs increase, and regress to baseline afterwards, while the average mEPSC amplitude does not change. mEPSCs are single vesicular fusion events, and an increase in the frequency but not amplitude is usually attributed to changes in presynaptic properties, e.g. an increased number of docked vesicles. This interpretation is based on the assumption that changes in postsynaptic strength, e.g. neurotransmitter receptor density, would result in an increased amplitude of a given vesicle fusion event. With regard to this classical interpretation of mEPSC frequency change, our data suggest a presynaptic effect of postsynaptically elevated cAMP levels by bPAC. This raises the question about the mechanism of retrograde signaling. As the mEPSC frequency increase

is transient, the presynaptic change would have to be transient as well. Possible retrograde messengers exist, such as the endocannabinoid system (ECS) and BDNF signaling. However, the ECS is known to suppress neurotransmitter release, and not increase it[104]. BDNF is known to increase mEPSC frequency and release probability in hippocampal neurons[105,106], but a cAMP-dependent mechanism of postsynaptic BDNF release has not been described. This is certainly a possibility worth investigating in the future.

An alternative explanation for the observed phenomenon would be that cAMP-induced changes in dendritic membrane properties were responsible for the observed increase in mEPSC frequency. In this case, the cause for the mEPSC increase would be a postsynaptic change, i.e. more mEPSCs generated at distal synapses coming out of the noise because of better propagation to the soma. As I measured a *drop* in input resistance during the light-induced inward current, mEPSC propagation should be worse and cannot account for the observed *increase* in frequency. However, there are a number additional caveats in interpreting mEPSC data from these very large neurons. mEPSC frequency was highly variable between experiments, and even within one experiment there were periods of mEPSC ‘burst’ like events which strongly skewed frequency measurements. Furthermore, it is not even clear whether spontaneous vesicle fusion happens within the active zone or rather outside the synapse. Due to these considerations, I decided to use stimulation-evoked synaptic transmission rather than mEPSCs to further characterize synaptic effects of bPAC.

5. bPAC modulation of synaptic long-term plasticity

Having shown that bPAC activation induces cAMP production in hippocampal pyramidal neurons, and that bPAC activation has acute effects on CA1 pyramidal neurons (inward currents, and modulation of mEPSC frequency), I performed experiments to assess whether synaptic strength can be manipulated by activating cAMP signaling cascades in hippocampal pyramidal cells. In the experiments for this thesis, I focused exclusively on manipulating cAMP signaling in the postsynaptic CA1 pyramidal neurons of the Schaffer collaterals.

Presynaptic cAMP signaling has already been shown to play a pivotal role for synaptic plasticity, for example in the amygdala[37]. In the hippocampus, mossy fiber LTP has been shown to be independent of NMDA receptors and to be mediated predominantly by presynaptic mechanisms as well[33,38,107–110]. For mossy fiber LTP, many studies point to a presynaptic locus and cAMP involvement of LTP; in the Schaffer collateral CA3-CA1 synapse, the picture is less clear. When LTP at the CA3-CA1 synapse is analyzed, two phases can be distinguished, an early phase (E-LTP) which lasts for 1-2 h, and a late phase (L-LTP) which can be probed several hours after induction[33]. E-LTP and L-LTP have different time courses, induction requirements, and involve different signaling mechanisms. For LTP at the CA3-CA1 synapse, it is thought that cAMP signaling is important mainly for L-LTP[33,111–113]. Forskolin, a drug which activates endogenous adenylyl cyclases, has been used to induce LTP simultaneously at all synapses, a strategy known as chemical LTP (cLTP)[81]. cLTP can also be induced with other cAMP elevating drugs, for example Sp-cAMPS, a cell membrane permeable cAMP analog[111,112,114]. A forskolin-induced NMDAR-independent early phase of synaptic potentiation in active synapses has also been described[81]. The locus of this early phase of forskolin-induced LTP is not defined, as bath application of forskolin acts on both pre- and postsynaptic sites. To my knowledge, there are no published studies addressing the question whether cAMP signaling in postsynaptic pyramidal neurons has modulates the induction of synaptic plasticity. To exploit the specificity of bPAC, I decided to address this question by optogenetic manipulation of the postsynaptic neuron.

5.1. bPAC activation does not change synaptic strength in active synapses

First, I investigated whether or not bPAC activation by itself changes connection strength of Schaffer collateral synapses. For this, I transfected cultures with channelrhodopsin-2 (ChR2) in CA3 and with bPAC in CA1 (see Methods). bPAC was activated by a blue LED coupled into the epifluorescence condenser. Presynaptic ChR2 expressing cells were stimulated by a green laser focused on CA3 through a 1.4 NA oil-immersion condenser. I performed intracellular recordings ('sharp electrode' recordings) in the CA1 region and activated excitatory inputs by optically spiking CA3 cells. The rationale behind doing intracellular recordings was to be able record without dialyzing out the contents of the cell. Typically, the intracellular recordings were maintained for 1 h, which was approximately the same duration that was obtained in whole-cell patch-clamp experiments. Wash-out due to dialyzing the cytoplasm with the contents of the low-resistance electrode is an inevitable consequence of whole-cell patch-clamp

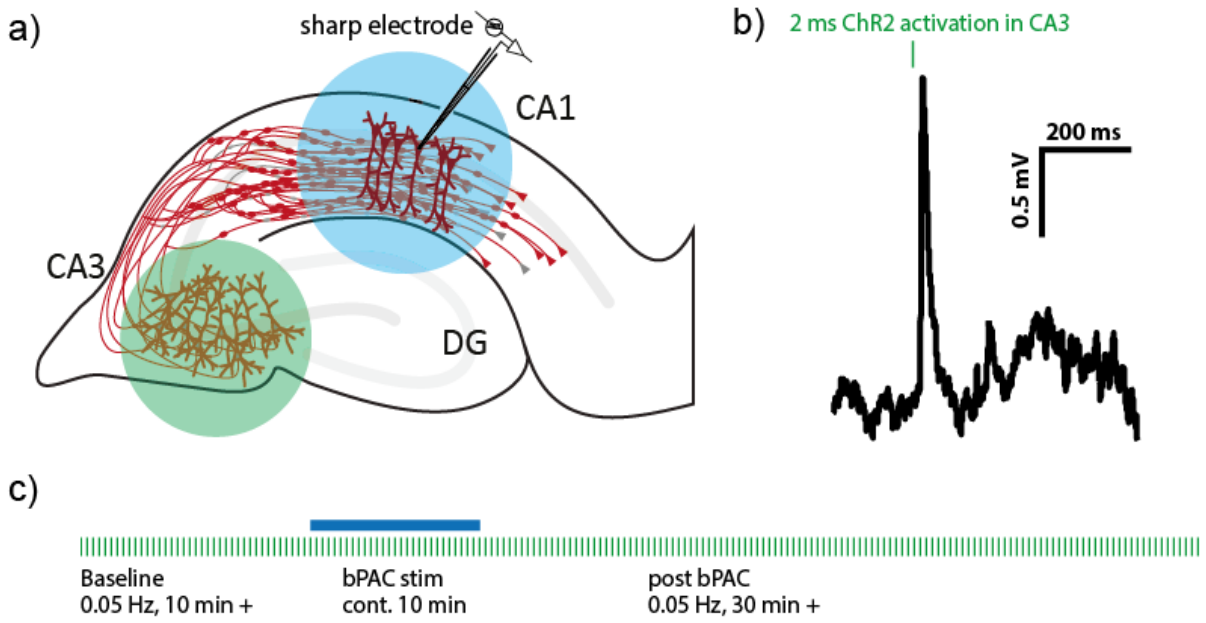

Figure 5.1.1: Intracellular recordings overview and experimental setup. (a) Intracellular recordings with sharp electrodes in CA1. Blue spot, illumination field (via 40x objective) of CA1 region containing bPAC transfected cells (n.t.s.). Green spot, illumination field (laser beam focused through the condenser) for stimulation of ChR2 expressing CA3 neurons (n.t.s). (b) Example EPSP measured in an impaled CA1 pyramidal neuron after ChR2 stimulation in CA1. (c) Experimental setup for intracellular recording experiments. CA3 stimulation continuously at 0.05 Hz (green lines) with a green laser, bPAC activation in CA1 during 10 min (blue bar) with blue LED, ~1mW/mm^2.

experiments (see general discussion), but is less of a concern during intracellular recordings. The tip diameter of a sharp electrode is at least an order of magnitude smaller, markedly reducing fluid exchange between pipette and cell. The general experimental setup is shown in Fig. 5.1.1a. The baseline was recorded over at least 10 min, in some cases longer until responses became stable. Before the baseline recording, the EPSP amplitude was adjusted to 2-4 mV by modulating the laser intensity illuminating CA3 (example shown in Fig. 5.1.1b).

I compared the effects of blue light illumination on synaptic strength in bPAC-expressing CA1 pyramidal neurons vs. non-transfected (WT) CA1 pyramidal neurons. Cells were transfected by local virus injection of pAAV-bPAC-2A-tdimer under the Synapsin promoter. bPAC expressing cells depolarized upon blue light illumination (see example in Fig. 5.1.2a), by about 2-4 mV. This is equivalent to the inward current that I saw in voltage clamp experiments (chapter 4.1), providing a positive control for successful optogenetic cAMP elevation in every single experiment. Illumination induced no depolarization in WT cells. Evoked EPSPs in CA1 did not change amplitude after illumination with blue light (Fig. 5.1.2b). This was true for WT neurons and bPAC-expressing neurons. Thus,

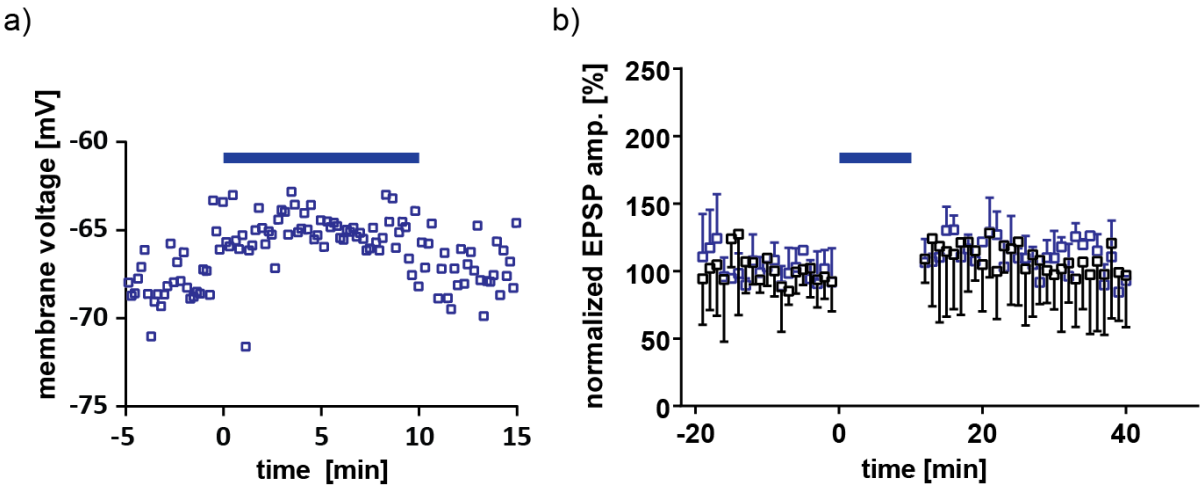

Figure 5.1.2: bPAC stimulation does not modulate synaptic strength in baseline spiking conditions (a) Example bPAC expressing CA1 pyramidal neuron. Membrane voltage over time, measured at 0.05 Hz. During bPAC activation (10 min starting at 0, blue bar, ~1 mW/ / mm^2), membrane voltage decreased by ~3 mV, and reverted to baseline voltage after light off. (b) Normalized evoked EPSP amplitude in WT (black squares, n= 6) and bPAC (blue squares, n=3) expressing CA1 pyramidal neurons before and after blue light illumination (10 min starting at 0, blue bar, ~1 mW/ / mm^2). No change in EPSP amplitude was observed.

strong increase of postsynaptic cAMP levels for 10 min is not sufficient to change the strength of Schaffer collateral synapses active at a low frequency (0.05 Hz).

5.2. bPAC activation does not seem to modulate theta burst protocol induced synaptic plasticity

I have shown in chapter 5.1 that bPAC activation in postsynaptic CA1 neurons did not seem to change synaptic strength in Schaffer collateral synapses by itself. One reason for this could be that we were in a stimulation regime where activation of the cAMP pathway does not influence synaptic plasticity. Next, I wanted to test whether postsynaptic cAMP affects the threshold for plasticity induction or the amplitude of long-term potentiation. For these experiments, I also used AAV virus transduction, but I designed different constructs. instead of the synapsin-1 promoter, I used a CamKII promoter to restrict expression to pyramidal cells and avoid expression in interneurons. The rationale behind this was that bPAC activation in interneurons in vicinity to CA1 pyramidal neurons could modulate their activity which could have an unwanted secondary effect on CA1 plasticity. In addition, I used a version of bPAC with a reduced dark activity *in vitro*[12] (pAAV-CamKII-bPAC$_{S27A}$-2A-timer). To induce plasticity, I chose a theta burst protocol (TBP), in which bursts of presynaptic and postsynaptic spikes are paired[115]. One theta-burst consisted of 4 short spike trains, delivered at 5 Hz; each spike train consisted of 5 spikes, delivered at 100 Hz. The postsynaptic CA1 spike trains were applied with a delay of several milliseconds, so that the postsynaptic spike occurred during the EPSP from the presynaptic spike, and not before (See Fig. 5.2.1). Theta bursts were repeated either 10x at 0.05 Hz (strong TBP), or 2x at 0.05 Hz (weak TBP). ChR2, however, cannot be reliably driven at frequencies above 20 Hz, at least not in hippocampal pyramidal neurons[116].

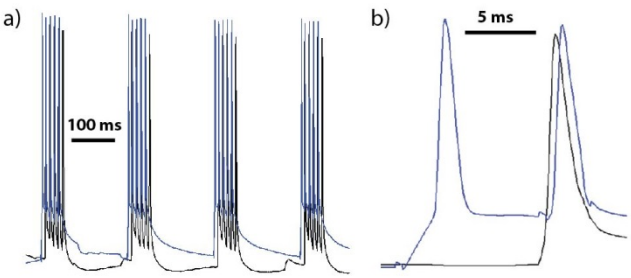

Figure 5.2.1: TBP protocol. Blue, presynaptic cell, black, post-synaptic cell. (a) A theta burst. (b) Spike delay pre-post.

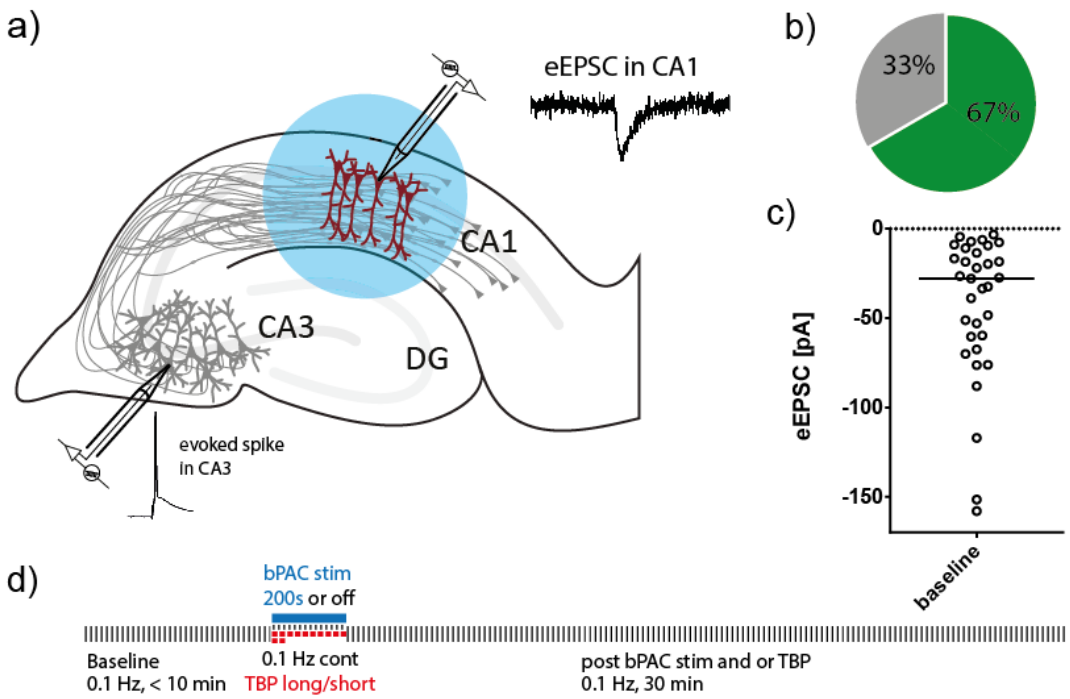

Figure 5.2.2: Paired recordings overview and experimental scheme. (a) Paired recordings of CA3 and CA1 pyramidal cells. Blue spot, illumination field of CA1 field containing bPAC transfected cells (n.t.s.). Top right, example evoked EPSC in CA1 after spiking a CA3 pyramidal neuron. (b) Average connectivity of CA1-CA3 pairs. 67 % of pairs were connected (n= 100). (c) Median baseline eEPSC in connected pairs was -27 ± 40 mV SD, n= 33. (d) Schematic of experiment. Spikes in the CA3 cell were evoked at 0.1 Hz. Plasticity induction protocol was delivered in a time window of 200 s, either with or without PAC activation.

To circumvent this problem and ensure reliable high-frequency activation of the presynaptic cell, I decided to perform paired recordings of CA3 and CA1 cells. This technique has several advantages but also disadvantages, which I will discuss in chapter 5.3.

A CA3 cell was patched and was kept in current clamp mode, subsequently a bPAC transfected CA1 cell was patched and held in voltage clamp (Fig. 5.2.2 a). Baseline responses were recorded at 0.1 Hz. Not all CA3-CA1 pairs were connected. If no EPSC could be detected in 15-20 trials, the experiment was terminated (67% of experiments, Fig. 5.2.2b). The strength of unitary connections was highly variable, with a median EPSC amplitude of -27 ± 40 mV (median ± SD; mean = -43 mV, Fig. 5.2.2 c). Recording of baseline responses at 0.1 Hz was kept below 10 min (8 min, typically) to minimize potential wash-out of plasticity relevant factors (5.2.2 d). The strong (long) theta burst protocol had a duration of 200 s, the bPAC-activating light stimulus had the same length. The light stimulus

was kept constant throughout the different protocols, including the weak (short) theta burst protocol (duration ~40 s) and continuous 0.1 Hz application (control). During plasticity induction via theta burst protocols, the CA1 cell was temporarily held in current clamp mode. After the end of the protocol (time point zero), the recording was kept up for as long as possible. Typically, a post-protocol recording duration of 30 min could be achieved before one of the two recordings were lost, or the series resistance in the CA1 cell went above a threshold (20 MΩ). As expected for Schaffer collateral synapses, a continuous 0.1 Hz test stimulus did not change synaptic strength of the activated synapses (Fig. 5.2.3b/c, black squares, Fig. 5.2.4 a). Stimulating bPAC with the 200 s light stimulus during a continuous 0.1 Hz spiking stimulus did not change the strength of the unitary connection (Fig. 5.2.3b/c, blue squares), consistent with our experiments using

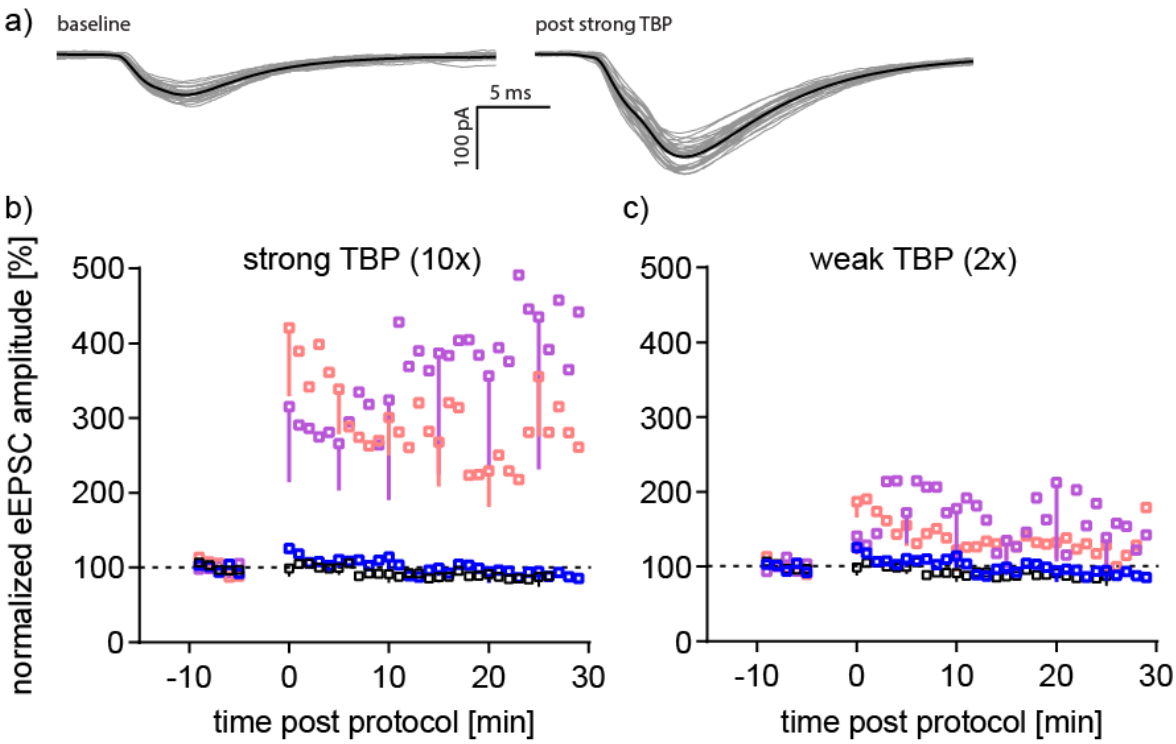

Figure 5.2.3: Paired Recordings – TBP. (a) Example traces, eEPSCs measured in CA1 during baseline (left) and 25 min after strong theta burst protocol induction. (b+c) Normalized eEPSC amplitude for baseline (black squares, n = 6) and baseline + bPAC activation (blue squares, n = 6). 1 square = 1 min bin (average response from 6 traces). Error bars (SEM) only shown every 5th data point. (b) Normalized eEPSC amplitude for strong TBP (red squares) and strong TBP + bPAC activation (purple squares). (c) same as in (b), except weak TBP instead of strong (n = 5 for weak TBP only, red squares, n = 3 for weak TPB + light, purple squares)

‘sharp’ intracellular recordings (chapter 5.1). When I applied the strong TBP, eEPSC magnitude increased to 299 ± 57 % mean ± SEM (Figure 5.2.3b, red squares) averaged from -5 min to protocol start, and from 25 - 30 min post protocol). An example of eEPSC traces before and after strong TBP is shown in figure 5.2.3a. Activation of bPAC with a blue light stimulus (200 s) during the strong theta burst protocol also resulted in strong potentiation (Fig. 5.2.3b, purple squares, 418 ± 192 % mean ± SEM), not significantly different from the experiments without bPAC activation. Initial connection strength and amount of potentiation was highly variable in individual experiments, both with and without bPAC activation (Fig. 5.2.4 c and d). Intriguingly, in the 30 min after plasticity induction, there was a slight decrease of EPSC amplitude in the non-illuminated

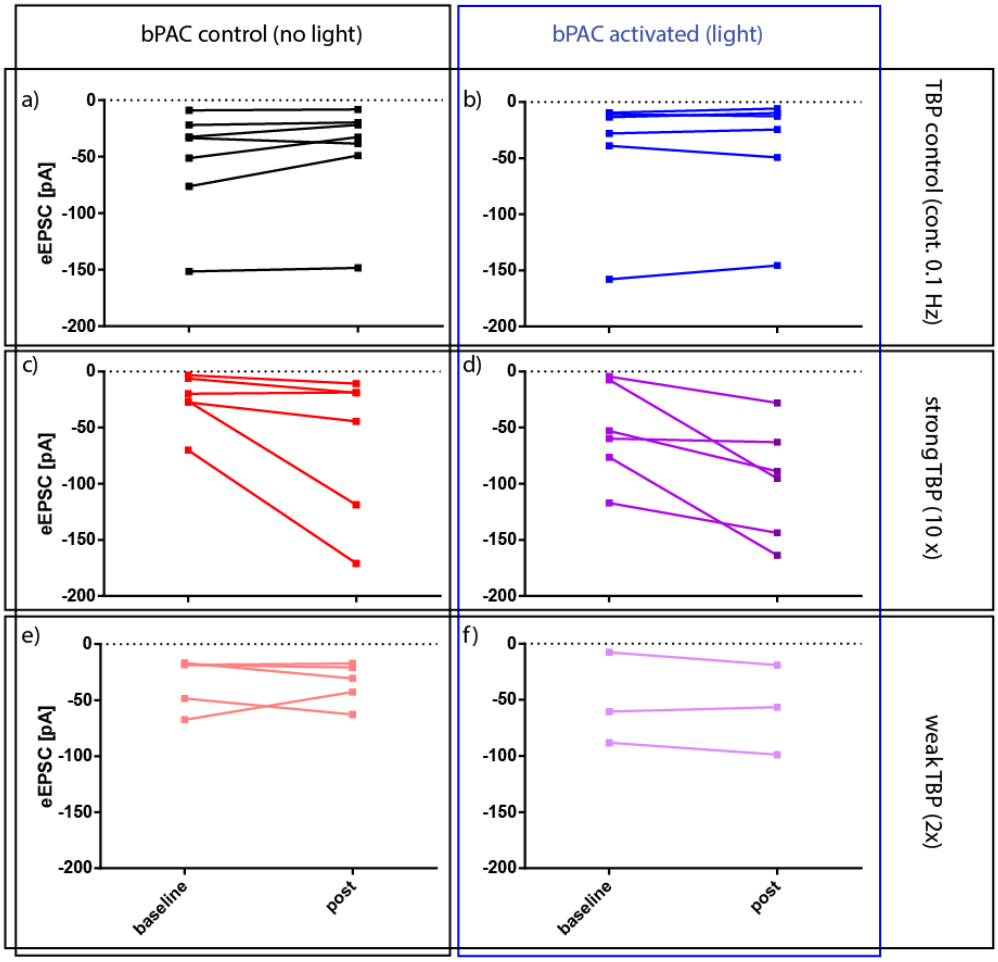

Figure 5.2.4: Paired recordings – non-normalized EPSC amplitudes. Average eEPSCs during baseline and 25 min after induction protocol for all experiments included in 5.2.3b+c. (a,c,e) Top to bottom: continuous 0.1 Hz baseline, strong TBP (10x), weak TBP. No bPAC activation during plasticity induction. (b,d,e) Top to bottom: same as (a,c,e), but bPAC activation during plasticity induction protocol.

cells, but an apparent increase in the cells in which bPAC was activated (Fig. 5.2.3 b,c). Unfortunately, patch clamp recordings cannot be extended in time to investigate potential effects of bPAC activation on late LTP (see discussion).
It is possible that by inducing plasticity with a strong TBP, the activated synapses were already strengthened to a saturating level, which could be one reason for the lack of a clear effect of bPAC stimulation on TBP-induced synaptic plasticity. To induce non-saturating potentiation, I used a TBP with less repeated iterations (2 instead of 10). We reasoned that a weak potentiation could be more easily modulated by bPAC activation during the induction. Indeed, the short TBP-induced weak potentiation (Fig. 5.2.3c, red squares, 130 ± 44 % mean ± SEM). bPAC activation for 200 s (starting with the first theta burst) in this protocol also did not significantly modulate synaptic plasticity induction (Fig. 5.2.3c, purple squares, 143 ± 41 % mean ± SEM). Thus, within 30 min after induction, neither threshold nor amplitude of TBP-induced LTP seems to be modulated by postsynaptic cAMP levels.

5.3. Discussion

To study the effects of bPAC stimulation on synaptic plasticity, I used two methods: intracellular recordings in CA1 together with an optogenetic stimulation in CA3, and whole-cell patch-clamp paired recordings of CA3-CA1 connected pyramidal neurons. I hoped to achieve a longer recording duration by using intracellular recordings, but it was not possible to maintain the intracellular recordings significantly longer than patch-clamp experiments in our recording configuration. This was not expected, because in principle intracellular recordings can be very stable, as series resistance changes over time are not an issue in current clamp mode recordings. However, intracellular recordings are much more sensitive to mechanical or thermal drift of pipet or slice compared to whole-cell recordings, and stability issues are the most likely cause for the modest achievable recording length.

ChR2 stimulation of a subpopulation of CA3 has both advantages and disadvantages. Light stimulation can be easily adjusted (laser pulse intensity or length) to achieve a postsynaptic response of a certain size. One disadvantage is

the limited maximum spike frequency which can be induced in a controlled way with ChR2. Also, during intracellular recordings, the cell cannot be voltage-clamped due to the high resistance of the intracellular electrode. The results show that activating bPAC alone for as long as ten minutes, and thereby dramatically elevating cAMP levels in postsynaptic CA1 pyramidal neurons, is not sufficient to elicit a change in the synaptic strength of the stimulated synapses within the 30 minutes after the induction protocol. This was confirmed in paired recording experiments, where a shorter bPAC stimulus (200s) during a 0.1 Hz protocol did not affect the strength of synaptic connections.

In the paired recording experiments, I induced synaptic plasticity with a stimulation protocol that has been shown to reliably potentiate CA3-CA1 synaptic connections[115]. In synaptic physiology, paired recordings are considered the gold standard, as they allow for perfect control over spike timing in the pre- and postsynaptic cell during the induction protocol. Other methods, such as ChR2 or extracellular stimulation, are less exact in this matter, as the number of cells or fibers spiking can change over time (drift or other fluctuations). In paired recordings, one also looks at a defined subset of synapses, because only one Schaffer collateral fiber is activated by spiking a CA3 cell (unitary connectivity). However, there are also drawbacks to this technique. First of all, the throughput is limited. Obtaining two stable, long lasting patches is not always possible and some CA3-CA1 patched pairs are not actually connected (about one third). Altogether, from 100 patched pairs, only 32 could be included for the analysis in above figures. In the connected pairs, initial connection strength was highly variable, a biological reality that is obscured in extracellular recordings.

With these experiments we were trying to find out whether or not the induction of synaptic plasticity can be manipulated by postsynaptically stimulating cAMP signaling with bPAC. I can now say with confidence that elevating cAMP levels in active synapses does not by itself induce an increase in connection strength. In chemical LTP experiments, forskolin-mediated activation of adenylyl cyclases was sufficient to induce a form of early LTP[81]. A possible explanation for these divergent results are cAMP-dependent processes in the presynaptic terminal, stimulated by forskolin/Rolipram, but not by (postsynaptic) bPAC. Strong effects

of cAMP on glutamate release are well documented, e.g. in the mossy fiber- CA3 connection. To test this hypothesis, presynaptic expression of bPAC in the context of TBP experiments would be a viable approach. The completely untargeted and unphysiological nature of cLTP, however, includes many possible targets such as various types of interneurons and glia cells. This lack of specificity makes sorting out the precise mechanism of cLTP not a very attractive proposition.

A frustrating aspect of paired recordings is their limited duration which essentially prevented us from studying the effects of cAMP on late LTP. Extracellular field potential recordings can last for several hours, but do not work well in organotypic cultures. An interesting approach for the future would be bPAC stimulation in acute hippocampal slices in combination with long-term field recordings. This requires precise stereotactic virus injections *in vivo* to express bPAC in targeted hippocampal areas, followed by preparation of acute slices after a suitable expression period.

6. Overall discussion and perspectives

During my thesis work I characterized bPAC, a small photoactivatable adenylyl cyclase from a bacterium (*Beggiatoa*) in hippocampal neurons. The aims were to test whether bPAC is a viable optogenetic tool to manipulate intracellular cAMP levels in neurons, and to use it in hippocampal organotypic slice cultures to study cAMP signaling in synaptic plasticity.

To characterize bPAC, I expressed it together with a sensitive CNG channel in hippocampal neurons. I compared it to euPACα, a previously published light activated adenylyl cyclase from a different organism (*Euglena*), but with the same BLUF light sensing domain and accordingly very similar spectral properties [10].
In our publication in JBC (see chapter 4), we pointed out that bPAC is very light sensitive. Even in low light conditions, bPAC activation could be detected. The high light sensitivity can be explained by the slow *off* time constant in the seconds range, leading to a high degree of photon integration during long illumination. From our comparison with euPACα we know that euPACα-induced CNG currents decay to baseline much faster than bPAC currents. Thus, the decay of intracellular cAMP levels after the end of PAC illumination is not limited by phosphodiesterase activity, but by the time constant of PAC inactivation. Fast inactivation is actually an advantageous feature of euPACα, because timing of cAMP elevations in the cell can be controlled with an even higher temporal resolution than with bPAC. However, euPACα has certain important drawbacks. First, it is ~ 3 times larger than bPAC (350 vs. 1019 a.a.), which limits its use in AAV-based viral transduction techniques. AAVs have a limited packing capacity of ~ 4.9 kb[117], which limits the vector construct size (including inverted terminal repeats[118] and promoter), and the euPACα sequence alone has a size of over 3 kb. The second drawback is the much higher dark activity and lower dynamic range of euPACα compared to bPAC. These properties were measured by Manuela Stierl in the Hegemann lab [12,67]. For most applications, bPAC is advantageous compared to euPACα. Even though the time constants of bPAC are slower, its temporal precision is still far superior to pharmacological methods using bath application of cAMP elevating drugs.

How does bPAC compare to similar optogenetic tools, which are not based on the BLUF-AC structure? Opto-XRs are chimeric GPCRs which were engineered to combine the light sensitive domain of rhodopsin with the intracellular signaling domain of other GPCRs, for example the $ß_2$-adrenergic receptor (Opto-$ß_2$AR) or the α_1-adrenergic receptor (Opto-α_1R) [4,5]. This allows for specific activation of signaling targets of these receptors, in the case of Opto-$ß_2$AR, activation stimulates endogenous adenylyl cyclases, elevating cAMP levels. Opto-XRs are very elegant optogenetic tools, not much bigger than bPAC (~ 400-500 a.a. vs 350 a.a.), and their kinetics is very fast. Opto-XRs are based on a fundamentally different principle, as the enzyme that produces the second messenger (endogenous, $G\alpha_s$ activated adenylyl cyclase) is activated via another intermediate step, and not by light directly. This means that the cAMP produced by Opto-$ß_2$AR is limited by the amount of available, activatable endogenous adenylyl cyclases. In case of bPAC, the amount of cAMP which can be produced is limited by the expression level of bPAC itself (and of available ATP in the cell). Another important difference between bPAC and Opto-XRs is the light activation spectrum. Opto-XRs are based on bovine rhodopsin, which has a wide activation spectrum reaching into the orange-red visible light spectrum up to λ = 600 nm [119]. bPAC is like euPACα based on the BLUF domain, which has a relatively sharp drop of activation around λ = 520 nm (green).

The sharp drop in the activation spectrum of bPAC in the green visible light spectrum provides it with the distinct advantage of being spectrally separated from other optogenetic tools, specifically from red-shifted channelrhodopsins (see Fig. 6.1). This allows for yellow-green light stimulation of ChR2-expressing cells in the same tissue, or even in the same cell, without activating bPAC. I have exploited this feature in chapter 5.1, where I spike the red shifted ChR2 variant ET/TC[116] with green light in CA3 while recording from a bPAC-expressing cell in CA1. With recently developed further red-shifted channelrhodopsin-variants such as ReaChR [120], it will be possible to achieve even better spectral separation from PAC. When combining ChR2 and bPAC, the slow time constant and high sensitivity of bPAC is advantageous, because low, constant blue light can be used to stimulate bPAC, sub-threshold for ChR2-induced spiking. This allows for a two-way separation of bPAC and ChR2 activation through intensity and wavelength.

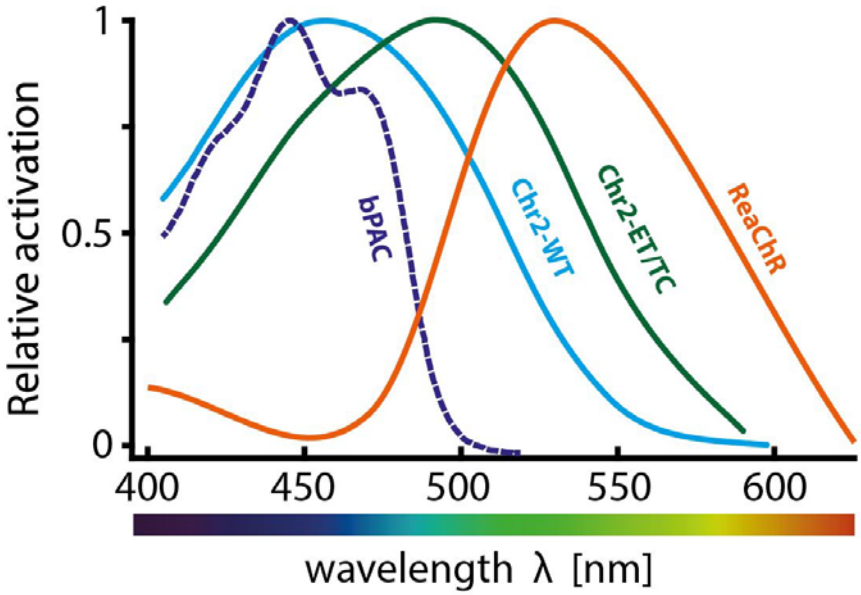

Figure 6.1: Comparison of activation spectrum of several optogenetic actuators. bPAC activation approaches zero close to λ = 520 nm. WT-ChR2 has a similar peak activation spectrum to bPAC. Chr2-ET/TC and ReaChR are significantly shifted towards the red light spectrum with peak activation at λ ~ 490 and λ ~ 530 nm, respectively. Figure combined from [116] and [67] and unpublished data from the Oertner lab.

The very high light sensitivity and photon integration properties of bPAC are a mixed blessing, as certain precautions are required for handling transfected tissue to avoid unwanted bPAC activation. Exposure to daylight, bright room light or other blue light emitting sources had to be avoided (see also methods, chapter 7.3). The spectral properties of bPAC were an advantage here, as it allowed us to use safely orange light sources for the handling of cultures, avoiding bPAC activation.

Two-photon laser scanning microscopy (2PLSM) technique allows for tissue imaging at greater depths than conventional laser scanning microscopy, because the excitation laser can be tuned to wavelengths in the near-infrared range (λ = 700 - 1080 nm). The main advantage of 2PLSM is the small volume of excitation in the range of about 1 nm^3. This is useful for high resolution imaging, but also to locally activate 'caged' compounds such as MNI-glutamate. I wanted to test whether two-photon excitation could be used to locally activate bPAC. Two-photon activation would make it possible to investigate intracellular signaling with an even higher spatial resolution, on the level of dendrites or even single spines. Fig. 6.2 contains an example trace as proof of concept for two-photon activation of bPAC. I scanned a

bPAC-positive CA1 pyramidal cell soma with a 890 nm laser while recording I_{hold} every 2 seconds. The observed inward current had a similar magnitude to the magnitude achieved with LED illumination in chapter 4.1. No inward currents were observed when scanning non-transfected cells with the same laser power. I conclude that 2PLSM as a technique to stimulate bPAC in neuronal subcellular compartments is possible and promising.

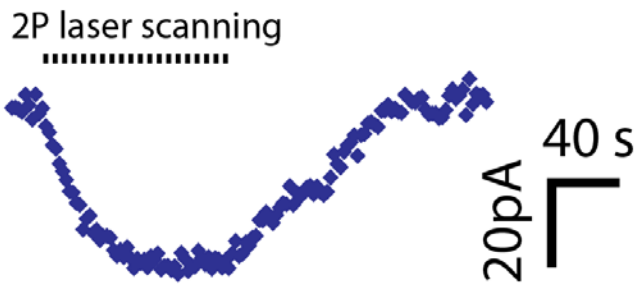

Figure 6.2 Proof of concept for 2PLSM bPAC activation. Scanning the soma of a bPAC expressing neuron with a λ = 890 nm 2P laser results in a slow inward current.

Which concentration ranges of cAMP do we expect in neurons with and without bPAC activation? In this study, we did not attempt to measure absolute cAMP concentrations in individual hippocampal neurons. The most elegant method would be a ratiometric FRET assay with an EPAC based sensor and CFP/YFP as FRET pair (EPAC-cAMPS[121]). Unfortunately, EPAC-cAMPS cannot be used together with bPAC, as the excitation of the CFP-YFP FRET pair with blue light also activates bPAC at the peak of its activation spectrum. In published EPAC-cAMPS measurements of intracellular cAMP concentrations in brain stem slice cultures[122], absolute intracellular cAMP concentration ($[cAMP]_i$) was about 0.01 µM. Under low-dose forskolin, $[cAMP]_i$ increased 100-fold to ~ 1 µM, showing the enormous dynamic range of endogenous cAMP signaling. We have measured relative changes in $[cAMP]_I$ by overexpressing a high-sensitivity CNG channel variant (CNG C460W/E583M) together with bPAC and recoding light-induced currents. K_m of this CNG channel is 1.2 µM cAMP[66]. As we could saturate the CNG channels by strongly activating bPAC (see Fig 3.2.4c), we estimate that bPAC is able to produce cAMP concentrations > 10 µM under bright light conditions.

Endogenous, G-protein-controlled adenylyl cyclases are activated by neurotransmitter receptors like D_1 and $ß_2$, but also by forskolin and Opto-XRs. G-protein-activated ACs have transmembrane domains, anchoring them to the plasma membrane (tmACs). bPAC, in contrast, is a soluble adenylyl cyclase (sAC). There

are also endogenous sACs in the brain which are activated by calcium [32,123]. Compartmentalization of cAMP signaling is an emerging concept[52] that could potentially explain how a single molecule like cAMP manages to integrate many different signaling pathways, combining extracellular and intracellular information. A-kinase-anchoring proteins (AKAPs) play a pivotal role in compartmentalized signaling, as they can tether PKA together with PDEs, creating microdomains of cAMP concentration[51,89]. It is quite possible that the spatio-temporal complexity of cAMP signaling is comparable to the much better studied calcium signaling system, but tools for controlled and local manipulation have been lacking. As 2PLSM activation of bPAC is feasible (Fig. 6.2), this new tool could be applied to study cAMP signaling in subcellular compartments. To this end, an engineered, membrane-anchored version of bPAC could be even more useful, as anchored bPAC cannot diffuse out of the focal volume.

In my experiments presented in chapter 5, I have demonstrated that strongly elevating cAMP levels in postsynaptic CA1 pyramidal cells does *not* change synaptic strength of the activated Schaffer collateral inputs in an early phase after the induction protocol. This is in line with what others have found using a pharmacological approach[124]. In this study, mEPSC frequency and amplitude were analyzed to distinguish pre- and postsynaptic effects. Compared to this traditional approach, optogenetic manipulation of cAMP signaling now improves the spatial and temporal resolution significantly. It is a much cleaner approach not only because the site of cAMP elevation is certain, but also because drug approaches, in particular forskolin, have multiple targets, leading to unspecific effects[125]. Despite of its side effects, forskolin has been widely used to study neuronal signaling (a PubMed search of “Forskolin AND Neurons” produces >2000 results), due to the lack of better alternatives. In my opinion, optogenetic tools like bPAC will revive the research interest in cAMP signaling like genetically encoded calcium sensors have stimulated the research on calcium signaling.

We were motivated to test the effects of bPAC on synaptic plasticity by the well documented modulatory effects of dopaminergic and adrenergic inputs. For example, Li et. al have shown *in vivo* that novelty-induced activation of D1/D5 receptors in CA1 pyramidal cells facilitates the induction of LTP[23]. Also, work from

John Lisman's lab shows an increase of the magnitude of early LTP in CA1 hippocampal cells by D1/D5 receptor activation, which can be mimicked by low-dose forskolin[126]. These and other studies[111,114,127] convey the concept that a novelty or reward stimulus activates dopaminergic inputs to the hippocampus, which facilitate the induction of synaptic plasticity in the hippocampus CA1 region via cAMP signaling downstream of D_1 receptors. We reasoned that by directly increasing cAMP levels with bPAC, we could perhaps mimic the dopaminergic facilitation of plasticity induction, comparable to shifting a Bienenstock-Cooper-Munro (BCM) type sliding threshold plasticity induction model (see figure 6.3). This would have supported a cAMP-dependent mechanism for dopaminergic signaling in facilitation of plasticity induction. However, our results at this stage do not support the claim that increasing postsynaptic cAMP signaling in CA1 modulates plasticity induction. This is unexpected and raises the possibility of dopamine effects on presynaptic properties.

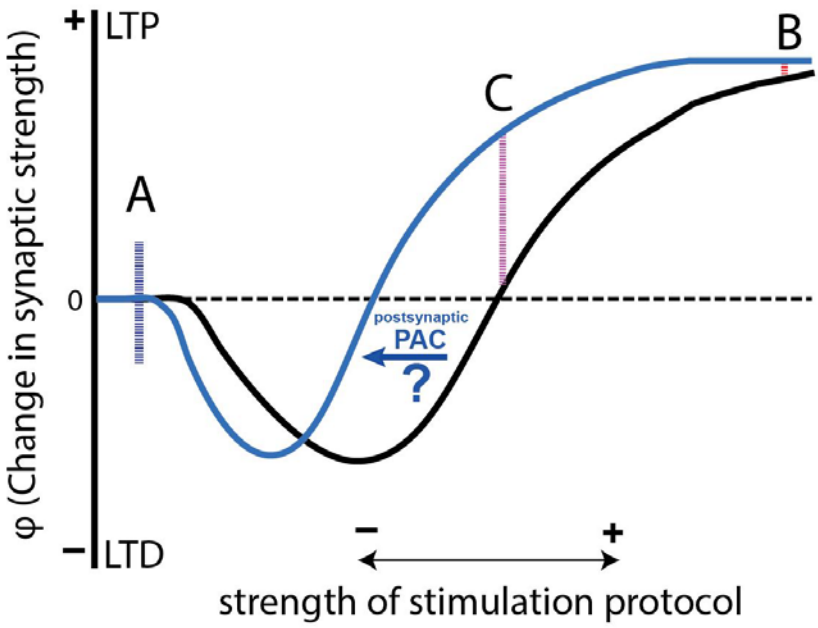

Figure 6.3: Speculative bPAC-induced shift in a BCM-like plasticity induction model. A certain stimulation protocol of synaptic inputs can lead to either a positive, negative or neutral change in synaptic strength. Situation A: weak stimulation situation, bPAC -induced plasticity shift has no effect on change in synaptic strength. Situation B: strong stimulation, plasticity saturated, bPAC shift has no effect on change in synaptic strength. Situation C: 'medium' stimulation. bPAC stimulation shifts plasticity induction curve, so that a previously neutral stimulus now leads to an increase in synaptic strength. The outcome of our study does <u>not</u> support a dependence of the BCM curve on postsynaptic cAMP elevation.

Optogenetic actuators such as Channelrhodopsin have been successfully applied *in vivo,* targeting specific cell types and regions. bPAC is very suitable for *in vivo* applications, as it is highly light sensitive and has no apparent cytotoxic effects. I have successfully undertaken viral vector-mediated transfection in living tissue, a prerequisite for *in vivo* application of the construct. By local activation of bPAC, for example in the hippocampus, cAMP signaling can be investigated in the context of learning and memory-related behaviors. *In vivo* experiments would also allow to asses the effects of cAMP elevation on longer time scales. The development of new tools has always been a major driving force in neuroscience. Optogenetics is a particularly striking example of a methodological breakthrough, endowing researchers with the capability to study neuronal function with unprecedented spatiotemporal resolution. The next step will be to develop experimental approaches that capitalize on the properties of bPAC to test the importance of cAMP signaling in the regulation of brain function. On a microscopic scale, studying subcellular compartmentalization with highly localized bPAC activation might reveal new levels of complexity in intracellular signaling.

7. Experimental Methods

Comprehensive methods for all experimental procedures, complementing the methods section in the JBC publication[67].
All experiments were in done in accordance with local regulations, either of Basel, Switzerland or Hamburg, Germany.

7.1. Organotypic hippocampal slice cultures

Organotypic hippocampal slice cultures were prepared from Wistar rats at postnatal day 4-5 as described elsewhere [17]. Briefly, newborn Wistar rats were decapitated after CO_2-induced anesthesia and following death, brains were removed and immediately placed in ice cold dissection medium (see chapter 8 for details about solutions and drugs). Hippocampi were dissected out under a stereomicroscope, chopped on a tissue chopper (coronal slices, 300 µm thick), and the resulting slices placed on PTFE membranes (Millipore) in 6-well cell culture plates containing 1 ml culture medium. With this technique, cultures are supplied with nutrients through the permeable membrane, while being exposed to a carbogen gas mix (95 % O_2, 5 % CO_2) in an incubator. Organotypic hippocampal cultures can then be kept for several weeks up to months in the incubator at 37 ˚C, provided the cells are fed twice-weekly by replacing 2/3 of the medium with fresh, pre-warmed culture medium.

7.2. Gene delivery to hippocampal neurons

For the vector constructs see chapter 7.5, molecular genetics.

Biolistic transfection

For biolistic transfection of hippocampal organotypic slice cultures, a Bio-Rad Helios® Gene-Gun system was used.
In short, plasmid constructs were bound to microcarrier gold particles (1.0 µm diameter) with a multistep protocol according to the supplier's instructions. DNA covered gold particles were transferred to Gold-Coat® -Tubing and the tubing cut to cartridge-size, then stored with desiccant at 4˚C. Shooting of the gold particles with high pressure helium was carried out on air-exposed organotypic slice cultures at days *in vitro* (DIV) 6-7 with a gene gun, through a filtering screen

made of fine nylon mesh. Expression was verified with a stereomicroscope and epifluorescence illumination, and experiments were done 6 or more days after transfection.

AAV injection and single-cell electroporation

For both gene-delivery methods, organotypic slice cultures were transferred to a special purpose microscope setup. To minimize exposure of the organotypic slice cultures to contaminants, the whole setup was under a sterile air flow fan, and critical parts disinfected before use with 70% EtOH. Culture membranes were placed in a small sterilized glass-bottom dish either covered by (single-cell electroporation) or underwashed with ACSF-HEPES 2/1, and transferred to the setup. At the setup, optics and micromanipulators with the appropriate electrode holder or headstage could be interchanged for the respective gene delivery method.

Transduction by local AAV injection

Adeno-associated virus (AAV) suspensions were stored in aliquots at -80˚C, and thawed freshly for injection in the slice. AAV virus titers varied from 10^{12} – $2x10^{13}$ vg/ml. Local AAV injection was done with a precision pressure injection system (Parker, 'Picospritzer') in the dedicated setup. Thin-wall glass pipets (WPI, Model TW150F-3) were pulled to hair thin closed ends on a horizontal putter (Sutter). 1µl of AAV suspension was filled into the pipet, the pipet tip was broken off with

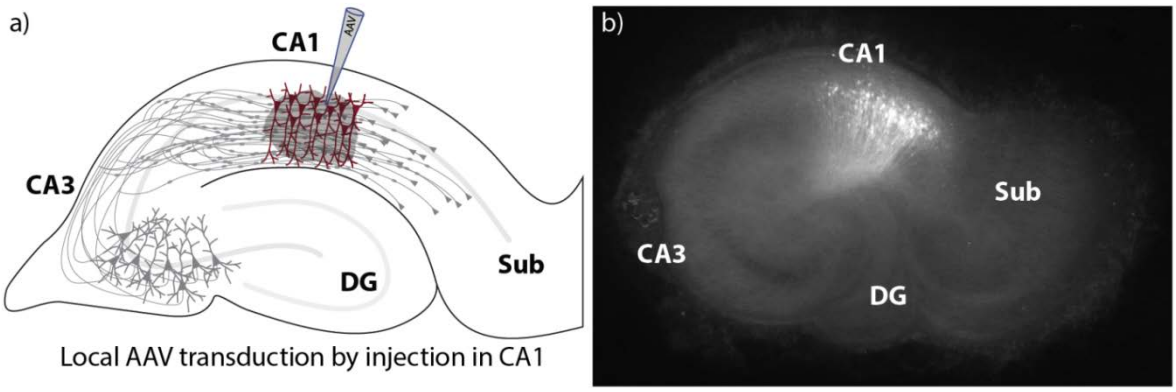

Figure 7.2.1: Local AAV injection
(a) Schematic for localized virus injection, in this case in the CA1 region of the hippocampus. (b) Epifluorescence image of a whole organotypic brain slice after injection with rAAV-*CamKII*-bPAC-(2A)-tDimer2. Transduction remains localized to the injection site in the CA1 region of the slice.

sterile tweezers. Under a 5x air objective, the pipette was inserted into the slice in the region where the somata of the targeted neurons were located. The AAV suspension was ejected into the tissue with short pressure pulses (30-50 ms, 1.5 - 2 bar). The extent of the injection site could be immediately recognized due to a change in local contrast in the tissue, and injection was adapted accordingly. Usually several days after injection, expression of tDimer2-FP was verified under a fluorescence stereomicroscope (Leica) (see Fig.7.2.1)

Single-cell electroporation

Single-cell electroporation is a technique to deliver polar or charged molecules (in this case negatively charged DNA) into cells by applying a train of voltage steps to a cell that has been approached with a pipet containing the molecule (see Fig. 7.2.2 for schematic). For single cell-electroporation the brain slices on the membrane insert were temporarily submerged in ACSF-HEPES 2/1 for the duration of the procedure, because a water-immersion objective was used.

Thin-wall glass pipettes (WPI, Type TW150F-3) had a pipette resistance of 12-15 MΩ when filled. The pipette was filled with K-gluconate based intracellular solution (IC(K-Gluc), see solutions chapter 8.5) containing the DNA constructs (1-100 ng/µl) and 20 µM Alexa-594 dye (Life Technologies). The pipette was inserted into the holder on the headstage of an Axoporator 800A (Molecular Devices). Positive pressure was applied and the pipette was manipulated to the

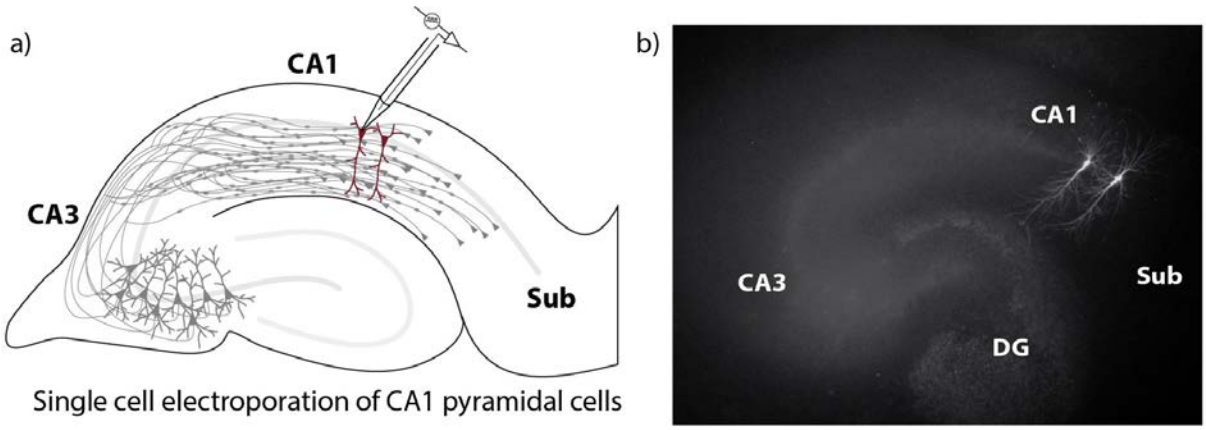

Figure 7.2.2: Single cell electroporation
(a) Schematic for single cell electroporation (b) Epifluorescence image of a whole organotypic brain slice after electroporation (example from our lab, transfection with cerulean and GCamP3, reproduced with modifications, courtesy of S. Wiegert [131])

soma of the targeted cell, the pressure was released, and the resistance increased to ~25-30 MΩ (loose patch mode). The electroporation pulse was delivered immediately after the resistance increase (50 pulses at 50 Hz, -12 mV, 500 µs). 8-20 cells per slice were electroporated, and transfection success was verified 2-5 days after transfection.

7.3. Electrophysiology and optogenetic stimulation

Electrophysiology recording equipment consisted of an amplifier (Axon, Models Multiclamp 700B, or Axopatch 200B) and appropriate headstages and micromanipulators (Sutter, Models MPC-200 and MPC-285) . Data was acquired with data acquisition boards (National Instruments, several models) in combination with custom modified Ephus software[128].

For electrophysiology experiments, a piece of membrane, containing an organotypic slice culture with a rim of empty membrane around it, was cut out with a scalpel, and placed in a custom made glass bottom chamber, weighed down with a piece of gold wire (touching only the membrane), and superfused with ACSF 4/4 or, in some experiments ACSF 2/1 (flow rate ~ 1.5 - 2 ml/min). The ACSF was constantly bubbled with carbogen, and heated to 30˚C (temperature measured in chamber). An Ag/Cl pellet was used as the reference electrode and a chloride coated silver wire was inserted into the pipette in contact with the pipette filling solution. Drugs were either always present in the ACSF or, for wash-in experiments, allowed to perfuse the slice culture for 10 min or more.

Whole-cell patch clamp experiments

Patch pipettes were pulled from thick-wall glass with filament (WPI, Model 1B150F-3) on a vertical pipette puller (Narishige) in a two-step protocol. Pipettes were pulled to achieve an initial pipette resistance of 3-5 MΩ and the tips were then filled with intracellular solution and approached to the tissue with positive pressure under DIC or Dodt-Gradient-Contrast imaging. The pressure was released upon contacting the soma of the neuron and the voltage clamp potential was set to -65 mV. After forming a GΩ seal, with negative pressure when necessary, sharp suction was applied to break the membrane and achieve a whole-cell recording configuration. Series resistance was less than 20 MΩ

(usually below 12 MΩ), initial membrane resistance was 80 MΩ or higher and initial holding current less than 100 pA. Recordings were discontinued if series resistance increased above 25 MΩ.

Intracellular recordings

For intracellular (sharp electrode) recordings, thin wall glass pipets (WPI, Type TW150F-3) were pulled on a horizontal puller (Sutter) to a pipet resistance of 50-100 MΩ. A concentrated salt solution (1.25 M K-Acetate) filled the pipette, and the pipette was approached to the tissue. To penetrate a cell, the buzz function of the amplifier was used and/or a stepping protocol for the micromanipulator (Sutter) was used. Penetration success was evidenced by a sudden voltage drop. Overshooting action potentials were evident in successful recordings. Verification of the transfection status of the recorded neuron was done post-hoc.

Optogenetic stimulation

Optogenetic stimulation was done in different ways depending on the tool (bPAC or ChR2). Illumination of bPAC was done through the water immersion objective (40x or 63x, depending on the experiment), with a blue LED illumination system (Prizmatix, 460 nm) coupled into the light-path of the microscope. For stimulation, the soma of the bPAC transfected pyramidal cell was centered in the field of view of the objective. Illumination was either controlled with TTL pulses generated by the Ephus software[128], or, manually for long periods of illumination. The stimulation parameters are provided in the results section for each experiment as either light intensity together with a time (e.g. 1 mW / mm^2 for 10 s), or as light dose (e.g. 0.1 mW * s / mm^2).

To activate ChR2 a green laser (530 nm) was used In the case of laser illumination, the laser was coupled into the microscope setup through a dichroic mirror underneath the 1.4 NA condenser. The size of the laser illumination spot in the tissue could be regulated with a telescope, and the position could be adjusted with a movable mirror system.

Precautions against unwanted PAC activation

To avoid unwanted activation of bPAC, several precautions were taken when handling bPAC expressing tissue. bPAC is very light sensitive and has a slow τ_{off},

which can lead to a quick accumulation of relatively high cAMP levels when exposed light at wavelengths below ~520 nm. Exposure to daylight was completely prevented. Exposure to room light was minimized during feeding and transport of transfected cultures. Light sources for stereomicroscopy (cutting out the slice from the membrane) and for microscope setup illumination were filtered with long-pass (orange) colored glass filters with transmission wavelengths above ~530 nm (Thorlabs). Transmission light for DIC or Dodt-Gradient-Contrast imaging was filtered with long-pass glass filters in the infrared range. Exposure to high-intensity green light (needed for fluorescence imaging of tDimer2) was limited to very brief periods of time, or if possible omitted completely.

7.4. Data analysis

For mEPSC analysis, the custom MATLAB data format from the Ephus software was converted for analysis with Clampfit-Software (Axon Instruments) with a custom written tool. mEPSC analysis was done with Clampfit's in-built Template Search module, and custom templates based on observed mEPSCs from the data. mEPSC detection was automated to reduce bias.

For all other data, custom software was used in MATLAB. Physanalyzer software (M. Mikulsky and T. Oertner, unpublished) and OnlineAnalysis software (D. Udwari, unpublished) based on MATLAB were used to calculate the basic cell parameters; membrane capacitance (C_{mem}), membrane potential (V_{mem}), holding current (I_{hold}), membrane input resistance (R_{mem}) and series resistance (R_s) and to measure and plot response peaks and slopes.

Statistical analysis was done with Prism Software (GraphPad) or Excel (Microsoft); statistical tests are given at each experiment if applicable.

OnlineAnalysis Software for electrophysiological experiments

To be able to monitor changes in basic cell parameters and response peaks, I developed a software tool which works in conjunction with Ephus software, specifically the user functions of Ephus [128]. The program was entirely written in MATLAB, and evolved from a basic data plotting tool to a more advanced tool for electrophysiological data analysis written for online and post-hoc analysis. The main principle of the online analysis function is the import of the last acquired

trace data structure from Ephus, which is then used to calculate a series of parameters including C_{mem}, V_{mem}, I_{hold}, R_{mem}, R_s, R_{total}, peak response and slope of a response. This can be done with data from one channel, or with two channels simultaneously, when a Multiclamp 200B amplifier is used. The user interface consists of a series of windows, which can be arranged to fit the needs of the user. All settings can be stored in a settings file to recall the setup when the software is next launched. Results are plotted live, and can be exported as an Excel file for further analysis. A plugin for post-hoc analysis was developed, to be able to re-analyze the experiment afterwards, for example with changed settings for detection-windows. The code for OnlineAnalysis software can be requested from the author (daniel@udwari.de).

7.5. Molecular genetics

Molecular cloning

Cloning strategies, restriction sites and PCR primer sequences were all done with the help of ApE (A plasmid Editor) software. Molecular cloning was done according to standard procedures and kits (Qiagen, Macherey-Nagel, Fermentas). Briefly, plasmids were produced in *Dam*-negative *E.coli* strains growing at 37°C in LB (Sigma). Plasmid isolation was done with plasmid prep kits based on anion-exchange resins. For cloning, restriction enzymes from different vendors were used according to the supplier's protocols (Fermentas, Roche, NEB). In case of PCR-based subcloning, oligonucleotides (primers) were ordered from companies and used according to the company's instructions (Microsynth, Eurofins).

Cloning vectors and promoters

Destination cloning vectors were either in pCI or pAAV backgrounds, both with resistance genes against Ampicillin. Two different promoters were used depending on the experiment, either Synapsin-1 (Syn), or Ca^{2+}/calmodulin-dependent protein kinase II alpha (CamKIIα).

The Syn promoter is a pan-neuronal promoter; neurons transfected with a construct under the Syn promoter reliably express the construct continuously. No expression in glial cells is driven by the Syn promoter[129].

The CamKIIα promoter is also neuronal, but expression of constructs under the CamKIIα promoter is strongly biased towards pyramidal neurons[129], and little to no expression can be found in interneurons.

Sequence of the Synapsin promoter, 469 bp (5'-3'):

CTGCAGAGGGCCCTGCGTATGAGTGCAAGTGGGTTTTAGGACCAGGATGAGGCGGGGTGGGGGTGCCTACCTGACGACCGACCCCGACC
CACTGGACAAGCACCCAACCCCCATTCCCCAAATTGCGCATCCCCTATCAGAGAGGGGGAGGGGAAACAGGATGCGGCGAGGCGCGTGC
GCACTGCCAGCTTCAGCACCGCGGACAGTGCCTTCGCCCCCGCCTGGCGGCGCGCGCCACCGCCGCCTCAGCACTGAAGGCGCGCTGA
CGTCACTCGCCGGTCCCCCGCAAACTCCCCTTCCCGGCCACCTTGGTCGCGTCCGCGCCGCCGCCGGCCCAGCCGGACCGCACCACGC
GAGGCGCGAGATAGGGGGGCACGGGCGCGACCATCTGCGCTGCGGCGCCGGCGACTCAGCGCTGCCTCAGTCTGCGGTGGGCAGCGG
AGGAGTCGTGTCGTGCCTGAGAGCGCAG

Sequence of the CamKIIα promoter, 1293 bp (5'-3'):

TTAACATTATGGCCTTAGGTCACTTCATCTCCATGGGGTTCTTCTTCTGATTTTCTAGAAAATGAGATGGGGGTGCAGAGAGCTTCCTCAGTG
ACCTGCCCAGGGTCACATCAGAAATGTCAGAGCTAGAACTTGAACTCAGATTACTAATCTTAAATTCCATGCCTTGGGGGCATGCAAGTACG
ATATACAGAAGGAGTGAACTCATTAGGGCAGATGACCAATGAGTTTAGGAAAGAAGAGTCCAGGGCAGGGTACATCTACACCACCCGCCCA
GCCCTGGGTGAGTCCAGCCACGTTCACCTCATTATAGTTGCCTCTCTCCAGTCCTACCTTGACGGGAAGCACAAGCAGAAACTGGGACAGG
AGCCCCAGGAGACCAAATCTTCATGGTCCCTCTGGGAGGATGGGTGGGGAGAGCTGTGGCAGAGGCCTCAGGAGGGGCCCTGCTGCTCA
GTGGTGACAGATAGGGGTGAGAAAGCAGACAGAGTCATTCCGTCAGCATTCTGGGTCTGTTTGGTACTTCTTCTCACGCTAAGGTGGCGGT
GTGATATGCACAATGGCTAAAAAGCAGGGAGAGCTGGAAAGAAACAAGGACAGAGACAGAGGCCAAGTCAACCAGACCAATTCCCAGAGG
AAGCAAAGAAACCATTACAGAGACTACAAGGGGGAAGGGAAGGAGAGATGAATTAGCTTCCCCTGTAAACCTTAGAACCCAGCTGTTGCCA
GGGCAACGGGGCAATACCTGTCTCTTCAGAGGAGATGAAGTTGCCAGGGTAACTACATCCTGTCTTTCTCAAGGACCATCCCAGAATGTGG
CACCCACTAGCCGTTACCATAGCAACTGCCTCTTTGCCCCACTTAATCCCATCCCGTCTGTTAAAAGGGCCCTATAGTTGGAGGTGGGGGA
GGTAGGAAGAGCGATGATCACTTGTGGACTAAGTTTGTTCGCATCCCCTTCTCCAACCCCCTCAGTACATCACCCTGGGGGAACAGGGTCC
ACTTGCTCCTGGGCCCACACAGTCCTGCAGTATTGTGTATATAAGGCCAGGGCAAAGAGGAGCAGGTTTTAAAGTGAAAGGCAGGCAGGTG
TTGGGGAGGCAGTTACCGGGGCAACGGGAACAGGGCGTTTCGGAGGTGGTTGCCATGGGGACCTGGATGCTGACGAAGGCTCGCGAGG
CTGTGAGCAGCCACAGTGCCCTGCTCAGAAGCCCCAAGCTCGTCAGTCAAGCCGGTTCTCCGTTTGCACTCAGGAGCACGGGCAGGCGAG
TGGCCCCTAGTTCTGGGGGCAGC

Multicistronic vectors with 2A ribosome skip sequence

For simultaneous, stoichiometric expression of two gene products with one transcript, a 2A ribosome skip method was chosen. This is necessary for AAV transduction with multiple genes, as only one plasmid can be packed in an AAV vector at a time. The 2A peptide sequence we use in the lab originates from the Tomato aspermy Virus (TaV)[130], a.a. sequence: EGRGSLLTCGDVEENPGP.

Vectors and sources

pCI-Syn-euPACα

euPACα from P. Hegemann's lab, subcloning into pCI-Syn by W. Schleich, Basel

Amino acid sequence euPACα ORF 5'-3', 1009 a.a.:

MYILVWKEGQQIRTFQDLEECGQFQTASNITDGQIFSINVTPTMSKGGETGETQLRRLMYLSASTEPEKCNAEYL
ADMAHVATLRNKQIGVSGFLLYSSPFFFQVIEGTDEDLDFLFAKISADPRHERCIVLANGPCTGRMYGEWHMKD
SHIDNITKHPAIKTILFQIARSFSSMWSYLPKNAANMLLLGKNPNKQAPEPMSVVVTFIYLVEFSSILAHPGLTEQC
ADILAAFVDACVRNVEGTGGQVAKFITGICMAYWPINRAEDALVGLQQLSEDLAELRSQQPPGSALSLIYSRCGV
HYGRALLCNAGFRKADFTLLGDCINTASRITSLSVKLKVPLLLSFEVRCLLGDEMREELESSGLHKVKGRDKPVQ
VYQFNAPELDSAMVRAKIEQFNPGRYRALCPVKPYESLHPAQRPPIFDDTPRENQPKLSQVQRRDSLVDRLSLI
AKLAFPSSMMAGGEGQLITLTYISQAAHPMSRLDLASIQRIAFARNESSNITGSLLYVSGLFVQTLEGPKGAVVSL
YLKIRQDKRHKDVVAVFMAPIDERVYGSPLDMTSATEEMLATFPPLQDVLSQLAKSFISLETYVPSTVVRYLTAG
NNPRNLQPVSVEVVMLATDICSFTPLSEKCSLTEVWTICNTFIDACTSAICNEGGEVIKLIGDCVTAYFPPTGADN
AVHACQEIVSFCAQLRDAFHDVLDCRSVVACGVGLDFGQVIMAQCGSLGMTEFVVAGEVSARVMEVEALTREA

GRAIVITEPVADRLSPKLRDTGIVPCQEGVDGVPCYGILGPEWELDVATIKKNIYGFHDARALAAMKKVDDGTNA
PGRGAPAGGIPSSPKVRPPGRTNSVSSYTPDPNEALDPRMAESVFLDMCHQRGDTANNSIAVKLRQAANDDRL
DLGRMLQGPHELMPVMQAIKHLTNLRMLNMSDNFVDDNNVGELVESCIPMRSLQVLDLSNNPGLTKVIALKRLI
KHNTQVREILLNGTRIAPTEQKLISEEDLKGSHKYEH*

pCI-Syn-bPAC

Humanized bPAC-cMyc from P. Hegemann's lab, cloning by D. Udwari

Amino acid sequence of bPAC ORF 5'-3', 364 a.a.:

MMKRLVYISKISGHLSLEEIQRIGKVSIKNNQRDNITGVLLYLQGLFFQILEGENEKVDKLYKKILVDDRHTNILCLK
TEYDITDRMFPNWAMKTINLNENSELMIQPIKSLLQTITQSHRVLEKYMPARVIYLINQGINPLTVEPQLVEKIIFFS
DILAFSTLTEKLPVNEVVILVNRYFSICTRIISAYGGEVTKFIGDCVMASFTKEQGDAAIRTSLDIISELKQLRHHVEA
TNPLHLLYTGIGLSYGHVIEGNMGSSLKMDHTLLGDAVNVAARLEALTRQLPYALAFTAGVKKCCQAQWTFINLG
AHQVKGKQEAIEVYTVNEAQKYYDTLQITQLIRQTLENDKPRTYEQKLISEEDL*

pAAV-Syn-bPAC-2A-tdimer2

Cloned by D. Udwari based on pCI-Syn-bPAC (see above) and pAAV-Syn-ChR2-2A-tdimer (S. Wiegert, Basel)

Amino acid sequence bPAC-2A-tdimer ORF 5'-3', 857 a.a. (2A sequence bold red, first 10 a.a. of bPAC and tdimer2 bold black):

MMKRLVYISKISGHLSLEEIQRIGKVSIKNNQRDNITGVLLYLQGLFFQILEGENEKVDKLYKKILVDDRHTNILCLK
TEYDITDRMFPNWAMKTINLNENSELMIQPIKSLLQTITQSHRVLEKYMPARVIYLINQGINPLTVEPQLVEKIIFFS
DILAFSTLTEKLPVNEVVILVNRYFSICTRIISAYGGEVTKFIGDCVMASFTKEQGDAAIRTSLDIISELKQLRHHVEA
TNPLHLLYTGIGLSYGHVIEGNMGSSLKMDHTLLGDAVNVAARLEALTRQLPYALAFTAGVKKCCQAQWTFINLG
AHQVKGKQEAIEVYTVNEAQKYYDTLQITQLIRQTLENDKPRTYEQKLISEEDLVPAA**EGRGSLLTCGDVEENPG**
PAPGSAAA**MVASSEDVIK**EFMRFKVRMEGSVNGHEFEIEGEGEGRPYEGTQTAKLKVTKGGPLPFAWDILSPQ
FQYGSKAYVKHPADIPDYKKLSFPEGFKWERVMNFEDGGVVTVTQDSSLQDGTLIYKVKFRGTNFPPDGPVMQ
KKTMGWEASTERLYPRDGVLKGEIHQALKLKDGGHYLVEFKTIYMAKKPVQLPGYYYVDTKLDITSHNEDYTIVE
QYERSEGRHHLFLGHGTGSTGSGSSGTASSEDVIKEFMRFKVRMEGSVNGHEFEIEGEGEGRPYEGTQTAKL
KVTKGGPLPFAWDILSPQFQYGSKAYVKHPADIPDYKKLSFPEGFKWERVMNFEDGGVVTVTQDSSLQDGTLIY
KVKFRGTNFPPDGPVMQKKTMGWEASTERLYPRDGVLKGEIHQALKLKDGGHYLVEFKTIYMAKKPVQLPGYY
YVDTKLDITSHNEDYTIVEQYERSEGRHHLFL*

pAAV-CamKIIα-bPAC$_{S27A}$-2A-tdimer

Same as pAAV-Syn-bPAC-2A-tdimer2, but with CamKIIα promoter instead of Syn. Point mutation in bPAC (Serine to Alanine at Pos. 27, ... IQRIGKV**S**IKNNQR ...)

Site-directed mutagenesis performed by I. Ohmert and D. Udwari.

For this construct, a mutated version of bPAC (bPAC$_{S27A}$) was used [12] *(collaboration with P. Hegemann, Berlin). This mutant has a reduced dark activity and slightly shifted excitation spectrum in vitro, and is equally efficient at producing cAMP*

pCI-Syn-tdimer2

Standard vector in the lab. tdimer2 from R.Y. Tsien (San Diego).

For amino acid sequence tdimer2 ORF 5'-3'see pAAV-Syn-bPAC-2A-tdimer

pCI-Syn-CNGA2

CNGA2 double mutation (C460W/E583M)[66], construct by W. Schleich (Basel)

Amino acid sequence CNGA2 ORF 5'-3', 664 a.a.:

MMTEKSNGVKSSPANNHNHHPPPSIKANGKDDHRAGSRPQSVAADDDTSPELQRLAEMDTPRRGRGGFQRIV
RLVGVIRDWANKNFREEEPRPDSFLERFRGPELQTVTTHQGDDKGGKDGEGKGTKKKFELFVLDPAGDWYYR
WLFVIAMPVLYNWCLLVARACFSDLQRNYFVVWLVLDYFSDTVYIADLIIRLRTGFLEQGLLVKDPKKLRDNYIHT
LQFKLDVASIIPTDLIYFAVGIHSPEVRFNRLLHFARMFEFFDRTETRTSYPNIFRISNLVLYILVIIHWNACIYYVISK
SIGFGVDTWVYPNITDPEYGYLAREYIYCLYWSTLTLTTIGETPPPVKDEEYLFVIFDFLIGVLIFATIVGNVGSMIS
NMNATRAEFQAKIDAVKHYMQFRKVSKDMEAKVIKWFDYLWTNKKTVDEREVLKNLPAKLRAEIAINVHLSTLKK
VRIFQDWEAGLLVELVLKLRPQVFSPGDYICRKGDIGKEMYIIKEGKLAVVADDGVTQYALLSAGSCFGEISILNIK
GSKMGNRRTANIRSLGYSDLFCLSKDDLMEAVTEYPDAKKVLEERGREILMKMGLLDENEVAASMEVDVQEKL
EQLETNMDTLYTRFARLLAEYTGAQQKLKQRITVLETKMKQNHEDDYLSDGINTPEPTAAE*

pAAV-Syn-Chr2$_{ET/TC}$-2A-tdimer2

Channelrhodopsin2 (E132T/T159C) mutant, construct by S.Wiegert (Basel)

Amino acid sequence Chr2$_{ET/TC}$-2A-tdimer2 ORF 5'-3', 801 a.a., 2A sequence bold red, first 10 a.a. of Chr2 and tdimer2 bold black):

MDYGGALSAVGRELLFVTNPVVVNGSVLVPEDQCYCAGWIESRGTNGAQTASNVLQWLAAGFSILLLMFYAYQ
TWKSTCGWEEIYVCAIEMVKVILEFFFEFKNPSMLYLATGHRVQWLRYATWLLTCPVILIHLSNLTGLSNDYSRRT
MGLLVSDIGCIVWGATSAMATGYVKVIFFCLGLCYGANTFFHAAKAYIEGYHTVPKGRCRQVVTGMAWLFFVSW
GMFPILFILGPEGFGVLSVYGSTVGHTIIDLMSKNCWGLLGHYLRVLIHEHILIHGDIRKTTKLNIGGTEIEVETLVED
EAEAGAVPAA**EGRGSLLTCGDVEENPGP**APGSAAA**MVASSEDVIK**EFMRFKVRMEGSVNGHEFEIEGEGEGR
PYEGTQTAKLKVTKGGPLPFAWDILSPQFQYGSKAYVKHPADIPDYKKLSFPEGFKWERVMNFEDGGVVTVTQ
DSSLQDGTLIYKVKFRGTNFPPDGPVMQKKTMGWEASTERLYPRDGVLKGEIHQALKLKDGGHYLVEFKTIYMA
KKPVQLPGYYYVDTKLDITSHNEDYTIVEQYERSEGRHHLFLGHGTGSTGSGSSGTASSEDVIKEFMRFKVRME
GSVNGHEFEIEGEGEGRPYEGTQTAKLKVTKGGPLPFAWDILSPQFQYGSKAYVKHPADIPDYKKLSFPEGFK
WERVMNFEDGGVVTVTQDSSLQDGTLIYKVKFRGTNFPPDGPVMQKKTMGWEASTERLYPRDGVLKGEIHQA
LKLKDGGHYLVEFKTIYMAKKPVQLPGYYYVDTKLDITSHNEDYTIVEQYERSEGRHHLFL*

AAV virus production

AAV virus production was outsourced to a virus facility (PennVector). DNA purification (endotoxin-free maxi-prep) was done in our lab. For the virus capsid, we chose serotype 7. The AAV backbone we used has serotype 2; the resulting AAV virus therefore has the mixed serotype AAV2/7. Virus titers were in the range of 10^{12} – 10^{13} vg/ml. AAV was stored in glycerin at -80°C.

8. Media, Solutions, Drugs

8.1. Dissection medium

Dissection medium for preparation of hippocampal organotypic slice cultures (a type of low sodium ACSF). Base ingredient is ddH_2O. Solution is sterile filtered before use.

Calcium chloride ($CaCl_2$)	1 mM
Magnesium chloride ($MgCl_2$)	5 mM
D-Glucose ($C_6H_{12}O_6$)	10 mM
Potassium chloride (KCl)	4 mM
Sodium bicarbonate ($NaHCO_3$)	26 mM
Phenol red	0.001 %
Kynurenic acid	2mM

8.2. Culture medium

Culture maintenance medium for long term culturing of hippocampal organotypic slice cultures. Base ingredient is minimal essential medium (MEM, Sigma). Solution is sterile filtered before use. pH ~ 7.28 and osmolality ~ 320 mOsm/kg.

Horse serum	20 %
L-glutamine	1mM
Ascorbic acid	0.00125 %
Insulin	1 µg/ml
Calcium chloride ($CaCl_2$)	1mM
Magnesium sulfate ($MgSO_4$)	2mM
D-Glucose ($C_6H_{12}O_6$)	13mM

8.3. Artificial Cerebrospinal Fluid (ACSF) for electrophysiology

ACSF 2/1 (2 mM $CaCl_2$, 1 mM $MgCl_2$)

ACSF for electrophysiology experiments, containing a more physiological ion composition compared to ACSF 4/4. ACSF gassed with carboxygen (5% CO_2 in 95% O_2) before adjusting pH to 7.4, osmolality = 315 mOsm/kg.

Sodium Chloride (NaCl)	127 mM
Sodium bicarbonate ($NaHCO_3$)	25 mM
D-Glucose ($C_6H_{12}O_6$)	25 mM
Potassium chloride (KCl)	2.5 mM
Sodium phosphate monobasic (NaH_2PO_4)	1.25 mM
Magnesium chloride ($MgCl_2$)	1 mM
Calcium Chloride ($CaCl_2$)	2 mM

ACSF 4/4 (4 mM $CaCl_2$, 4 mM $MgCl_2$)

ACSF for electrophysiology experiments, containing a high concentration of divalent cations, which reduces spontaneous activity. ACSF gassed with carbogen (5% CO_2 / 95% O_2) before adjusting pH to ~7.4, osmolality ~ 315 mOsm/kg.

Sodium Chloride (NaCl)	119 mM
Sodium bicarbonate ($NaHCO_3$)	26.2 mM
D-Glucose ($C_6H_{12}O_6$)	11 mM
Potassium chloride (KCl)	2.5 mM
Sodium phosphate monobasic (NaH_2PO_4)	1 mM
Magnesium chloride ($MgCl_2$)	4 mM
Calcium Chloride ($CaCl_2$)	4 mM

8.4. Artificial Cerebrospinal Fluid (ACSF) for virus injection and electroporation

ACSF-HEPES 2/1 (2 mM $CaCl_2$, 1 mM $MgCl_2$)

ACSF for virus injection and electroporation. Solution is sterile filtered before use. pH = 7.4, osmolality = 318 mOsm/kg.

Sodium Chloride (NaCl)	135 mM
HEPES	10 mM
D-Glucose ($C_6H_{12}O_6$)	25 mM
Potassium chloride (KCl)	2.5 mM
Magnesium chloride ($MgCl_2$)	1 mM
Calcium Chloride ($CaCl_2$)	2 mM

8.5. Intracellular Solutions

IC(K-Gluc)

Potassium gluconate based intracellular solution. Filtered before use. pH = 7.2, osmolality 295 mOsm/kg.

Potassium gluconate	135 mM
HEPES	10 mM
Na_2-ATP	4 mM
Na-GTP	0.4 mM
Magnesium chloride ($MgCl_2$)	4 mM
Ascorbate	3 mM
Na_2-phosphocreatine	10 mM

IC(Cs-Gluc)

Cesium-Gluconate based intracellular solution. Cesium replaces intracellular potassium, and blocks potassium channels. Filtered before use. pH = 7.2, osmolality 295 mOsm/kg.

Cesium gluconate	135 mM
HEPES	10 mM
Na_2-ATP	4 mM
Na-GTP	0.4 mM
Magnesium chloride ($MgCl_2$)	4 mM
Ascorbate	3 mM
Na_2-Phosphocreatine	10 mM

8.6. Drugs for electrophysiological experiments

Tetrodotoxin (TTX)
Antagonist of voltage gated sodium channels
Tocris (Cat.No:1069)
1 mM stock solution in ddH2O
Final concentration in bath: 1 µM (1:1000)

D-Serine (D-Ser)
Co-agonist of NMDARs
Tocris (Cat. No: 0226)
30 mM stock solution in ddH2O
Final concentration in bath: 30 µM (1:1000)

(-)-Bicuculline methochloride (Bic)
Competitive antagonist of GABAA-Receptors
Tocris (Cat. No: 0131)
10 mM stock solution in ddH2O
Final concentration in bath 10 µM (1:1000)

D-CPP-ene (CPPene)
Competitive antagonist of NMDARs
Tocris (Cat. No: 1265)
10 mM stock solution in ddH2O
Final concentration in bath: 10 µM (1:1000)

H 89 dihydrochloride (H89)
Antagonist of PKA catalytic subunit
Tocris (Cat. No: 2910)

10 mM stock solution in ddH2O
Final concentration in bath: 10 µM (1:1000)

L-cis-Diltiazem (LcD)
Blocker of cyclic nucleotide gated channels
Abcam (ab120532)
50 mM stock solution in ddH2O
Final concentration in IC: 1 mM (1:50)

ZD7288 (*ZD)*
Blocker of HCN-Channels
Tocris (Cat. No: 1000)
20mM stock solution in ddH2O
Final concentration in bath 20 µM (1:1000)

Forskolin
Activator of adenylyl cyclases
Sigma (F6886)
500mM stock solution in DMSO
Final concentration in bath 100 µM (1:5000)

IBMX
Inhibitor of phosphodiesterases
Sigma (I5879)
100 mM stock solution in DMSO
Final concentration in bath 100 mM (1:1000)

9. Abbreviations, Symbols, Suppliers

Abbreviations

2P	2-photon
a.a.	amino acid
AAV	adeno-associated virus
AC	adenylyl cyclase
ACSF	artificial cerebrospinal fluid
approx.	approximate / approximately
ATP	adenosine triphosphate
bPAC	photoactivated adenylyl cyclase from *Beggiatoa*
CA1, CA3	*cornu ammonis* 1, 3 regions of the hippocampus
cAMP	cyclic adenosine monophosphate
CFTR	cystic fibrosis transmembrane conductance regulator
cGMP	cyclic guanosine monophosphate
ChR2	channelrhodopin-2
C_{mem}	membrane capacitance
CNG	cyclic nucleotide gated
CNS	central nervous system
ddH_2O	double distilled water
DG	*gyrus dentatus* region of the hippocampus
DIV	days in vitro
DMSO	dimethyl sulfoxide
e.g.	*exempli gratia*
EC	entorhinal cortex
ECS	Endocannabinoid system
ELISA	enzyme linked immunoabsorbent assay
EPAC	exchange protein activated by cAMP
EPSC	excitatory postsynaptic current
EPSP	excitatory postsynaptic potential
EtOH	ethanol, C_2H_6O
euPACα	photoactivated adenylyl cyclase alpha from *Euglena gracilis*
FOV	field of view
FP	fluorescent protein
FRET	Förster resonance energy transfer
$GABA_AR$	γ-aminobutyric acid receptor class A
$GABA_BR$	γ-aminobutyric acid receptor class B
GCaMP	GFP Calcium Monomeric Protein
GECO	Genetically Encoded Calcium sensor for Optical imaging
GPCR	G-protein coupled receptor
GTP	guanosine triphosphate

HCN	hyperpolarization activated cyclic nucleotide gated channels
HEPES	4-(2-hydroxyethyl)-1-piperazineethanesulfonic acid
i.e.	*id est*
IBMX	3-isobutyl-1-methylxanthine (see drugs)
IC	intracellular solution
I_h	HCN channel current, 'funny current'
I_{hold}	holding current
IP_3	inositol triphosphate
LB	lysogeny broth
LcD	L-cis-Diltiazem
LED	light-emitting diode
MEM	modified Eagle medium
mEPSC	miniature excitatory postsynaptic current
n.t.s.	not to scale
NMDAR	N-methyl-D-aspartate receptor
ns	statistical significance: not significant, p-value > 0.05
PCR	polymerase chain reaction
PDE	phosphodiesterase
PKA	protein kinase A
PTFE	Polytetrafluoroethylene
rAAV	recombinant adeno-associated virus
RFP	red fluorescent protein
R_{mem}	membrane resistance
ROI	region of interest
R_s	series resistance
SD	standard deviation
SEM	standard error of the mean
Sub	Subiculum
TEVC	two electrode voltage clamp
TTL	transistor-transistor logic
VGSC	voltage gated sodium channels
V_{mem}	membrane voltage

Symbols and units

*, **, ***, ****	statistically significant, p-value * < 0.05, ** <0.01, *** < 0.001, **** < 0.0001
⌀	diameter
°C	derived SI unit for temperature (degrees Celsius)
µs, ms, s, min, h	derived SI units for time (microsecond, millisecond, second, minute, hour)
A, mA, pA	SI unit for electric current (ampere, milliampere, picoampere)
bp, kb	basepairs, kilobasepairs (unit for DNA size)
Hz, kHz, MHz	derived SI unit for frequency (hertz, kilohertz, megahertz) Hz = 1 / s

m, mm, µm, nm	SI unit for distance (meter, millimeter, micrometer, nanometer)
t	time
V, mV	derived SI unit for voltage (volt, millivolt), V = W / A
vg/ml	virus genomes per milliliter, unit to express virus titer
W, mW	derived SI unit for electric power (watt, milliwatt), W = V * A
τ_{off}	Off time-constant (tau off)
Ω, MΩ, GΩ	derived SI unit for electric resistance (ohm, megaohm, gigaohm), Ω = V / A

Suppliers

A plasmid Editor	written by M. Wayne Davis, http://biologylabs.utah.edu/jorgensen/wayned/ape/
Abcam	Abcam plc, Cambridge, UK
Axon	Axon Instruments, part of Molecular Devices, LLC, Sunnyvale, CA, USA
Calbiochem	Calbiochem, part of Merck KGaA, Darmstadt, Germany
Eurofins	Eurofins MWG Operon, Ebersberg, Germany
Fermentas	Fermentas, part of Thermo-Fisher Scientific, Waltham, MA, USA
GraphPad	GraphPad Software Inc., La Jolla, CA, USA
Leica	Leica Microsystems, Wetzlar, Germany
Life Technologies	Life Technologies, Carlsbad, CA, USA
Macherey-Nagel	Macherey-Nagel, Düren, Germany
MathWorks	The Math Works, Natick, MA, USA
Microsoft	Microsoft, Redmond, WA, USA
Microsynth	Microsynth AG, Balgach, Switzerland
Mightex	Mightex Systems, Toronto, Canada
Molecular Devices	Molecular Devices LLC, Sunnyvale, CA, USA
Narishige	Narishige, Tokyo, Japan
National Instr.	National Instruments, Austin, TX, USA
NEB	New England Biolabs, Ipswitch, MA, USA
Parker	Parker Hannifin Corp, Cleveland, OH, USA
PennVector	University of Pennsylvania, Vector Core Facility, Philadelphia, PA, USA
Prizmatix	Prizmatix Ltd., Givat-Shmuel, Israel
Qiagen	QIAGEN, Venlo, Netherlands
Roche	F. Hoffmann-La Roche Ltd, Basel, Switzerland
Sigma	Sigma-Aldrich, St. Louis, MO, USA
Sutter	Sutter Instruments, Novado, CA, USA
Thorlabs	Thorlabs, Newton, NJ, USA
Tocris	Tocris, part of R&D Systems, Minneapolis, MN, USA
WPI	World Precision Instruments, Inc., Sarasota, FL, USA

10. Bibliography

1. Miesenböck, G. The optogenetic catechism. *Science* **326,** 395–9 (2009).

2. Deisseroth, K. Optogenetics. *Nat. Methods* **8,** 26–29 (2010).

3. Method of the Year 2010. *Nat. Methods* **8,** 1–1 (2010).

4. Kim, J.-M. *et al.* Light-driven activation of beta 2-adrenergic receptor signaling by a chimeric rhodopsin containing the beta 2-adrenergic receptor cytoplasmic loops. *Biochemistry* **44,** 2284–92 (2005).

5. Airan, R. D., Thompson, K. R., Fenno, L. E., Bernstein, H. & Deisseroth, K. Temporally precise in vivo control of intracellular signalling. *Nature* **458,** 1025–9 (2009).

6. Zincarelli, C., Soltys, S., Rengo, G. & Rabinowitz, J. E. Analysis of AAV serotypes 1-9 mediated gene expression and tropism in mice after systemic injection. *Mol. Ther.* **16,** 1073–80 (2008).

7. Burger, C. *et al.* Recombinant AAV viral vectors pseudotyped with viral capsids from serotypes 1, 2, and 5 display differential efficiency and cell tropism after delivery to different regions of the central nervous system. *Mol. Ther.* **10,** 302–17 (2004).

8. Ntefidou, M., Iseki, M., Watanabe, M., Lebert, M. & Häder, D.-P. Photoactivated adenylyl cyclase controls phototaxis in the flagellate Euglena gracilis. *Plant Physiol.* **133,** 1517–1521 (2003).

9. Iseki, M. *et al.* A blue-light-activated adenylyl cyclase mediates photoavoidance in Euglena gracilis. *Nature* **415,** 1047–51 (2002).

10. Schröder-Lang, S. *et al.* Fast manipulation of cellular cAMP level by light in vivo. *Nat. Methods* **4,** 39–42 (2007).

11. Linder, J. U. Class III adenylyl cyclases: molecular mechanisms of catalysis and regulation. *Cell. Mol. Life Sci.* **63,** 1736–51 (2006).

12. Stierl, M. Kleine Enzyme mit großer Perspektive: funktionelle Beschreibung und optogenetische Anwendung von photoaktivierbaren Adenylatzyklasen. 157 (2013). at <http://d-nb.info/1042992142/>

13. Raffelberg, S. *et al.* A LOV-domain-mediated blue-light-activated adenylate (adenylyl) cyclase from the cyanobacterium Microcoleus chthonoplastes PCC 7420. *Biochem. J.* **455,** 359–65 (2013).

14. Yasukawa, H. *et al.* Identification of photoactivated adenylyl cyclases in Naegleria australiensis and BLUF-containing protein in Naegleria fowleri. *J. Gen. Appl. Microbiol.* **369,** (2012).

15. Amaral, D. & Lavenex, P. in *Hippocampus B.* (Andersen, P., Morris, R., Amaral, D., Bliss, T. & O'Keefe, J.) 37–114 (2007).

16. Andersen, P., Bliss, T. V, Lomo, T., Olsen, L. I. & Skrede, K. K. Lamellar organization of hippocampal excitatory pathways. *Acta Physiol. Scand.* **76,** 4A–5A (1971).

17. Stoppini, L., Buchs, P. a & Muller, D. A simple method for organotypic cultures of nervous tissue. *J. Neurosci. Methods* **37,** 173–182 (1991).

18. Amaral, D. & Witter, M. The three-dimensional organization of the hippocampal formation: a review of anatomical data. *Neuroscience* **31,** 571–591 (1989).

19. Spruston, N. Pyramidal neurons: dendritic structure and synaptic integration. *Nat. Rev. Neurosci.* **9,** 206–21 (2008).

20. Spruston, N. & McBain, C. in *Hippocampus B.* (Andersen, P., Morris, R., Amaral, D., Bliss, T. & O'Keefe, J.) 133–201 (2007).

21. Sudhof, T. C. The synaptic vesicle cycle. *Annu. Rev. Neurosci.* **27,** 509–47 (2004).

22. Freund, T. & Buzsáki, G. Interneurons of the hippocampus. *Hippocampus* **470,** (1996).

23. Li, S., Cullen, W. K., Anwyl, R. & Rowan, M. J. Dopamine-dependent facilitation of LTP induction in hippocampal CA1 by exposure to spatial novelty. *Nat. Neurosci.* **6,** 526–31 (2003).

24. Edelmann, E. & Lessmann, V. Dopamine Modulates Spike Timing-Dependent Plasticity and Action Potential Properties in CA1 Pyramidal Neurons of Acute Rat Hippocampal Slices. *Front. Synaptic Neurosci.* **3,** 6 (2011).

25. Lin, Y.-W., Min, M.-Y., Chiu, T.-H. & Yang, H.-W. Enhancement of associative long-term potentiation by activation of beta-adrenergic receptors at CA1 synapses in rat hippocampal slices. *J. Neurosci.* **23,** 4173–81 (2003).

26. Kalia, D. *et al.* Nucleotide, c-di-GMP, c-di-AMP, cGMP, cAMP, (p)ppGpp signaling in bacteria and implications in pathogenesis. *Chem. Soc. Rev.* **42,** 305–41 (2013).

27. Linder, J. U. & Schultz, J. E. The class III adenylyl cyclases: multi-purpose signalling modules. *Cell. Signal.* **15,** 1081–1089 (2003).

28. Gehring, C. Adenyl cyclases and cAMP in plant signaling - past and present. *Cell Commun. Signal.* **8,** 15 (2010).

29. Lodish, H., Berk, A. & Zipursky, S. in *Mol. cell Biol.* Section 20.1 (W. H. Freeman, 2000). at <http://www.ncbi.nlm.nih.gov/books/NBK21517/>

30. Shichida, Y. & Matsuyama, T. Evolution of opsins and phototransduction. *Philos. Trans. R. Soc. Lond. B. Biol. Sci.* **364,** 2881–95 (2009).

31. Halls, M. & Cooper, D. Regulation by Ca2+-signaling pathways of adenylyl cyclases. *Cold Spring Harb. …* (2011). at <http://cshperspectives.cshlp.org/content/3/1/a004143.short>

32. Chen, J., Martinez, J., Milner, T. a, Buck, J. & Levin, L. R. Neuronal expression of soluble adenylyl cyclase in the mammalian brain. *Brain Res.* **1518,** 1–8 (2013).

33. Nguyen, P. V & Woo, N. H. Regulation of hippocampal synaptic plasticity by cyclic AMP-dependent protein kinases. *Prog. Neurobiol.* **71,** 401–37 (2003).

34. Esteban, J. a *et al.* PKA phosphorylation of AMPA receptor subunits controls synaptic trafficking underlying plasticity. *Nat. Neurosci.* **6,** 136–43 (2003).

35. Banke, T. G. *et al.* Control of GluR1 AMPA receptor function by cAMP-dependent protein kinase. *J. Neurosci.* **20,** 89–102 (2000).

36. Schrader, L. a, Anderson, A. E., Mayne, A., Pfaffinger, P. J. & Sweatt, J. D. PKA modulation of Kv4.2-encoded A-type potassium channels requires formation of a supramolecular complex. *J. Neurosci.* **22,** 10123–33 (2002).

37. Fourcaudot, E. *et al.* cAMP/PKA signaling and RIM1alpha mediate presynaptic LTP in the lateral amygdala. *Proc. Natl. Acad. Sci. U. S. A.* **105,** 15130–5 (2008).

38. Kaeser-Woo, Y. J. *et al.* Synaptotagmin-12 phosphorylation by cAMP-dependent protein kinase is essential for hippocampal mossy fiber LTP. *J. Neurosci.* **33,** 9769–80 (2013).

39. Craven, K. B. & Zagotta, W. N. CNG and HCN channels: two peas, one pod. *Annu. Rev. Physiol.* **68,** 375–401 (2006).

40. Kaupp, U. B. & Seifert, R. Cyclic nucleotide-gated ion channels. *Physiol. Rev.* **82,** 769–824 (2002).

41. Matulef, K. & Zagotta, W. N. Cyclic nucleotide-gated ion channels. *Annu. Rev. Cell Dev. Biol.* **19,** 23–44 (2003).

42. Kingston, P. a, Zufall, F. & Barnstable, C. J. Rat hippocampal neurons express genes for both rod retinal and olfactory cyclic nucleotide-gated channels: novel targets for cAMP/cGMP function. *Proc. Natl. Acad. Sci. U. S. A.* **93,** 10440–5 (1996).

43. Barbuti, A. & DiFrancesco, D. Control of cardiac rate by “funny” channels in health and disease. *Ann. N. Y. Acad. Sci.* **1123,** 213–23 (2008).

44. Kase, D. & Imoto, K. The Role of HCN Channels on Membrane Excitability in the Nervous System. *J. Signal Transduct.* **2012,** 619747 (2012).

45. Robinson, R. B. & Siegelbaum, S. a. Hyperpolarization-activated cation currents: from molecules to physiological function. *Annu. Rev. Physiol.* **65,** 453–80 (2003).

46. Gloerich, M. & Bos, J. L. Epac: defining a new mechanism for cAMP action. *Annu. Rev. Pharmacol. Toxicol.* **50,** 355–75 (2010).

47. Gelinas, J. N. *et al.* Activation of exchange protein activated by cyclic-AMP enhances long-lasting synaptic potentiation in the hippocampus. *Learn. Mem.* **15,** 403–11 (2008).

48. Ster, J. *et al.* Epac mediates PACAP-dependent long-term depression in the hippocampus. *J. Physiol.* **587,** 101–13 (2009).

49. Ma, N., Abel, T. & Hernandez, P. J. Exchange protein activated by cAMP enhances long-term memory formation independent of protein kinase A. *Learn. Mem.* **16,** 367–70 (2009).

50. Laurent, A.-C., Breckler, M., Berthouze, M. & Lezoualc'h, F. Role of Epac in brain and heart. *Biochem. Soc. Trans.* **40,** 51–7 (2012).

51. Conti, M. & Beavo, J. Biochemistry and physiology of cyclic nucleotide phosphodiesterases: essential components in cyclic nucleotide signaling. *Annu. Rev. Biochem.* **76,** 481–511 (2007).

52. Baillie, G. S. Compartmentalized signalling: spatial regulation of cAMP by the action of compartmentalized phosphodiesterases. *FEBS J.* **276,** 1790–9 (2009).

53. Dessauer, C. Adenylyl cyclase–A-kinase anchoring protein complexes: the next dimension in cAMP signaling. *Mol. Pharmacol.* **76,** 935–941 (2009).

54. Cooper, D. Compartmentalization of adenylate cyclase and cAMP signalling. *Biochem. Soc. Trans.* **8,** 1319–1322 (2005).

55. Baillie, G. S., Scott, J. D. & Houslay, M. D. Compartmentalisation of phosphodiesterases and protein kinase A: opposites attract. *FEBS Lett.* **579,** 3264–70 (2005).

56. Zhong, H. *et al.* Subcellular dynamics of type II PKA in neurons. *Neuron* **62,** 363–74 (2009).

57. Kim, M. *et al.* Colocalization of protein kinase A with adenylyl cyclase enhances protein kinase A activity during induction of long-lasting long-term-potentiation. *PLoS Comput. Biol.* **7,** e1002084 (2011).

58. Lu, Y. *et al.* AKAP150-anchored PKA activity is important for LTD during its induction phase. *J. Physiol.* **586,** 4155–64 (2008).

59. Lu, Y. *et al.* A kinase anchor protein 150 (AKAP150)-associated protein kinase A limits dendritic spine density. *J. Biol. Chem.* **286,** 26496–506 (2011).

60. Bauman, A. L., Goehring, A. S. & Scott, J. D. Orchestration of synaptic plasticity through AKAP signaling complexes. *Neuropharmacology* **46,** 299–310 (2004).

61. Kirschner, L. S., Yin, Z., Jones, G. N. & Mahoney, E. Mouse models of altered protein kinase A signaling. *Endocr. Relat. Cancer* **16,** 773–93 (2009).

62. Kandel, E. R. The biology of memory: a forty-year perspective. *J. Neurosci.* **29,** 12748–56 (2009).

63. Davis, R. Physiology and biochemistry of Drosophila learning mutants. *Physiol. Rev.* **0,** (1996).

64. Silva, a J., Kogan, J. H., Frankland, P. W. & Kida, S. CREB and memory. *Annu. Rev. Neurosci.* **21,** 127–48 (1998).

65. Narayanan, R. & Johnston, D. The h current is a candidate mechanism for regulating the sliding modification threshold in a BCM-like synaptic learning rule. *J. Neurophysiol.* 1020–1033 (2010). doi:10.1152/jn.01129.2009.

66. Rich, T. C., Tse, T. E., Rohan, J. G., Schaack, J. & Karpen, J. W. In vivo assessment of local phosphodiesterase activity using tailored cyclic nucleotide-gated channels as cAMP sensors. *J. Gen. Physiol.* **118,** 63–78 (2001).

67. Stierl, M. *et al.* Light modulation of cellular cAMP by a small bacterial photoactivated adenylyl cyclase, bPAC, of the soil bacterium Beggiatoa. *J. Biol. Chem.* **286,** 1181–8 (2011).

68. Ryu, M.-H., Moskvin, O. V, Siltberg-Liberles, J. & Gomelsky, M. Natural and engineered photoactivated nucleotidyl cyclases for optogenetic applications. *J. Biol. Chem.* **285,** 41501–8 (2010).

69. Gorostiza, P. & Isacoff, E. Optical switches for remote and noninvasive control of cell signaling. *Science* **322,** 395–399 (2008).

70. Miller, G. Shining new light on neural circuits. *Science* **314,** 1674–1676 (2006).

71. Schoenenberger, P., Schärer, Y.-P. Z. & Oertner, T. G. Channelrhodopsin as a tool to investigate synaptic transmission and plasticity. *Exp. Physiol.* **96,** 34–9 (2011).

72. Gomelsky, M. & Klug, G. BLUF: a novel FAD-binding domain involved in sensory transduction in microorganisms. *Trends Biochem. Sci.* **27,** 497–500 (2002).

73. Hinck, S. *et al.* Physiological adaptation of a nitrate-storing Beggiatoa sp. to diel cycling in a phototrophic hypersaline mat. *Appl. Environ. Microbiol.* **73,** 7013–7022 (2007).

74. Mills, H. J., Martinez, R. J., Story, S. & Sobecky, P. A. Identification of members of the metabolically active microbial populations associated with Beggiatoa species mat communities from Gulf of Mexico cold-seep sediments. *Appl. Environ. Microbiol.* **70,** 5447–5458 (2004).

75. Weinreich, F., Wood, P. G., Riordan, J. R. & Nagel, G. Direct action of genistein on CFTR. *Pflugers Arch.* **434,** 484–491 (1997).

76. Liman, E. R., Tytgat, J. & Hess, P. Subunit stoichiometry of a mammalian K+ channel determined by construction of multimeric cDNAs. *Neuron* **9,** 861–871 (1992).

77. Rich, T. C. *et al.* A uniform extracellular stimulus triggers distinct cAMP signals in different compartments of a simple cell. *Proc. Natl. Acad. Sci. U. S. A.* **98,** 13049–54 (2001).

78. Schoenenberger, P., Gerosa, D. & Oertner, T. G. Temporal control of immediate early gene induction by light. *PLoS One* **4,** e8185 (2009).

79. Karimova, G., Pidoux, J., Ullmann, A. & Ladant, D. A bacterial two-hybrid system based on a reconstituted signal transduction pathway. *Proc. Natl. Acad. Sci. U. S. A.* **95,** 5752–5756 (1998).

80. Masuda, S. & Bauer, C. E. AppA is a blue light photoreceptor that antirepresses photosynthesis gene expression in Rhodobacter sphaeroides. *Cell* **110,** 613–623 (2002).

81. Otmakhov, N. *et al.* Forskolin-induced LTP in the CA1 hippocampal region is NMDA receptor dependent. *J. Neurophysiol.* **91,** 1955–62 (2004).

82. Bonetti, C. *et al.* The role of key amino acids in the photoactivation pathway of the Synechocystis Slr1694 BLUF domain. *Biochemistry* **48,** 11458–11469 (2009).

83. Christie, J. M., Swartz, T. E., Bogomolni, R. A. & Briggs, W. R. Phototropin LOV domains exhibit distinct roles in regulating photoreceptor function. *Plant J.* **32,** 205–219 (2002).

84. Matsuoka, D. & Tokutomi, S. Blue light-regulated molecular switch of Ser/Thr kinase in phototropin. *Proc. Natl. Acad. Sci. U. S. A.* **102,** 13337–13342 (2005).

85. Wu, Y. I. *et al.* A genetically encoded photoactivatable Rac controls the motility of living cells. *Nature* **461,** 104–108 (2009).

86. Strickland, D., Moffat, K. & Sosnick, T. R. Light-activated DNA binding in a designed allosteric protein. *Proc. Natl. Acad. Sci. U. S. A.* **105,** 10709–10714 (2008).

87. Möglich, A., Ayers, R. A. & Moffat, K. Design and signaling mechanism of light-regulated histidine kinases. *J. Mol. Biol.* **385,** 1433–1444 (2009).

88. Dunn, T. A. & Feller, M. B. Imaging second messenger dynamics in developing neural circuits. *Dev. Neurobiol.* **68,** 835–844 (2008).

89. Zaccolo, M. & Pozzan, T. Discrete microdomains with high concentration of cAMP in stimulated rat neonatal cardiac myocytes. *Science* **295,** 1711–1715 (2002).

90. Bailey, C. H., Bartsch, D. & Kandel, E. R. Toward a molecular definition of long-term memory storage. *Proc. Natl. Acad. Sci. U. S. A.* **93,** 13445–13452 (1996).

91. Chen, C. & Regehr, W. G. The mechanism of cAMP-mediated enhancement at a cerebellar synapse. *J. Neurosci.* **17,** 8687–8694 (1997).

92. Makhinson, M., Chotiner, J. K., Watson, J. B. & O'Dell, T. J. Adenylyl cyclase activation modulates activity-dependent changes in synaptic strength and Ca2+/calmodulin-dependent kinase II autophosphorylation. *J. Neurosci.* **19,** 2500–10 (1999).

93. Schroll, C. *et al.* Light-induced activation of distinct modulatory neurons triggers appetitive or aversive learning in Drosophila larvae. *Curr. Biol.* **16,** 1741–1747 (2006).

94. Zhang, F. *et al.* Red-shifted optogenetic excitation: a tool for fast neural control derived from Volvox carteri. *Nat. Neurosci.* **11,** 631–633 (2008).

95. Tang, W. *et al.* Faithful expression of multiple proteins via 2A-peptide self-processing: a versatile and reliable method for manipulating brain circuits. *J. Neurosci.* **29,** 8621–9 (2009).

96. Levitan, I. Modulation of ion channels by protein phosphorylation and dephosphorylation. *Annu. Rev. Physiol.* (1994).

97. Notomi, T. & Shigemoto, R. Immunohistochemical localization of Ih channel subunits, HCN1-4, in the rat brain. *J. Comp. Neurol.* **471,** 241–76 (2004).

98. Magee, J. Dendritic Ih normalizes temporal summation in hippocampal CA1 neurons. *Nat. Neurosci.* **2,** 848 (1999).

99. Magee, J. C. Dendritic hyperpolarization-activated currents modify the integrative properties of hippocampal CA1 pyramidal neurons. *J. Neurosci.* **18,** 7613–24 (1998).

100. Harris, N. C. & Constanti, a. Mechanism of block by ZD 7288 of the hyperpolarization-activated inward rectifying current in guinea pig substantia nigra neurons in vitro. *J. Neurophysiol.* **74,** 2366–78 (1995).

101. Noble, D. *et al.* Mechanism of isoprenaline- and forskolin induced depolarization of single guinea-pig ventricular myocytes. 299–320 (1988).

102. Nargeot, J., Nerbonne, J. M., Engels, J. & Lester, H. a. Time course of the increase in the myocardial slow inward current after a photochemically generated concentration jump of intracellular cAMP. *Proc. Natl. Acad. Sci. U. S. A.* **80,** 2395–9 (1983).

103. Poolos, N. P., Bullis, J. B. & Roth, M. K. Modulation of h-channels in hippocampal pyramidal neurons by p38 mitogen-activated protein kinase. *J. Neurosci.* **26,** 7995–8003 (2006).

104. Lovinger, D. M. Presynaptic modulation by endocannabinoids. *Handb. Exp. Pharmacol.* 435–77 (2008). doi:10.1007/978-3-540-74805-2_14

105. Tyler, W. J. *et al.* BDNF increases release probability and the size of a rapidly recycling vesicle pool within rat hippocampal excitatory synapses. *J. Physiol.* **574,** 787–803 (2006).

106. Tyler, W. & Pozzo-Miller, L. BDNF enhances quantal neurotransmitter release and increases the number of docked vesicles at the active zones of hippocampal excitatory synapses. *J. Neurosci.* **21,** 4249–4258 (2001).

107. Huang, Y. Y., Li, X. C. & Kandel, E. R. cAMP contributes to mossy fiber LTP by initiating both a covalently mediated early phase and macromolecular synthesis-dependent late phase. *Cell* **79,** 69–79 (1994).

108. Weisskopf, M. G., Castillo, P. E., Zalutsky, R. a & Nicoll, R. a. Mediation of hippocampal mossy fiber long-term potentiation by cyclic AMP. *Science* **265,** 1878–82 (1994).

109. Nicoll, R. a & Schmitz, D. Synaptic plasticity at hippocampal mossy fibre synapses. *Nat. Rev. Neurosci.* **6,** 863–76 (2005).

110. Chater, T. E. & Goda, Y. CA3 Mossy Fiber Connections: Giant Synapses that Gain Control. *Neuron* **77,** 4–6 (2013).

111. Frey, U., Huang, Y. & Kandel, E. Effects of cAMP simulate a late stage of LTP in hippocampal CA1 neurons. *Science (80-.).* **260,** 1661–1664 (1993).

112. Bolshakov, V. Y., Golan, H., Kandel, E. R. & Siegelbaum, S. a. Recruitment of new sites of synaptic transmission during the cAMP-dependent late phase of LTP at CA3-CA1 synapses in the hippocampus. *Neuron* **19,** 635–51 (1997).

113. Duffy, S. N. & Nguyen, P. V. Postsynaptic application of a peptide inhibitor of cAMP-dependent protein kinase blocks expression of long-lasting synaptic potentiation in hippocampal neurons. *J. Neurosci.* **23,** 1142–50 (2003).

114. Huang, Y. & Kandel, E. D1/D5 receptor agonists induce a protein synthesis-dependent late potentiation in the CA1 region of the hippocampus. *Proc. Natl. …* **92,** 2446–2450 (1995).

115. Huber, D. *et al.* Multiple dynamic representations in the motor cortex during sensorimotor learning. *Nature* **484,** 473–8 (2012).

116. Berndt, A. *et al.* High-efficiency channelrhodopsins for fast neuronal stimulation at low light levels. *Proc. Natl. Acad. Sci. U. S. A.* **108,** 7595–600 (2011).

117. Grieger, J. & Samulski, R. Packaging capacity of adeno-associated virus serotypes: impact of larger genomes on infectivity and postentry steps. *J. Virol.* **79,** (2005).

118. Bohenzky, R. A., LeFebvre, R. B. & Berns, K. I. Sequence and symmetry requirements within the internal palindromic sequences of the adeno-associated virus terminal repeat. *Virology* **166,** 316–27 (1988).

119. Shichi, H. Spectrum and purity of bovine rhodopsin. *Biochemistry* **9,** 1973–7 (1970).

120. Lin, J. Y., Knutsen, P. M., Muller, A., Kleinfeld, D. & Tsien, R. Y. ReaChR: a red-shifted variant of channelrhodopsin enables deep transcranial optogenetic excitation. *Nat. Neurosci.* **16,** 1499–1508 (2013).

121. Ponsioen, B. *et al.* Detecting cAMP-induced Epac activation by fluorescence resonance energy transfer: Epac as a novel cAMP indicator. *EMBO Rep.* **5,** 1176–80 (2004).

122. Mironov, S. L. *et al.* Imaging cytoplasmic cAMP in mouse brainstem neurons. *BMC Neurosci.* **10,** 29 (2009).

123. Buck, J., Sinclair, M. L., Schapal, L., Cann, M. J. & Levin, L. R. Cytosolic adenylyl cyclase defines a unique signaling molecule in mammals. *Proc. Natl. Acad. Sci. U. S. A.* **96,** 79–84 (1999).

124. Chavez-Noriega, L. E. & Stevens, C. F. Modulation of synaptic efficacy in field CA1 of the rat hippocampus by forskolin. *Brain Res.* **574,** 85–92 (1992).

125. Laurenza, a, Sutkowski, E. M. & Seamon, K. B. Forskolin: a specific stimulator of adenylyl cyclase or a diterpene with multiple sites of action? *Trends Pharmacol. Sci.* **10,** 442–7 (1989).

126. Otmakhova, N. a & Lisman, J. E. D1/D5 dopamine receptor activation increases the magnitude of early long-term potentiation at CA1 hippocampal synapses. *J. Neurosci.* **16,** 7478–86 (1996).

127. O'Carroll, C. M., Martin, S. J., Sandin, J., Frenguelli, B. & Morris, R. G. M. Dopaminergic modulation of the persistence of one-trial hippocampus-dependent memory. *Learn. Mem.* **13,** 760–9 (2006).

128. Suter, B. A. *et al.* Ephus: multipurpose data acquisition software for neuroscience experiments. *Front. Neural Circuits* **4,** 100 (2010).

129. Dittgen, T. *et al.* Lentivirus-based genetic manipulations of cortical neurons and their optical and electrophysiological monitoring in vivo. *Proc. Natl. Acad. Sci. U. S. A.* **101,** 18206–11 (2004).

130. Szymczak, A. L. *et al.* Correction of multi-gene deficiency in vivo using a single "self-cleaving" 2A peptide-based retroviral vector. *Nat. Biotechnol.* **22,** 589–94 (2004).

131. Wiegert, J. S. & Oertner, T. G. Long-term depression triggers the selective elimination of weakly integrated synapses. *Proc. Natl. Acad. Sci. U. S. A.* **110,** E4510–9 (2013).

132. Bannister, N. & Larkman, A. Dendritic morphology of CA1 pyramidal neurones from the rat hippocampus: I. Branching patterns. *J. Comp. Neurol.* **160,** 150–160 (1995).

11. Picture credits

The following pictures were taken from publications:

- Fig 1.1 modified from Miesenböck [1]
- Fig 1.3 and 1.5 modified from The Hippocampus Book [15]
- Fig 7.2.2b modified from S. Wiegert in [131]

12. Acknowledgements

I would like to thank Thomas Oertner for the opportunity to do this thesis, for discussions and for his guidance and patience.

Christine Gee was a very important help for me and the project, I would like to thank her very much for her support and expertise.

I also would like to thank the rest of the Oertner lab in Basel and Hamburg for the good times in the lab. I would like to specifically thank Simon Wiegert and Philipp Schönenberger for many discussions and their friendship.

Thanks to Iris Ohmert and Daniela Gerosa for great technical support and the good atmosphere in the lab.

Thanks to Manuela Stierl and Peter Hegemann, with whom we collaborated for this project, and who provided us with new constructs and insights about PAC.

Many thanks to my parents and my grandmother who have always supported me in my academic career, wherever it drew me all over Europe.

I would also like to thank my godchild Ben for being a generally very awesome little toddler.

Funding for this project was provided by the Novartis Research Foundation and the University Medical Center Hamburg-Eppendorf (UKE)

13. Statement of Contribution

Organotypic cell cultures were prepared by Iris Ohmert (Hamburg) or Daniela Gerosa (Basel). Technical assistance, especially culture media preparation and assistance in molecular cloning was provided by Iris Ohmert (Hamburg) and Daniela Gerosa (Basel). Christine Gee performed some of the intracellular recording experiments and helped analyzing data. Christine Gee and Thomas Oertner proofread the thesis. Wolfram Schleich and Jiang Hao performed preliminary experiments with euPACα and bPAC respectively, data not included in this thesis.

14. Eidesstattliche Versicherung

Hiermit erkläre ich an Eides statt, dass ich die vorliegende Dissertationsschrift selbst verfasst und keine anderen als die angegebenen Quellen und Hilfsmittel benutzt habe.

Hamburg, den 31. Januar 2014

Unterschrift

15. Eidesstattliche Erklärung

Ich erkläre hiermit, dass ich mich bisher keiner weiteren Doktorprüfung unterzogen habe. Ich habe die Dissertation in der gegenwärtigen oder einer anderen Fassung an keiner anderen Fakultät eingereicht.

Hamburg, den 31. Januar 2014

Unterschrift